Spectrally Efficient Multicarrier Communication Systems: Signal Detection, Mathematical Modelling and Optimisation

A thesis submitted for the degree of Doctor of Philosophy (Ph.D)

by

Ioannis D. Kanaras

Communications and Information Systems Research Group

Department of Electronic and Electrical Engineering

University College London

June 2010

Statement of Originality

I, Ioannis D. Kanaras confirm that the work presented in this thesis is my own. Where information has been derived from other sources, I confirm that this has been indicated in the thesis.

To my beloved parents and to Nina, Kiki and the young Dimitris

'Honor to those who in the life they lead define and guard a Thermopylae. Never betraying what is right, consistent and just in all they do but showing pity also, and compassion; generous when they're rich, and when they're poor, still generous in small ways, still helping as much as they can; always speaking the truth, yet without hating those who lie. And even more honor is due to them when they foresee (as many do foresee) that Ephialtis will turn up in the end, that the Medes will break through after all.'

'Thermopylae'

C. P. Cavafy (1903)

Abstract

This thesis considers theoretical, analytical and engineering design issues relating to non-orthogonal Spectrally Efficient Frequency Division Multiplexing (SEFDM) communication systems that exhibit significant spectral merits when compared to Orthogonal FDM (OFDM) schemes. Alas, the practical implementation of such systems raises significant challenges, with the receivers being the bottleneck.

This research explores detection of SEFDM signals. The mathematical foundations of such signals lead to proposals of different orthonormalisation techniques as required at the receivers of non-orthogonal FDM systems. To address SEFDM detection, two approaches are considered: either attempt to solve the problem optimally by taking advantage of special cases properties or to apply sub-optimal techniques that offer reduced complexities at the expense of error rates degradation. Initially, the application of sub-optimal linear detection techniques, such as Zero Forcing (ZF) and Minimum Mean Squared Error (MMSE), is examined analytically and by detailed modelling. To improve error performance a heuristic algorithm, based on a local search around an MMSE estimate, is designed by combining MMSE with Maximum Likelihood (ML) detection. Yet, this new method appears to be efficient for BPSK signals only. Hence, various variants of the sphere decoder (SD) are investigated. A Tikhonov regularised SD variant achieves an optimal solution for the detection of medium size signals in low noise regimes. Detailed modelling shows the SD detector to be well suited to the SEFDM detection, however, with complexity increasing with system interference and noise. A new design of a detector that offers a good compromise between computational complexity and error rate performance is proposed and tested through modelling and simulation. Standard reformulation techniques are used to relax the original optimal detection problem to a convex Semi-Definite Program (SDP) that can be solved in polynomial time. Although SDP performs better than other linear relaxations, such as ZF and MMSE, its deviation from optimality also increases with the deterioration of the system inherent interference. To improve its performance a heuristic algorithm based on a local search around the SDP estimate is further proposed. Finally, a modified SD is designed to implement faster than the local search SDP concept. The new method/algorithm, termed the pruned or constrained SD, achieves the detection of realistic SEFDM signals in noisy environments.

Acknowledgement

I would like to express my sincere gratitude to my three fellow travellers in this magic trip of innumerous intellectual challenges and psychological transitions: my supervisor Professor Izzat Darwazeh for his guidance, wisdom and offering me the happiness of accomplishing one of my childhood dreams, Professor Miguel Rodrigues for his suggestions, numerous corrections and fruitful guidelines and Dr. Arsenia Chorti for her invaluable contributions, daily discussions and continuous motivation. But above all, I would like to thank them for their moral support and their true friendship.

I would also like to thank Ms Safa Ahmed for her useful explanations on the SEFDM transmitters and the problem properties and Dr. Richard Clegg for his kind collaboration. Furthermore, all the people in the 804 lab for their help. Especially Dr. Miguel Pimenta, Dr. Fabio Verdicchio and Mr. Samir Sayed for sharing their knowledge and their feelings and thoughts with me.

Last but not least, I would like to express my deep gratitude to my mother, my sister and all my friends for their tolerance, interest and love; and to Kiki that always brought and keeps on bringing so much light in my life. Finally, I could not forget my father and grand parents whose memory and example are still inspirational for me and Aristides without whom I would probably have never been here.

I hope, life will give them back multiply help and happiness they have so generously offered me.

Contents

List of Figures

List of Tables

Glossary and Abbreviations

.*	Element by element multiplication
$\downarrow$	Decreasing
$(\hat{\cdot})$or$(\tilde{\cdot})$	Estimate
$\in$	In
∞	Infinity
$(\cdot)^*$	Optimum
$(\cdot)^H$	Hermitian of a vector/matrix
$(\cdot)^T$	Transpose of a vector/matrix
$(\cdot)^{-1}$	Inverse of a matrix
$\langle\cdot\rangle$	Inner product
$\lceil\cdot\rceil$	Floor function
$\lfloor\cdot\rceil$	Slicing function
$\lfloor\cdot\rfloor$	Ceiling function
$\mathbf{A}$	Where a symbol appears in bold, it refers to a matrix of any dimension including a $(1xN)$ dimension which is a vector
$\mathbf{S}^N$	The set of symmetric matrices of N dimension
$\mathbf{S}_+^N$	The set of positive semidefinite matrices of N dimension
ceil$\{\cdot\}$	Ceiling function
cholesky$\{\cdot\}$	Cholesky decomposition function
conj$\{\cdot\}$	Conjugate
Diag$\{\cdot\}$	Diagonal matrix
diag$\{\cdot\}$	Diagonal of a matrix

dom$\{\cdot\}$	The domain of a function
enum$\{\cdot\}$	Integer enumeration function
E$\{\cdot\}$	Expected value
floor$\{\cdot\}$	Floor function
HD$\{\cdot\}$	Hamming distance calculation function
Im$\{\cdot\}$	Imaginary
init_radius	Initial radius of the SD hypersphere
length$\{\cdot\}$	Vector length function
max.	Maximise
min.	Minimise
randomise$\{\cdot\}$	Randomisation function
rank$\{\cdot\}$	Rank of a matrix
recomp$\{\cdot\}$	Real to complex vector converter function
Re$\{\cdot\}$	Real
s.t.	Subject to
sortSE$\{\cdot\}$	SE strategy reordering function
Tr$\{\cdot\}$	Trace of a matrix
∇	The gradient of a function
$\subset$	Subset
$\succeq$	Inequality over the set $\mathbf{S}_+^N$
$\uparrow$	Increasing
$\vee$	Or
$d_H\{\cdot,\cdot\}$	Hamming distance
E_b/N_0	Energy of Bit to Noise Power Density Ratio
l_2	Euclidean norm
$O(\cdot)$	Order
ACI	Adjacent Channel Interference
ADSL	Asymmetric Digital Subscriber Loop
ASK	Amplitude Shift Keying

19

AWGN	Additive White Gaussian Noise
BER	Bit Error Rate
BPSK	Binary Phase Shift Keying
CDMA	Code Division Multiplexing Access
CGS	Classical Gram Schmidt
CSD	Complex Sphere Decoder
CVX	Convex optimisation tool
DAB	Digital Audio Broadcasting
DEV	Dominant Eigen Vector
DFT	Discrete Fourier Transform
DVB	Digital Video Broadcasting
ETSI	European Telecommunications Standards Institute
FDM	Frequency Division Multiplexing
FFT	Fast Fourier Transform
FP	Fichke-Pohst reordering strategy
FPGA	Field Programmable Gate Array
FrFT	Fractional Fourier Transform
FT	Fourier Transform
FTN	Faster Than Nyquist
GA	Genetic Algorithms
GS	Gram Schmidt
HC-MCM	High Compaction Multicarrier Modulation
I	In-phase
IC	Iterative Cancellation
IC-Lo	Iterative Cancellation Lowdin based
ICI	Intercarrier Interference
IFFT	Inverse Fast Fourier Transform
IFrFT	Inverse Fractional Fourier Transform
ILS	Integer Least Squares

IMGS	Iterative Modified Gram Schmidt
IOTA	Isotropic Orthogonal Transform Algorithm
IPM	Interior Point Methods
ISI	Intersymbol Interference
KKT	Karush-Kuhn-Tucker conditions
LAS	Likelihood Ascent Sequence
LB	Lower Bound
LHS	Left Hand Side
LMI	Linear Matrix Inequality
Lo	Lowdin orthonormalisation
LS	Least Squares
LTE	Long Term Evolution
MAP	Maximum a Posteriori
MC-CDMA	Multi-Carrier CDMA
MCM	Multi Carrier Modulation
MGS	Modified Gram Schmidt
MIMO	Multiple Input Multiple Output
ML	Maximum Likelihood
MMSE	Minimum Mean Squared Error
NP	Non Polynomial
OFDM	Orthogonal Frequency Division Multiplexing
OQAM	offset QAM
OvFDM	Overlapped Frequency Division Multiplexing
OvTDM	Overlapped Time Division Multiplexing
PAM	Pulse Amplitude Modulation
PAPR	Peak to Average Power Ratio
PLC	Power Line Communications
PoSD	Power Spectrum Density
PSD	Pruned Sphere Decoder

PSK	Phase Shift Keying
Q	Quadrature
QAM	Quadrature Amplitude Modulation
Rand	Randomisation
RegSD	Regularised Sphere Decoder
RHS	Right Hand Side
RSD	Sphere Decoder based on real decomposition
SD	Sphere Decoder
SDP	Semidefinite Programming
SDP-ML	Combined SDP with brute force ML
SE	Schnorr-Euchner reordering strategy
SeDuMi	Self Dual Minimization
SEFDM	Spectrally Efficient Frequency Division Multiplexing
SNR	Signal to Noise Ratio
SpE	Spectral Efficiency
SV	Shortest Vector
SVD	Singular Value Decomposition
TSVD	Truncated Singular Value Decomposition
UB	Upper Bound
WCDMA	Wideband Code Division Multiplexing Access
WiMAX	Worldwide interoperability for Microwave Access
ZF	Zero Forcing

Chapter 1

Introduction

Communications have played a significant role in the transformation of social lives and structures all around the world. Mobile phones and the Internet are no longer luxuries, but absolute necessities in the daily life of millions of people. The support of bandwidth demanding applications by these two means, has become feasible thanks to advanced transmission techniques like Wideband Code Division Multiple Access (WCDMA) and Orthogonal Frequency Division Multiplexing (OFDM). The latter has been adopted in many state of the art communication systems due to its ability of coping efficiently with frequency selective and time dispersive propagation channels.

OFDM's first analogue variants were proposed in 1950s/1960s [1], [2], [3], [4] and its practical digital implementation became tangible much later by making use of the Inverse Discrete Fourier Transformation (IDFT) [5] . Hence, OFDM has been applied in numerous commercial applications. To mention but a few, it was first used in late 80s in Asymmetric Digital Subscriber Loop (ADSL) [6] for the transmission of high data rates over ordinary copper telephone lines. Around the same time, OFDM was adopted by the European Telecommunications Standards Institute (ETSI) for the development of Digital Audio (DAB) [7] and Digital Video Broadcasting (DVB) systems [8], [9]. Furthermore, for more than a decade it has constituted the physical layer of wireless

networks standards like the 802.11a/g/n [10], [11]. Nowadays, the development and deployment of wireless broadband OFDM systems like Worldwide interoperability for Microwave Access (WiMAX) [12], [13] and Long Term Evolution (LTE) systems are in progress [14], [15]. For LTE, system proposals include a combination of OFDM with Multiple-Input Multiple-Output (MIMO) techniques [16], [17] that promise the reliable transmission of hundreds of Megabits per second (Mbps) over distorting mobile communications channels. OFDM commercial applications are not limited to wireless or ADSL systems. Because of its ability of meeting tight spectral masks, OFDM is further used in Power Line Communications (PLC) [18], [19], [20]. In addition, recent research has taken place for OFDM implementation in optical communications [21], [22] as a mean of handling the dispersion effects in fibre media.

While the use of rectangular pulses establishes the orthogonality between the OFDM signal carriers, such use creates OFDM's with two main weaknesses: first, it results in an infinite bandwidth that renders OFDM signal vulnerable to frequency dispersion caused by Doppler effect and/or other frequency offsets. Second, the robustness of OFDM against time dispersion requires the introduction of a redundant guard band between transmitted symbols. As a consequence, the OFDM spectral efficiency is reduced. Regarding the first issue, diverse pulse shaping based solutions have been proposed in order to improve the localisation of the OFDM signal in both time and frequency domain [23], [24], [25]. As far as the spectral efficiency is concerned, offset QAM (OQAM) OFDM [4], [26] was an initial attempt to enhance OFDM throughput by discarding the guard band overhead. This was achieved through transmitting the in phase (I) and quadrature (Q) parts of the data symbols separately in half-OFDM signaling period intervals.

In the beginning of this decade, the issue of improving the spectral efficiency of OFDM signals was addressed again. Rodrigues and Darwazeh in [27] and Xiong in [28] introduced similar to OQAM-OFDM schemes with half in-

tercarrier frequency separation. Fast OFDM (FOFDM) and M-ASK OFDM, respectively, preserve the orthogonality for one dimensional data, e.g. M-PAM, doubling real data OFDM spectral efficiency. However, the transmission of two-dimensional symbols suffers from intercarrier interference. Ultimately, these systems do not offer bandwidth saving when compared to systems using higher order modulation such as M-QAM or M-PSK OFDM.

In 2003, Rodrigues and Darwazeh later proposed in [29] an M-QAM Spectrally Efficient FDM (SEFDM) system where carrier orthogonality is intentionally violated so that the transmitted signal occupies less bandwidth than an equivalent OFDM system. Hence, relevant research started becoming popular and other variants of SEFDM like the High Compact Multicarrier Modulation (HC-MCM) [30] and the Overlapped FDM (OvFDM) [31] were presented. Last but not least, Rusek and Anderson in [32], [33] proved very recently that the detection of such signals in AWGN should not suffer any error penalty as long as the carriers frequency separation is larger than 0.8 of the orthogonal one. Nevertheless, the perfect reconstruction of SEFDM signals constitutes a very hard problem, even in the presence of AWGN only, due to the lack of orthogonality and the resulting interference between the signal sub-bands.

Following the first SEFDM proposal of [29], the work of this thesis aims to fill in the research gap of reliable and computationally reasonable SEFDM detection. Initially, the optimal - in terms of error rate - ML detector is derived and showing that the detection is reduced to a Non Polynomial (NP) hard combinatorial problem. Consequently, other detection methods are investigated. In particular, suboptimal linear techniques like Zero Forcing (ZF), Minimum Mean Squared Error (MMSE) and different flavors of Sphere Decoder (SD), a method that achieves the optimum result with a lower than ML complexity, are studied . In addition, detection algorithms based on convex optimisation, such as Semidefinite Programming (SDP), and combinations of either MMSE or SDP estimates with brute force ML are mathematically mod-

elled and verified through detailed simulation studies.

1.1 Thesis Organisation

This thesis is divided into seven chapters that discuss the background and the detailed modelling as well as design issues of the different detectors studied.

Chapter 2 introduces the reader to the concept of multicarrier communication signals. Starting from the Nyquist fundamental communication principle, the chapter presents the concept and benefits of using orthogonal bases for the signal representation and underlines the weaknesses of typical orthogonal systems in terms of poor frequency domain localisation as well as of reduced spectral efficiency due to the use of pulse guard bands. Consequently, various proposals to improve OFDM spectral efficiency, such as offset QAM-OFDM, Fast OFDM and M-ASK OFDM, are described. Finally, the Mazo limit [34] for faster than Nyquist transmission and recent work on the dual Mazo limit [32], [33] are outlined. These different systems and studies provide the theoretical framework that stimulates the author's research in the area of spectrally efficient multicarrier signals that violate the orthogonality principle.

Chapter 3 describes the main principles of the SEFDM system [29] and highlights the main issues that should be addressed for its practical implementation. First, the problem of the signal generation is discussed and different alternatives are briefly described. In particular, it is demonstrated that the samples of the discrete transmitted SEFDM signal can be generated by the Inverse Fractional Fourier Transform (IFrFT) of the transmitted data symbols. Recent proposals for the generation of such signals based on the typical IDFT transformation are also presented. Besides the transmitter, the receiver structure is also analytically explained. The justification for the use of an orthonormalisation process at the receiver side is given and different methods for the generation of the receiver projections base are examined. Furthermore, the properties of the matrix of the projections between the orthonormal base and

the SEFDM carriers are investigated. Useful simulation based observations are stated with key results being mathematically confirmed. Finally, it is proved that the noise variables at the output of the receiver demodulator are Gaussian independent with zero mean and variance equal to the power spectral density of the channel noise. Following the study of the noise properties, the optimum maximum a posteriori (MAP) detector is derived and it is shown that an optimal SEFDM detection reduces to a combinatorial optimisation problem that is NP hard.

Chapter 4 investigates the appropriateness of linear detectors for the detection of SEFDM signals. Specifically the ZF and MMSE detectors are investigated in detail. In addition, new iterative receivers taking advantage of the properties of the receiver projections matrix, generated either by Gram Schmidt variants or the Löwdin method, are also proposed. The studies of MMSE show that it forms a special case of the regularised solution of the initial ML problem. It is demonstrated by simulation that although all the above detectors offer a fixed polynomial complexity, they suffer severe error penalties. Finally, a combined MMSE-ML method is designed and shown to result in significant improvement of the error rate of MMSE and to approximate the optimal solution for BPSK SEFDM signals but have degraded error behaviour for 4-QAM SEFDM signals.

In Chapter 5 a different approach to the detection problem is proposed. A well known method of dynamic programming called SD is investigated for the purpose of SEFDM detection. The new detection method is based on splitting the overlapped SEFDM sub-bands into a number of consecutive processes that lead to a global optimum. The real and the complex variants of the algorithm are investigated and compared in terms of complexity and error behaviour. Finally, the application of a modified SD based on the regularisation of the ML cost function is proposed in order to cope with the ill conditioning of the projections matrix. It is demonstrated that the regularised SD offers the

optimal solution at a reasonable complexity for medium sized SEFDM signals in high SNR regimes.

Chapter 6 studies SEFDM detection utilising a newly proposed convex optimisation technique known as Semidefinite Programming (SDP). This is based on relaxing the optimal detection least squares problem to a convex SDP. It is demonstrated by simulation that SDP relaxation is superior to both ZF and MMSE. However, the gap between the SDP and the optimal solutions deteriorates with the increase of interference in the system. Consequently, a novel SDP-ML combined detector is proposed. Simulation results show that the new scheme tightens the SDP relaxation gap. Moreover, a pruned SD (PSD) is designed to implement a faster and more efficient SDP-ML concept. PSD achieves a near-optimal detection for medium dimensional SEFDM signals in low SNR regimes.

Finally, Chapter 7 summarises the results of this work, citing the designs and advantages of the investigated and proposed detection techniques. In addition, the possibility of further research is discussed and directions of future work are given.

The mathematical proof of Eq. (5.46) is in Appendix A and brief introductions to lattice theory and convex optimisation are in Appendices B and C, respectively.

1.2 Main Contributions

This work comprises investigations of existing and design of novel detection techniques suitable for non orthogonal SEFDM systems. The main contributions within the course of this research are the following:

- Prove that the Gram Schmidt coefficient matrix of the SEFDM linear statistical model is upper triangular and that its diagonal elements are equal or less than unity;

- Address the problem of the numerical error in the orthonormalisation process and study its effect on the system performance. It has been shown that the Modified GS (MGS) and the Iterative Modified GS (IMGS) are numerically superior to the standard Classic GS method. In addition, it was shown by simulation that IMGS can generate numerically orthonormal bases for a large dimensional SEFDM signal.

- Apply the Löwdin orthonormalisation method, typically used in the Quantun chemistry, to the orthonormalisation of multicarrier communication signals;

- Prove that the noise variables at the receiver correlators outputs are Gaussian independent with zero mean and variance equal to the channel noise power spectral density;

- Derive the optimal MAP detector for the SEFDM system;

- Design a detection method based on a combination of MMSE and ML that offers a good approximation of ML error performance for BPSK modulated FDM signals with a significant reduction in brute force ML complexity;

- Apply SD to the SEFDM signals detection and derivation of its main constraints;

- Design a regularised version of SD that overcomes one of standard SD main limitations, i.e. the projections matrix singularity. This technique has practical advantages in that it is computationally efficient in high SNR regimes;

- Introduce a new a boxed ML technique that combines SDP with brute force ML;

- Design a novel SD that performs much faster than the equivalent SDP-ML detector. The new scheme reduces considerably the computational effort of the regularised SD and would potentially fill the gap of detection for medium size SEFDM signals in low SNR regimes;

The above contributions and results based on this work have resulted in the following publications (listed chronologically):

1. I. Kanaras, A. Chorti, M. Rodrigues, and I. Darwazeh, 'Analysis of Sub-Optimum Detection Techniques for Bandwidth Efficient Multi-Carrier Communication Systems,' in Cranfield Multi-Strand Conference, CMC 2008, May 2008.

2. I. Kanaras, A. Chorti, M. Rodrigues, and I. Darwazeh, 'A combined MMSE-ML detection for a spectrally efficient non orthogonal FDM signal,' 5th International Conference on Broadband Communications, Networks and Systems, 2008. BROADNETS 2008., pp. $421 - 425$, Sept. 2008.

3. I. Kanaras, A. Chorti, M. Rodrigues, and I. Darwazeh, 'An Optimum Detection for a Spectrally Efficient non Orthogonal FDM System,' in 13th International OFDMWorkshop 2008, InOWo'08, Hamburg, Germany. OFDM International Workshop 2008, August 2008.

4. I. Kanaras, A. Chorti, M. Rodrigues, and I. Darwazeh, 'Spectrally Efficient FDM Signals: Bandwidth Gain at the Expense of Receiver Complexity,' in IEEE International Conference on Communications, 2009. ICC '09., June 2009, pp. $1 - 6$.

5. I. Kanaras, A. Chorti, M. Rodrigues, and I. Darwazeh, 'An Overview of Optimal and sub-Optimal Detection Techniques for a Non Orthogonal Spectrally Efficient FDM,' in London Communications Symposium, LCS 2009, September 2009.

6. I. Kanaras, A. Chorti, M. Rodrigues, and I. Darwazeh, 'An Investigation of Semidefinite Programming Detection for a non orthogonal FDM system,' 20th Personal, Indoor and Mobile Radio Communications Conference 2009, IEEE PIMRC'09, Japan, Tokyo, September 2009, pp. $2827 - 2832$.

7. I. Kanaras, A. Chorti, M. Rodrigues, and I. Darwazeh, 'A New Quasi-Optimal Detection Algorithm for a Non Orthogonal Spectrally Efficient FDM,' in 9th International Symposium on Communications and Information Technologies 2009, IEEE ISCIT 2009, Incheon, Korea, September 2009, pp. $460 - 465$.

8. A. Chorti, I. Kanaras, M. Rodrigues, and I. Darwazeh, 'Joint Channel Equalization and Detection of Spectrally Efficient FDM Signals,' in proceedings with the 20th Personal, Indoor and Mobile Radio Communications Conference 2010, IEEE PIMRC'10, Turkey, Istanbul, September 2010.

9. I. Kanaras, A. Chorti, M. Rodrigues, and I. Darwazeh, 'A fast constrained sphere decoder for ill conditioned communication systems,' to appear in IEEE Communications Letters, 2010.

10. R. Clegg, S. Ahmed, I. Kanaras, and I. Darwazeh, 'A practical system for improved efficiency in frequency division multiplexed wireless networks,' submitted to IEEE Transactions on Communications, 2010.

Further on the basis of ideas driven from this work the paper below, proposing the application of overlapped FDM to enhance the physical layer security of communication systems, was recently published.

A. Chorti and I. Kanaras, 'Masked M-QAM OFDM: A Simple Approach for Enhancing the Security of OFDM Systems,' in 20th Personal, Indoor and Mobile Radio Communications Conference 2009, IEEE PIMRC'09, Japan, Tokyo, September 2009, pp. $1682 - 1686$.

Chapter 2

Multicarrier modulation: Basics

This chapter introduces the basic concepts of multicarrier modulation (MCM) systems with the aim of revealing the motivation behind the research work of this thesis. The goal is not to provide a detailed analytical/mathematical description of the different communication systems but to highlight their key merits and demerits from basic communication and signal theory principles.

2.1   MCM representations

In general, in a multicarrier system the transmitted signal may be expressed as

$$s(t) = \sum_{m=-\infty}^{+\infty} \sum_{n=0}^{N-1} S_{m,n} x_{m,n}(t), \qquad (2.1)$$

where $S_{m,n}$ are the information symbols, e.g. M-QAM symbols, and $x_{m,n}(t)$ are a set of functions used for the generation/representation of the samples of the transmitted signal. These functions comprise translated and modulated pulses, i.e. $x_{m,n}(t)$ can be expressed as

$$x_{m,n}(t) = g(t - mT)e^{j2\pi n\Delta ft}. \qquad (2.2)$$

where the time translation step T is equal to the symbol period, the frequency step Δf is equal to the carriers frequency separation, and $g(t)$ is the pulse function.

In orthogonal multicarrier systems like OFDM, $g(t)$ is normally selected to be the rectangular function rect($\cdot$) defined as

$$\text{rect}(\frac{t}{T}) = \begin{cases} 1, & |t| \leq \frac{T}{2} \\ 0, & |t| > \frac{T}{2} \end{cases} . \tag{2.3}$$

In addition, systems are designed in such a way so that Δf and T meet the following orthogonality principle

$$\Delta f = \frac{1}{T}. \tag{2.4}$$

Satisfying (2.4) guarantees the orthogonality between the basis functions, i.e.

$$\int_{-m\frac{T}{2}}^{m\frac{T}{2}} x_{m,n}(t) x_{m,k}^*(t) dt = \begin{cases} 1, & n = k \\ 0, & n \neq k \end{cases} , \tag{2.5}$$

where $(\cdot)^*$ denotes the complex conjugate.

Thanks to orthogonality, the reconstruction of the transmitted data symbols at the receiver side becomes simple. Such reconstruction is accomplished by projecting the signal onto the same orthogonal base used for the signal generation at the transmitter side. This is implemented by a bank of correlators that generate independent samples, $S'_{m,0}, S'_{m,1}, \ldots, S'_{m,N-1}$, of the data symbols corrupted by noise as illustrated in Fig. 2.1.

Nevertheless, in Hilbert spaces [35], [36] - such as the vector space of communication signals - this is not the only option. An alternative could be signal generation by projecting the data symbols onto a non orthogonal base. In that case, a simple signal reconstruction relies upon the respective biorthogonal base [36], [37]. The biorthogonal set comprises of functions that lack mutual orthogonality, yet they are orthogonal over the base of the transmitted signal,
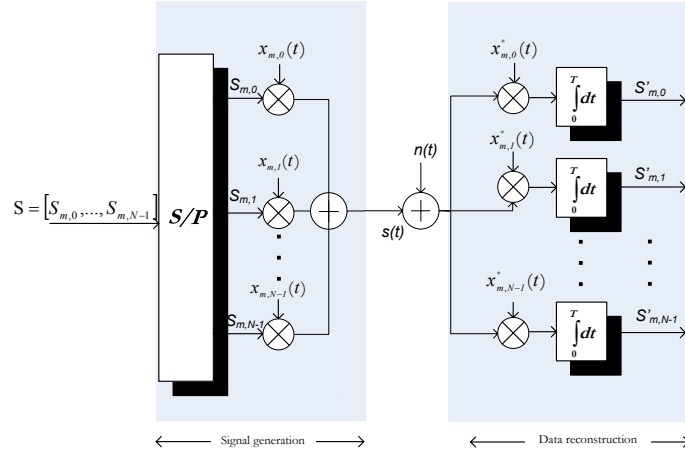
Figure 2.1: Illustration of the OFDM signal generation/reconstruction.

i.e.

$$\int_{-m\frac{T}{2}}^{m\frac{T}{2}} x_{m,n}(t)y_{m,k}^{*}(t)dt = \begin{cases} 1, & n = k \\ 0, & n \neq k \end{cases}, \qquad (2.6)$$

where $x_{m,n}$ and $y_{m,n}$ are the signal generation and its biorthogonal base functions, respectively. Notwithstanding, orthogonal bases demonstrate a major advantage when compared to the biorthogonal ones. They minimise the effect of the additive white noise (AWGN) on the detection error [25].

Apart from the ease of signal reconstruction and the optimal error rate in AWGN channels [24], meeting orthogonality implies that the OFDM signal further satisfies the fundamental communication principle set by Nyquist and described also by Gabor in [38] [1]. Following this, the number N of data symbols that are conveyed independently by a signal of duration T and bandwidth W, must meet the following inequality

$$N \leq WT \qquad (2.7)$$

---

[1]In [38] Gabor shows that a time limited signal can be developed in a fourier series that comprise an infinite number of spectral lines with $\frac{1}{T}$ separation. Consequently, within a band W the signal is represented by a maximum $N = WT$ complex exponentials, i.e. the fourier functions, or $2N$ real cosines and sines that can convey independent, data equal to the number of the fourier coefficients.

In practical OFDM systems, the overall bandwidth approximates $N\Delta f$. Consequently, in OFDM the bandwidth-symbol period product will be

$$WT = (N\Delta f)T = N \tag{2.8}$$

Hence, the OFDM signal contains the maximum number of linear independent functions within a band, or equivalently the OFDM orthogonal base is described as 'complete' [36], meaning that OFDM makes the most out of the signal space in terms of capacity [39].

This, of course, does not mean that OFDM can be used to transmit at faster rates than single carriers schemes. Actually, in OFDM the input high data rate stream is split to N low rate streams, equal to the number of carriers, that are transmitted in parallel (see Fig. 2.2). The main motivation behind this is what
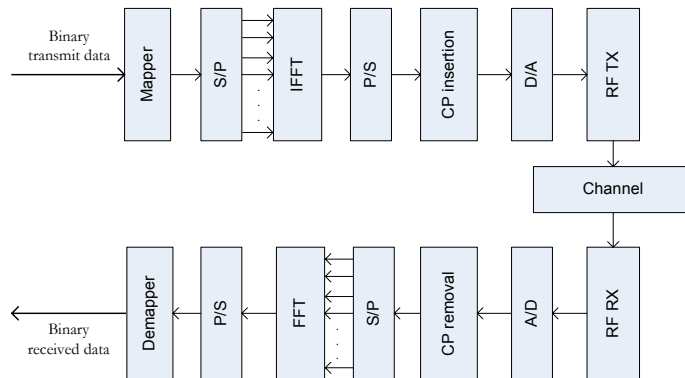
Figure 2.2: Block diagram of an OFDM transceiver.

established OFDM as one of today's most attractive transmission technique in wireless communication systems. That is OFDM's ability to cope easily and efficiently with multipath propagation effects. Specifically, the destructive effects of the latter are intersymbol interference (ISI) and fading that can be either flat or frequency selective depending on the delay spread τ of the channel [40]. ISI is handled by introducing a guard band between consecutive OFDM symbols that is larger than τ. Thus, the delayed samples of a symbol do not fall in the detection window of consecutive symbols, as illustrated in Fig. 2.3. As
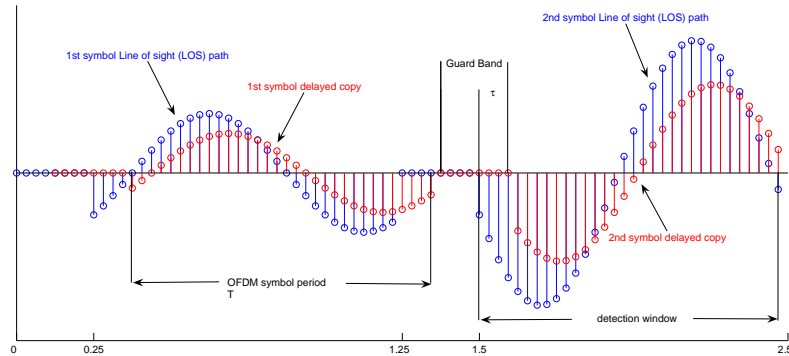
Figure 2.3: OFDM use of guard band against ISI.

far as the frequency selectivity is concerned, due to the parallel transmission of N lower rate streams the OFDM signaling period is large enough so that each OFDM sub-band is smaller than the coherence bandwidth $w \approx \frac{1}{\tau}$ of the channel, i.e. the range of frequencies that undergo the same channel response [40]. Consequently, each of OFDM sub-bands undergoes effectively flat fading that requires much less complex equalisation. In particular, the transformation of the intersymbols guard band into a kind of symbol cyclic repetition, called cyclic prefix and illustrated in Fig. 2.4, allows the diagonalisation of the channel matrix by the IFFT-FFT pair. Hence, an easy equalisation for each OFDM sub-band can be accomplished separately.
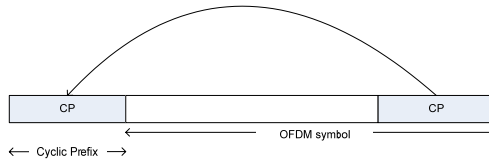
Figure 2.4: Cyclic prefix.

However, the use of orthogonal functions appears to have disadvantages. In particular, OFDM signals are vulnerable to the frequency dispersion mostly met in mobile communication systems. It is well known that the change in the propagation path between mobile transmitters and receivers results in fre-

quency offsets known as Doppler frequencies [40] that would result in the loss of orthogonality. Moreover, because of the infinite spread of each of the signal sub-band [2] - due to the use of the orthogonal pulses - any deviation from orthogonality leads to high intercarrier interference (ICI). A solution to this problem is the good 'localisation' of the multicarrier base functions. This implies that the base functions in eq. (2.2) do not deviate significantly from their time and frequency mean values mT and $n\Delta f$, respectively [39]. A measure of this deviation is given by the base functions second order moments (dispersions),

$$
\begin{aligned}
\Delta T &= \int_{-\infty}^{+\infty} t^2 \, |x(t)|^2 \, dt, \\
\Delta \Phi &= \int_{-\infty}^{+\infty} f^2 \, |X(f)|^2 \, df,
\end{aligned}
\tag{2.9}
$$

where ΔT and $\Delta \Phi$ are the time and frequency dispersions of the base functions, respectively, and $X(f)$ is the signal representation in the frequency domain.

Gabor was the first to investigate the issue of the well localised functions in his famous 1945 'Communications Theory' paper [38]. Extending the Heisenberg uncertainty principle to the communications field, he derived a minimal bound for the product of the time and frequency dispersion. In particular, he showed that

$$
\Delta \Phi \Delta T \geq \frac{1}{2}
\tag{2.10}
$$

In the same paper Gabor also demonstrated that the ideally localised functions is a set generated upon a new prototype function $x_{m,n}(t)$ given by

$$
x_{m,n}(t) = e^{-\alpha^2 (t-mT)^2} e^{j2\pi\Delta ft}.
\tag{2.11}
$$

where α is a constant and the function $e^{-\alpha^2 (t-mT)}$ represents a Gaussian pulse. An example of such a pulse is illustrated in comparison with a rectangular pulse

---

[2]According to the Balian-Low theorem [39], [24], [25], orthogonal systems, using prototype functions $x_{m,n}(t)$ having the same orthogonality properties as the rectangular window, have infinite dispersion either in the time or the frequency domain, suffering ISI or ICI, respectively. Fig. 2.5 illustrates the bad localisation of typical OFDM in frequency due to the frequency representation of the rect pulses by Sinc functions.
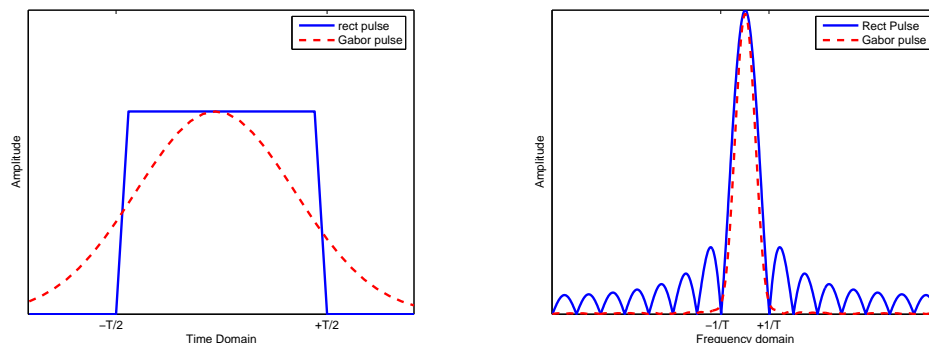
(a) Time domain representation.

(b) Frequency domain representation.

Figure 2.5: Comparisons of rectangular and Gabor pulses in the time and frequency domain, as illustrated in left and right sub-figure, respectively.

in Fig. 2.5. It is apparent that due to the lack of sidelobes the former is much superior than the latter in terms of frequency dispersion.

Although Gabor functions are well localised, they do not constitute an orthogonal base. Notwithstanding, the lack of orthogonality is not always a limitation [24]. For example, in mobile communication channels, where the noise is not the dominant distorting effect, good localisation and not orthogonality is the first priority. In addition, for $\Delta fT > 1$ Gabor functions compose an incomplete set of linear independent functions, i.e. they can convey independent data, yet sub-optimally in terms of signal space utilisation. These observations drove major research in the field of another class of systems that combine efficient pulse shaping, e.g. Hermite pulses, with multicarrier transmission [23], [24], [41].

2.2 Communication Below Orthogonality

Hitherto, we referred to multicarrier systems that are based on signal representations over complete or incomplete bases, i.e. when $\Delta fT \geq 1$. Next

question comes naturally: what happens when the frequency separation between the FDM carriers is squeezed beyond the orthogonality point; and then, what could be the benefits and the disadvantages of such a design. In the literature, it is well known that in this case there can be frames of such functions, i.e. non orthogonal and overcomplete sets [24]. The overcompleteness implies that the frame functions are no longer linear independent [36]. An immediate corollary of this is the lack of invertibility of the matrix of the linear transformation of data symbols S to the multicarrier signal $s(t)$. Note that, in OFDM this is guaranteed by the invertibility of the Fourier transformation matrix. Consequently, at first sight, perfect reconstruction, i.e. detection, of the data symbols, even in the case of an ideal channel is not possible.

Nevertheless, Saltzberg first introduced in [4] the possibility of reducing the carriers frequency separation by 50%, i.e. half OFDM frequency separation. Although the new set is apparently overcomplete in the complex Hilbert space, a more thorough look shows that the system preserves the orthogonality principle, and consequently the completeness, when the signal is examined in the real Hilbert space. In particular, Saltzberg proposed the separate transmission of the real and imaginary parts of the complex M-QAM symbols with an offset of $T/2$ between them. The perfect reconstruction of the half OFDM symbol signals required orthogonality only between the real parts of the base functions. In contrast to OFDM where the prototype function is

$$x_{m,n}(t) = g(t - mT)e^{j2\pi\Delta ft}, \text{ with } \Delta FT = 1 \tag{2.12}$$

in OQAM-OFDM system the base functions are translated as time and frequency copies of the following prototype function,

$$x_{m,n}(t) = g(t - mT)j^{m+n}e^{j2\pi\Delta ft}, \text{ with } \Delta FT = \frac{1}{2}. \tag{2.13}$$

Note that the term j^{m+n} corresponds to $\pi/2$ rotation between adjacent carriers. A block diagram of this system, called Offset QAM-OFDM (OQAM-OFDM) transceiver is illustrated in Fig. 2.6.
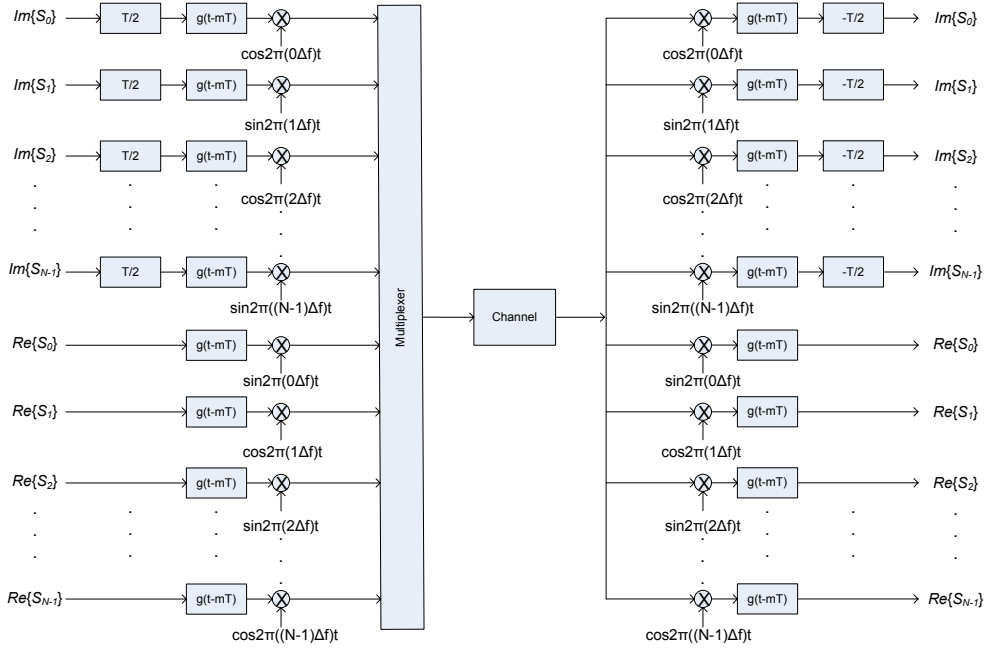
Figure 2.6: OQAM-OFDM transceiver block diagram [26].

The main advantage of the OQAM-OFDM is that it combines the base completeness with the possibility of applying pulses other than rectangular in order to achieve better localisation [42]. Good examples are the use of pulses of optimised time domain characteristics [42] and the use of the Isotropic Orthogonal Transform Algorithm (IOTA) pulses [39] that enable OFDM to get rid of the cyclic prefix overhead. Consequently, OQAM-OFDM appears to be more spectrally efficient than standard OFDM [43].

Further design issues are of interest when operating below orthogonality, mainly the digital implementation for the signal generation and the receiver projections. A solution based on a $N/2$ length IFFT-FFT pair and a bank of filters was first proposed in [26]. Furthermore, a less computationally expensive proposal based on the discrete cosine transform was presented in [28]. All these systems perform similarly to the equivalent (in terms of symbol period) OFDM in case the baseband modulation symbols are real. However, the fact that the advantage of the reduced frequency separation is lost to systems employing

complex modulation compromises the superiority of the proposed schemes in terms of spectral efficiency. The next section outlines recent research on the design of non orthogonal multicarrier systems that are capable of complex modulation to convey more data than OFDM systems occupying equivalent bandwidth.

2.3   Overlapped FDM

In the last decade sporadic research efforts took place for the design of over-complete non orthogonal multicarrier systems. The main motivation was the potential increase of spectral efficiency fitting more signals - than the orthogonality principle allows - in a specific frequency range. Initially, Rodrigues and Darwazeh [29] proposed an FDM system where the orthogonality principle was deliberately violated, i.e. $\Delta fT < 1$. The signal generation at the transmitter side was based on a bank of analogue local oscillators and mixers. Thanks to the overlapping between the sub-bands the overall signal bandwidth was a fraction of the bandwidth of an equivalent OFDM for the same transmission rate. The error performance of the system was evaluated in AWGN. Consequently, the projection of the noise signal onto an orthonormal base was a prerequisite for optimal detection. Since the base of transmission functions were no longer orthogonal, an orthogonalisation method was used in order to generate an orthonormal base suitable for the receiver projections. In addition, the receiver correlations were based on a bank of analogue filters that output a set of statistics for detection purposes. For the projections base was different from the signal generation base, a simple-OFDM likewise signal detection was not possible and required exhaustive search over the entire set of possible transmitted FDM symbols. However, the complexity of such a solution increases exponentially over the number of signal carriers and the constellation cardinality. In [29] ZF and Genetic Algorithms (GA) were investigated to circumvent the detection complexity. Both these solutions were proved inefficient in terms

of error performance, leaving a gap for further research.

Apart from the detection issue [29] revealed other design challenges such as finding a digital signal generation mechanism that could get rid off the bulky structure of an analogue transmitter. Hamamura et al proposed in [30] a solution based on the use of typical IFFT-FFT pair for the generation and projection of the signal at the transmitter and receiver side, respectively. In particular, following the principle of [26], the generation of the OFDM symbol by discarding some of the output samples of a longer IFFT was introduced. This is equivalent to the truncation by a rectangular window in the time domain that results into the extension of each of the sub-band. In addition, the requirement of an orthonormal base for the projections was met by the use of the FFT and a detector based on the calculation of the Euclidean distance between the received vector and all the possible results/hypotheses was used as in [29]. Notwithstanding, the detector proposed by Hamamura also suffered a very high complexity.

Further to the previous efforts [44] and [45] introduce systems termed Overlapped Time Division Multiplexing (OvTDM) and Overlapped FDM (OvFDM) that overlap symbols or channels in time or frequency domain, respectively. The signal generation and demodulation is based on the use of typical IFFT-FFT pair [31]. Nevertheless, detection was proved to be the main challenge and results were presented for small dimensional signals, i.e. $N \leq 12$, [46], [47], [48]. It is useful though to highlight an intriguing observation reported in [45]. The authors mention that although independent demodulation is not possible due to the overlapping between consecutive pulses in OvTDM systems - the same applies for overlapped FDM sub-bands - joint detection would be tangible as long as there is one-to-one correspondence between the symbols sequence and the overall transmitted waveform. Fig. 2.7 illustrates such an example. Two overlapped binary pulses A and B are transmitted. Because of their unique shapes their overlapping can lead to only 4 discrete waveforms corresponding

one-to-one to the 4 different combinations of A and B, i.e. $A + B$, $A - B$, $-A - B$ and $-A + B$. Consequently, comparing the received waveform with all 4 possible transmitted waveforms achieves correct detection.
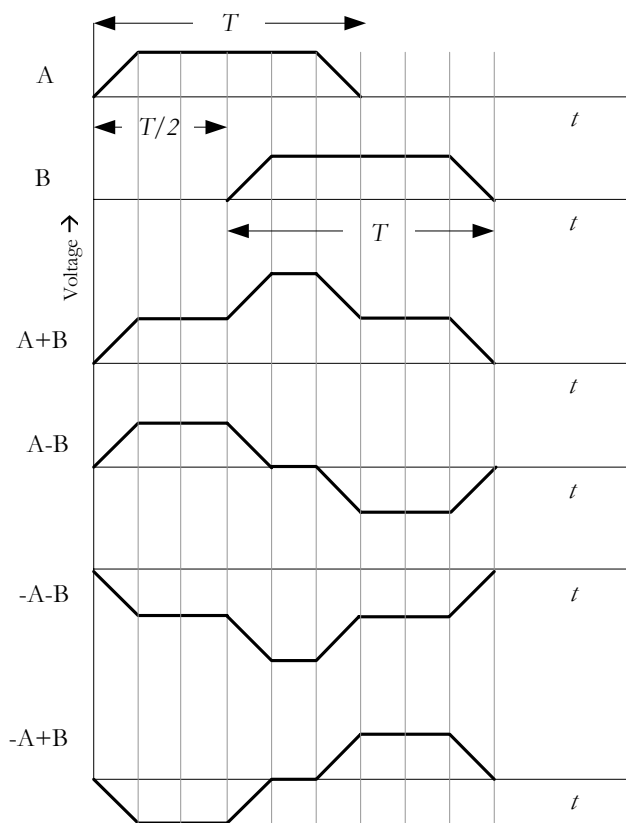
Figure 2.7: Principle of overlapped multiplexing after [45].

2.4 Mazo limit

Most interestingly, Rusek and Anderson recently dealt with the problem of deriving the minimum Euclidean distance between transmitted BPSK or 4-QAM symbols that overlap in time and/or frequency [32], [33]. They were inspired by the 1975 work of Mazo, at Bell Labs, for systems that can transmit faster than the Nyquist signaling criterion [34]. Mazo proved that the transmission bandwidth of Sinc pulses can be reduced to 80% of the Nyquist signaling rate, i.e.

the transmission is by 25% faster, with no Euclidean distance loss. Although the shorter transmission time results in overlapping between consecutive pulses, this result implies that ISI should degrade the detection error rate in AWGN.

Rusek and Anderson further proved that the frequency separation between FDM sub-bands could also be reduced down to a close to Mazo bound without noticeable degradation in the error performance. Notwithstanding, the detection implementation for such systems relies on very complex techniques since the transmitted symbols cannot be detected independently due to the system inherent ISI and/or ICI [34], [49].

2.5 Conclusions

In this chapter, a short review of multicarrier communications basics was given. It was shown that OFDM demonstrates significant advantages like simple signal reconstruction, detection optimality in AWGN and ease of handling of time dispersive channels. But above all, OFDM makes the most of the available signal bandwidth in terms of transmitting the maximum possible number of independent data. Still, sporadic efforts have taken place in order to improve OFDM spectral efficiency. Initially, half symbol OFDM systems managed to transmit one-dimensional data symbols at rates twice as fast as those of OFDM systems. Nevertheless, they did not offer bandwidth advantage when compared to standard OFDM conveying 2-dimensional data apart from discarding the cyclic prefix overhead needed by OFDM to cope with ISI and frequency selective fading. Then, non orthogonal overlapped in time and/or frequency systems were proposed to reduce the bandwidth of an equivalent to OFDM transmitted signal. The deliberate lack of orthogonality rendered an independent detection of the transmitted symbols impossible. However, detection could be possible as long as there is a one by one correspondence between the information symbols sequence and the overall transmitted waveform. In addition, recent work has shown that as long as overlapping does not exceed some specific bounds,

the Euclidean distance between the transmitted waveforms does not shrink and consequently the detection error rate should not degrade. Yet, a feasible implementation of detection is an open research area. Motivated by these observations and results, this thesis aims to explore the limits of a computationally practical detection. In the following chapters, various detection techniques are studied, designed and tested using appropriate mathematical and numerical simulation modelling. The next chapter however is specifically dedicated to studies of the SEFDM signals and systems for which the detection is the focus of this thesis.

Chapter 3

The SEFDM system

3.1 Introduction

The idea of squeezing the frequency separation between the OFDM carriers in order to improve OFDM spectral efficiency is not something new. Saltzberg was the first to propose offset QAM/OFDM [4] that offered increased spectral efficiency of a conventional OFDM by the cyclic prefix overhead [43]. Later, Rodrigues and Darwazeh in [27] and Xiong in [28] proposed the idea of combining 1-dimensional modulation schemes with half symbol period of OFDM systems and introduced the use of typical discrete fourier and fast-cosine transformations, respectively, for their implementations. Notwithstanding, both schemes did not offer the benefits of M-dimensional modulated OFDM systems. Since then, various efforts have come to the light. High compaction multicarrier modulation (HC-MCM) [30], [50], overlapped FDM (OvFDM) [31] and more recently faster than Nyquist (FTN) signaling [33], [49], [51] are the most prominent proposals of spectrally efficient multicarrier systems.

This thesis deals specifically with the study of the first attempt for a non orthogonal spectrally efficient FDM (SEFDM) as proposed by Rodrigues and Darwazeh in [29]. Such system has an advantage in its use of a demodulation architecture that facilitates the detection process. This is due to the triangular shape of the projections matrix that could either assist the implementation

of iterative receivers or simplify techniques like SDs by discarding relevant decomposition steps.

In this chapter, firstly, a general description of the SEFDM concept is given and its spectral efficiency gains are demonstrated. Following, the main SEFDM implementation challenges are pointed out. In particular, three main areas of potential research are identified: the design of a digital transmitter, the design of a demodulator able to extract sufficient statistics for the transmitted SEFDM waveform and finally, the design of a reliable and computationally cheap detector.

Regarding the transmitter, the use of an inverse fractional fourier transform (IFrFT) is introduced. In addition, recent proposals based on the conventional inverse discrete fourier transform (IDFT) are presented. As far as the demodulator is concerned, it is shown that the Gram Schmidt (GS) orthonormalisation method proposed in [29] is numerically stable only for a small number of carriers. Consequently, other orthonormalisation techniques like modified GS (MGS), iterative MGS (IMGS) and Löwdin method are described and their use for SEFDM is studied and compared in terms of orthonormalisation errors. Additionally, various properties of the matrix of the projections of the SEFDM carriers on the demodulator orthonormal base are derived and discussed. Relevant proofs are also given either based on mathematical calculations or on numerical modelling results.

Then, starting from the noise properties at the demodulator output, it is shown that the optimal detector for the SEFDM system is reduced to a combinatorial optimisation problem. An initial solver is modelled following an exhaustive enumeration method and some preliminary bit error rate (BER) results are demonstrated. Finally, all three main parts of the SEFDM system are discussed in terms of computational effort in order to identify potential bottlenecks for the SEFDM performance. The mathematical developments of this chapter serve as a necessary introduction to the following Chapters (4, 5

and 6) that present different detection techniques of varying complexity and performance.

3.2 SEFDM system general description

The original SEFDM transceiver is described in [29]. A high data rate input stream is split into N parallel low data rate streams. The latter modulate, according to a specific modulation scheme of level M, N SEFDM subcarriers $f_{\alpha,n}(t)$, $n = 0, \ldots, N-1$, whose frequency separation Δf is only a fraction α of the inverse of the SEFDM symbol period T, i.e.

$$\Delta f = \frac{\alpha}{T}, \text{ with } \alpha < 1. \tag{3.1}$$

Thus, the required bandwidth is reduced by a factor $1 - \alpha$, at the expense of the loss of orthogonality between the carriers. The transmitted signal, in an SEFDM symbol period, is given by

$$s(t) = \frac{1}{\sqrt{T}} \sum_{n=0}^{N-1} S_n f_{\alpha,n}(t) = \frac{1}{\sqrt{T}} \sum_{n=0}^{N-1} S_n e^{j2\pi n \Delta f t}, \tag{3.2}$$

where S_n represents the nth modulation symbol. Thanks to the squeeze of the carriers frequency separation SEFDM optimally offers a spectral efficiency gain of $\frac{1}{\alpha}$, approximately. Further details on the SEFDM spectral efficiency issue will be given in the next section.

For proof of concept and assuming the only impairment introduced by the communication channel is Additive White Gaussian Noise (AWGN) $n(t)$, the received signal $r(t)$ can be expressed as

$$r(t) = s(t) + n(t). \tag{3.3}$$

The proposed receiver consists conceptually of two stages. The first stage uses a bank of N correlators to extract N sufficient [1] statistics from the received signal. The second stage uses a detector. Fig. 3.1 depicts the SEFDM transceiver.

---

[1]Roughly, a statistic is sufficient when it carries all of the useful information about the parameter to estimate [35].
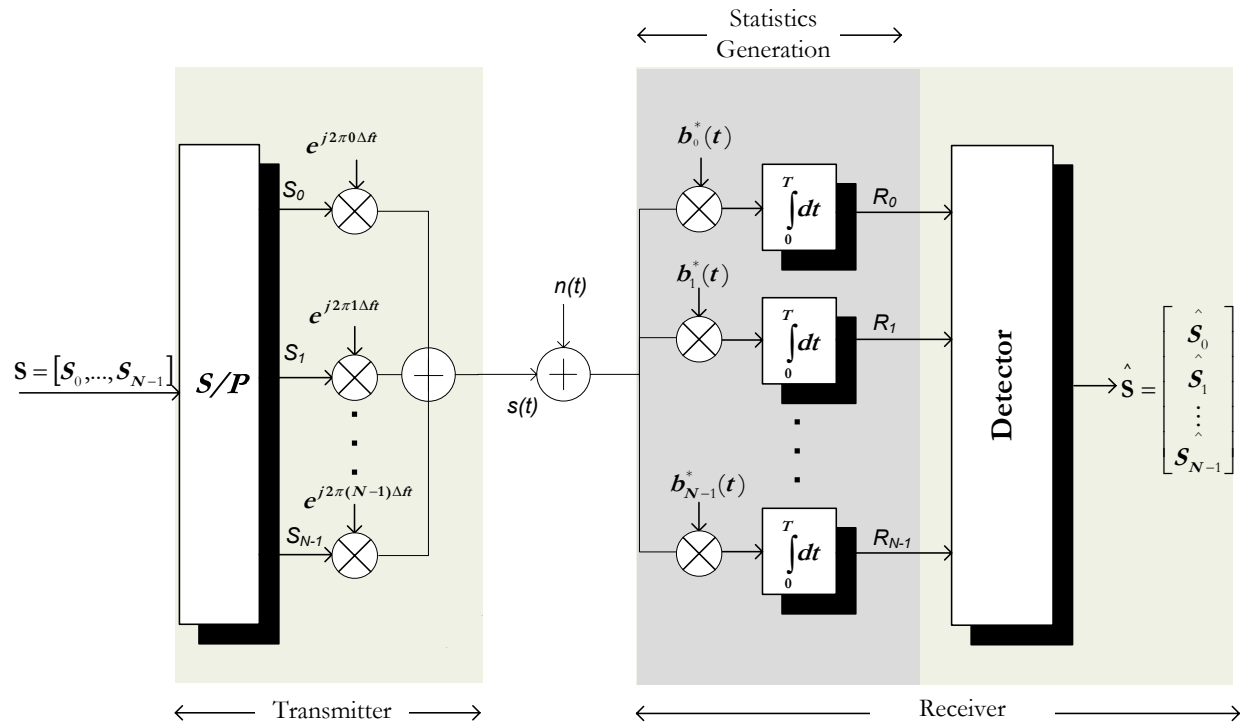
Figure 3.1: Conceptual GS SEFDM System Architecture [29].

The particular choice of the correlation functions at the receiver outer stage is driven by two important requirements: (i) the correlation functions should be orthonormal in order to prevent noise coloring, and (ii) that detection of the SEFDM signal must be computationally feasible. Both requirements can be met by generating an orthonormal base that spans the SEFDM signal space using the Gram Schmidt (GS) orthonormalisation method [52], [53]. However, it is well established in the literature [53], [54] that the classic GS algorithm is vulnerable to numerical errors and even for small values of N the generated base functions are not orthogonal. For example, in the case of SEFDM carriers, the classic GS base functions are not orthogonal for $N > 16$ when $\alpha = 0.75$. Consequently, we employ instead the computationally stable Iterative Modified Gram Schmidt (IMGS) [55] for the generation of the orthonormal base (see section 3.5). Denoting $b_k(t)$ the kth IMGS orthonormal base, the output of the kth receiver correlator is given by

$$R_k = \int_0^T r(t)b_k^*(t)dt, \ k = 0, \ldots, N-1. \tag{3.4}$$

The equivalent system linear statistical model can be described in matrix representation [2] as follows

$$\mathbf{R} = \mathbf{MS} + \mathbf{N}, \tag{3.5}$$

where $\mathbf{R} = [R_i]$ is the vector of the N observation statistics, $\mathbf{S} = [S_i]$ is the vector of the N transmitted symbols, $\mathbf{M} = [M_{ij}]$ is the $N \times N$ covariance matrix of the SEFDM carriers and the orthonormal base, and $\mathbf{N} = [N_i]$ is a vector containing N independent Gaussian noise time samples of zero mean and covariance matrix $\sigma^2 \mathbf{I}$ ($\mathbf{I}$ being an identity matrix of $N \times N$ dimension and σ^2 is the noise variance). The elements of $\mathbf{R}$ and $\mathbf{M}$ are given by

$$R_i = \int_0^T r(t)b_i^*(t)dt, \ i = 0, \ldots, N-1, \tag{3.6}$$

$$M_{ij} = \int_0^T f_{a,i}(t)b_j^*(t)dt, \ i,j = 0, \ldots, N-1. \tag{3.7}$$

[2]Throughout this thesis standard matrix notation is used; where a symbol appears in bold, it refers to a matrix of any dimension including a $(1 \times N)$ dimension which is a vector.

3.3 SEFDM spectral efficiency

The time domain SEFDM signal is given by

$$s(t) = \frac{1}{\sqrt{T}} \sum_{k=-\infty}^{+\infty} \sum_{n=0}^{N-1} S_{k,n} g(t - kT) e^{\frac{j2\pi\alpha n t}{T}}, \tag{3.8}$$

where $g(t - kT)$ are taken as rectangular (with no loss of generality) pulses of duration T. Consequently, $g(t - kT) = \text{rect}(\frac{t}{T} - k)$, with $\text{rect}(\cdot)$ denoting the rectangular function, defined as

$$\text{rect}(\frac{t}{T}) = \begin{cases} 1 & -\frac{T}{2} \leq t \leq \frac{T}{2} \\ 0 & \text{elsewhere} \end{cases}. \tag{3.9}$$

The frequency domain $S_k(f)$ representation of the kth SEFDM symbol is

$$\begin{aligned} S_k(f) &= \mathcal{F}\{\frac{1}{\sqrt{T}} \sum_{n=0}^{N-1} S_{k,n} \text{rect}(\frac{t}{T} - k) e^{n\frac{j2\pi\alpha t}{T}}\} \\ &= \frac{1}{\sqrt{T}} \sum_{n=0}^{N-1} \mathcal{F}\{S_{k,n} \text{rect}(\frac{t}{T} - k) e^{n\frac{j2\pi\alpha t}{T}}\} \\ &= \frac{1}{\sqrt{T}} \sum_{n=0}^{N-1} S_{k,n} \mathcal{F}\{\text{rect}(\frac{t}{T} - k)\} \otimes \mathcal{F}\{1 \times e^{n\frac{j2\pi\alpha t}{T}}\}, \end{aligned} \tag{3.10}$$

where $\mathcal{F}\{\cdot\}$ and $\otimes$ denote the fourier transformation and the convolution, respectively. Applying basic fourier properties Eq. (3.10) reduces to

$$S_k(f) = \sqrt{T} \sum_{n=0}^{N-1} S_{k,n} \text{Sinc}(fT) e^{j2\pi fkT} \otimes \delta(f - n\frac{\alpha}{T}), \tag{3.11}$$

where $\delta(\cdot)$ denotes the Dirac function. Finally,

$$S_k(f) = \sqrt{T} \sum_{n=0}^{N-1} S_{k,n} \text{Sinc}\left((f - n\frac{\alpha}{T})T\right) e^{j2\pi(f-n\frac{\alpha}{T})kT}. \tag{3.12}$$

It is apparent that the spectrum of the SEFDM symbol comprises a series of Sinc functions of $\frac{1}{T}$ width centrally located at $n\frac{\alpha}{T}$ frequencies. Fig. 3.2 illustrates an SEFDM symbol in the frequency domain for $\alpha = 1$ and 0.5, corresponding to OFDM and FOFDM, respectively. It is clear that in OFDM, the center of each Sinc function coincides with the zero crossings of all other

(a) OFDM.

(b) SEFDM for $\alpha = 0.5$.
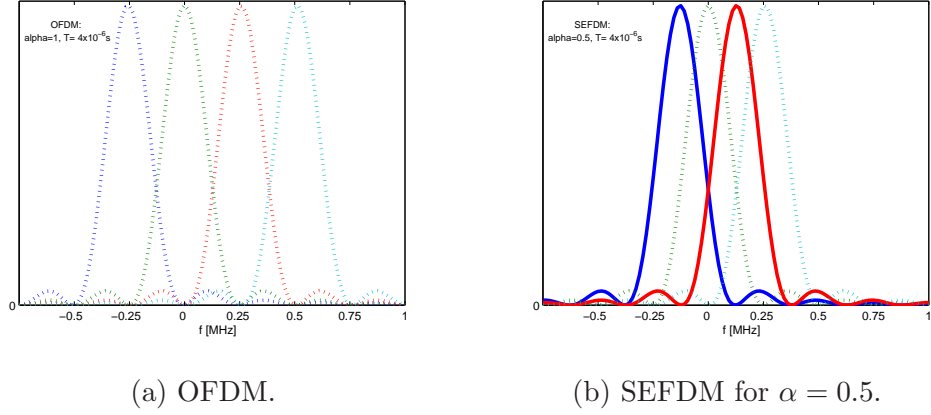
Figure 3.2: Frequency domain representation of OFDM and SEFDM with $N = 4$ subcarriers, in the right and left sub-figure, respectively. T was set to 4×10^{-6}s.

functions. Notwithstanding, this is not the case in SEFDM scenarios with $\alpha < 1$.

The overall bandwidth B of the SEFDM signal is roughly given by

$$B = (N-1)\frac{\alpha}{T} + 2\frac{1}{T}. \tag{3.13}$$

The SEFDM spectral efficiency β is defined as the ratio of the data bit rate $N\frac{\log_2 M}{T}$ over the signal bandwidth B. Hence, β is

$$\beta = \frac{N\frac{\log_2 M}{T}}{(N-1)\frac{\alpha}{T} + 2\frac{1}{T}} = \frac{N\log_2 M}{(N-1)\alpha + 2}. \tag{3.14}$$

It is clear that for large N

$$\beta \approx \frac{\log_2 M}{\alpha}. \tag{3.15}$$

To confirm the above result, the noise equivalent bandwidth B_N of SEFDM was measured by simulation for $N = \{32, 256\}$ and $\alpha = 0.5 \rightarrow 1$. Its calculation was performed according to

$$B_N = \frac{\int_{-\infty}^{+\infty} S^2(f)df}{\max |S^2(f)|}, \tag{3.16}$$

where $S(f)$ is the signal representation in the signal domain.

Fig. 3.3 shows the Power Spectrum Density $G(f)$ of the SEFDM signal for different values of the factor $\alpha = \Delta fT$. $G(f)$ is normalised over $\max\{|G(f)|^2\}$, and calculated according to the following [56]

$$G(f) = \frac{|S(f)|^2}{\max\{|S(f)^2|\}},\tag{3.17}$$

Fig. 3.4 demonstrates the SEFDM spectral gain calculated in two ways: either using Eq. (3.15) or by simulation as the ratio of the measured B_N over the bandwidth of the equivalent OFDM signal, i.e. B_N measured for $\alpha = 1$.
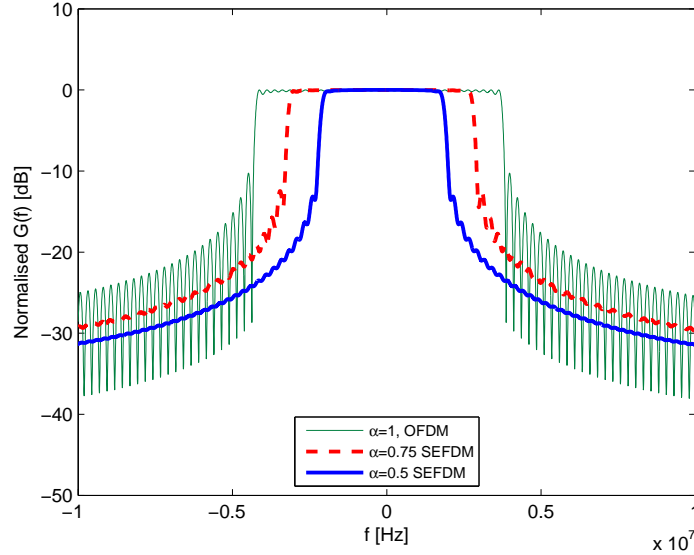
Figure 3.3: SEFDM $G(f)$ for $\alpha \in \{0.5, 0.75, 1\}$ and $N = 32$.

It is notable that simulation measurements coincide with the closed formula calculations of (3.15) for large $N = 256$ confirming that as the normalised carriers frequency separation α decreases, the noise equivalent bandwidth decreases and the SEFDM spectral gain increases proportionally.

Finally, Fig. 3.5 demonstrates spectral efficiency of BPSK and 4-QAM SEFDM schemes, versus the E_b/N_0 required to achieve a BER of 6×10^{-3}. It is assumed that an optimal detection for such systems is tangible and that
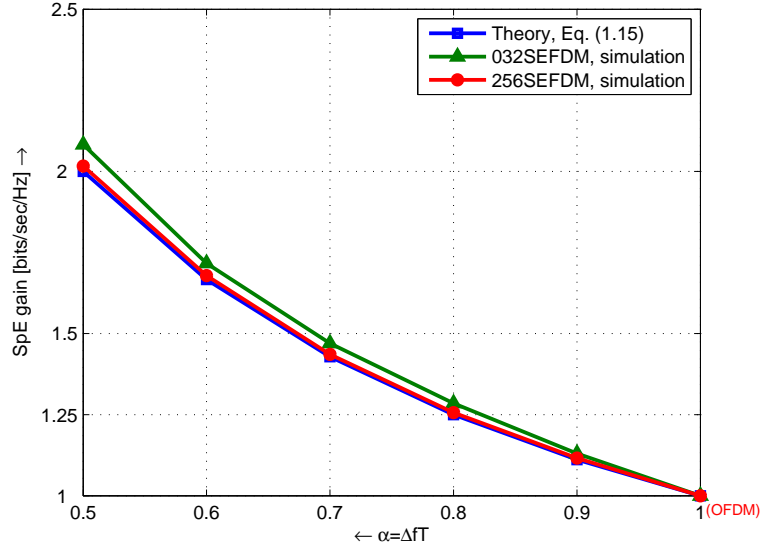
Figure 3.4: SEFDM spectral efficiency gain for $\alpha = \{1 \to 0.5\}$ and $N = \{32, 256\}$.

the error rate does not degrade due to the sub-bands overlapping for (BPSK, $\alpha \geq 0.401$) and (4-QAM, $\alpha \geq 0.802$) settings, in line with assumptions reported in [34], [32], [33]. The spectral efficiency of such SEFDM is compared to the spectral efficiency of a symbol rate/equivalent OFDM. The Shannon limit for the normalised capacity of a band-limited AWGN channel [52] serves as an upper bound. It is clear that 4-QAM SEFDM is superior as opposed to OFDM for $\alpha \geq 0.8$ (that achieves a spectral efficiency of 2.5) and closer to Shannon limit. Notwithstanding, a further decrease in α value does not necessarily offer a spectral efficiency benefit though the SEFDM signal occupies a smaller bandwidth than OFDM. This is due to the power penalty that should be paid because of the deterioration in the error rate of the SEFDM detection caused by the increase of the system inherent interference.
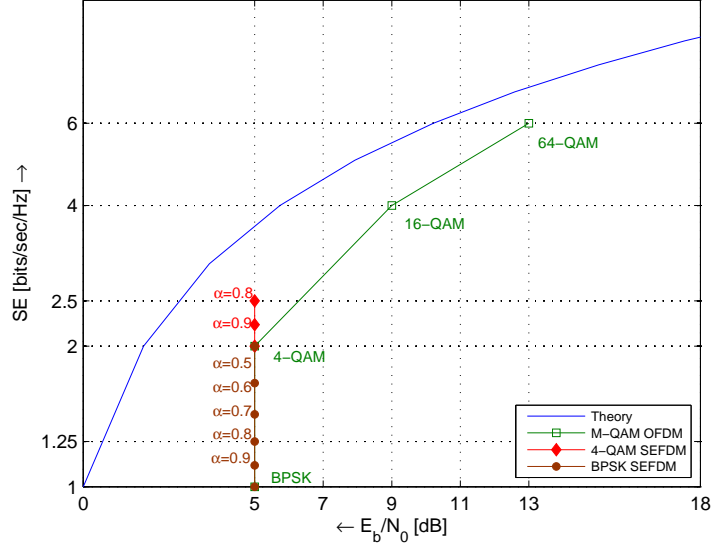
Figure 3.5: SEFDM spectral efficiency and the Shannon channel capacity bound.

3.4 SEFDM transmitter implementations

The implementation of an analogue SEFDM transmitter, depicted in Fig. 3.1, is overly complex when the number of the SEFDM carriers N becomes large. Consequently, alternative implementation methods should be investigated. Although this thesis focuses on the receiver design and specifically in the detector part, for the completeness the following paragraphs briefly present potential solutions for a feasible SEFDM transmitter. These can be classified in two main categories: the fractional fourier transform (FrFT) based and the discrete fourier transform (DFT) based transmitters.

3.4.1 Fractional Fourier based transmitter

In analogy to a classic OFDM transmitter that uses an Inverse Fast Fourier Transform (IFFT), an Inverse FrFT (IFrFT) algorithm can be employed for the generation of the SEFDM signal. The IFrFT is described in detail in [57].

The kth output of the IFrFT can be expressed as

$$x_k(\alpha) = \sum_{n=0}^{N-1} S_n e^{2\pi jk\alpha n/N}, \qquad (3.18)$$

so that the Inverse DFT (IDFT) is the IFrFT for $\alpha = 1$.

The IFrFT matrix is expressed as

$$\mathbf{F}_\alpha^{-1} = \begin{bmatrix} 1 & 1 & \cdots & 1 \\ 1 & \zeta^\alpha & \cdots & \zeta^{\alpha(N-1)} \\ \vdots & \vdots & \ddots & \vdots \\ 1 & \zeta^{\alpha(N-1)} & \cdots & \zeta^{\alpha(N-1)(N-1)} \end{bmatrix}, \qquad (3.19)$$

with $\zeta = e^{2\pi j/N}$. From the above it is clear that the time domain SEFDM samples within the signaling period T can be derived according to $\mathbf{F}_\alpha^{-1}\mathbf{S}$.

The attractiveness of the FrFT is the existence of efficient fast algorithms [58], [57] for its computation that require only $20N\log_2 N$ flops . As opposed to Radix-2 algorithms used in the standard FFT implementations, this implies an increase in computational cost by 4 times. Notwithstanding, the order of complexity of fast FrFT is still $N\log N$ and independent of α.

3.4.2 DFT based transmitter

For the first time, IDFT was used for the generation of non orthogonal FDM signals for an OQAM OFDM system in [26]. The author proposed the system implementation through a half OFDM length, i.e. $\frac{N}{2}$ IFDT-DFT pair. In addition, to reduce further complexity the IDFT-DFT was replaced by their respective IFFT-FFT implementations. A similar concept was adopted later in fast OFDM (FOFDM) systems [27], i.e. M-PAM SEFDM with $\alpha = 0.5$. Noticing that for real inputs IFFT generates symmetric outputs, half of the samples of the FOFDM symbol were discarded before transmission. The truncation of the IFFT output resulted in a transmitted signal occupying a reduced bandwidth. The same approach was also adopted in [30] and [31] for the transmission of SEFDM systems with arbitrary α.

More recently Ahmed and Darwazeh [59], [60] presented new variations of IDFT implementations for the generation of SEFDM signals where α is equal to a rational number, i.e. $\alpha = \frac{b}{c}$ with $b < c$ and both being integer prime numbers. It is notable that in this case according to [57], FrFT can be easily reduced to a larger dimensional DFT. In particular, the inverse FrFT (IFrFT) for an N carriers SEFDM system is given by

$$x_k\left(\frac{b}{c}\right) = \sum_{n=0}^{N-1} S_n e^{j2\pi\frac{kn}{N}\frac{b}{c}}, \text{ with } k = 0, \ldots, N-1. \tag{3.20}$$

Setting $N' = cN$ and adding $cN - N$ zeros in the previous sum, Eq. (3.20) reduces to

$$x_k\left(\frac{b}{c}\right) = \sum_{n=0}^{cN-1} S_{(np)} e^{j2\pi\frac{k(np)b}{N'}}, \text{ with } k = 0, \ldots, N-1, \tag{3.21}$$

where p is an integer chosen so that $(pb)\mathrm{mod}(N') = 1$, with $\{\cdot\}\mathrm{mod}\{\cdot\}$ denoting the modulo operator [3]. This is equivalent to $\frac{pb}{N'} = \rho + \frac{1}{N'}$, where ρ is an integer. Consequently, Eq. (3.21) is reduced to

$$x_k\left(\frac{b}{c}\right) = \sum_{n=0}^{cN-1} S_{(np)} e^{j2\pi kn\frac{pb}{N'}} = \sum_{n=0}^{cN-1} S_{(np)} e^{j2\pi kn(\rho+\frac{1}{N'})}, \tag{3.22}$$

Finally,

$$x_k\left(\frac{b}{c}\right) = \sum_{n=0}^{cN-1} S_{(np)} \underbrace{e^{j2\pi kn\rho}}_{1} e^{j2\pi\frac{kn}{N'}} = \sum_{n=0}^{cN-1} S_{(np)} e^{j2\pi\frac{kn}{cN}}. \tag{3.23}$$

An obvious choice for p is $p = \frac{1}{b}$ [60] so that $(pb)\mathrm{mod}(cN) = 1$. Then, the RHS of Eq. (3.23) is equivalent to an IDFT of size cN where the $np = \left(\frac{n}{b}\right)^{th}$, $n = 0, b, 2b, \ldots, (N-1)b$, inputs are the transmit symbols and the remaining inputs are zero padded. This IDFT can be computed through a Radix-2 IFFT using $5cN \log Cn$ floating operations. Furthermore, because only the first N outputs of the IDFT are required, the computational cost of the respective IFFT is finally reduced to $5cNlogN$ operations, i.e. c times more than an IFFT implementation of an equal sized OFDM transmitter.

---

[3]The $a\,\mathrm{mod}\,b$ operation finds the remainder of the division of a with b

A numerical example could be the following: consider an SEFDM system with $N = 16$ carriers and $\alpha = 5/6$ normalised frequency separation. The transmitted SEFDM signal can be generated using a $N' = 6 \times 16 = 96$ length IDFT, inserting the transmit data symbols at the $0, 6, 12, \ldots, 90$ indexed inputs and zero padding the rest. Then, the output of the IDFT is truncated so that only the first $N = 16$ samples are transmitted.

Recent work at UCL [60] also introduced two modifications of the above scenario. First, it was shown that an N carrier SEFDM signal can be generated using a larger $N\alpha = cN\frac{1}{b}$ IDFT under the assumption that $\frac{N}{\alpha}$ is an integer number. The main advantage with respect to the previous concept is that the IDFT used is b times smaller which results in a reduced complexity. Secondly, the use of multiple smaller size IDFTs combined with some post processing is proposed resulting in further reduction of complexity.

Fig. 3.6 illustrate possible SEFDM transmitters based on single IDFTs of either cN or $\frac{N}{\alpha} = \frac{cN}{b}$ length.

3.5 SEFDM Demodulator

As mentioned in section 3.2, the noise whiteness at the demodulator output requires the projection of the received signal onto an orthonormal base that spans the same vector space as the transmit SEFDM carriers. In the introduction of the SEFDM model [29], the Classical Gram Schmidt (CGS) method was proposed for the generation of the receiver base. Although CGS appears to have a very simple structure, it performs inefficiently even for a medium number of SEFDM carriers due to its large rounding error. In order to handle this effect, other techniques like the Modified Gram Schmidt (MGS) and its iterative variance (IMGS) are investigated in this work. Both promise a higher orthonormalisation accuracy [53], [54].

Alternatively to GS variants, the application of the symmetric Löwdin orthonormalisation is also investigated. This method exhibits interesting
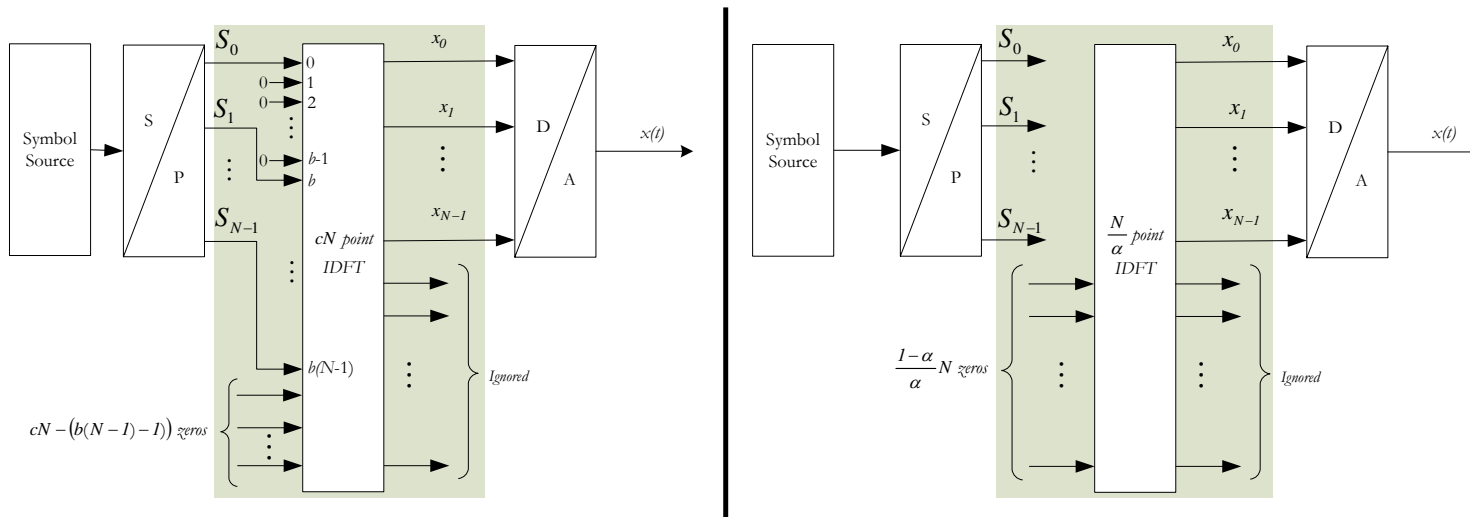
Figure 3.6: Potential IDFT based SEFDM transmitters [59] and [60].

properties like the greater resemblance in the least square sense between the orthonormal functions and the transmit SEFDM carriers. The next sections describe the development and use of the different orthonormalisation techniques for the generation of the demodulator base, and provide a short comparison of these techniques in terms of orthonormalisation error.

3.5.1 Classic Gram Schmidt (CGS) orthonormalisation

Consider a set of N linear independent but non orthogonal vectors $[v_1, v_2, ..., v_N]$ that constitute a base of a complex vector space. CGS generates an orthonormal base of N vectors $[u_1, u_2, ..., u_N]$ following an iterative process: first, the seed vector u_1 of the new base is derived as

$$u_1 = \frac{v_1}{\|v_1\|_2},\tag{3.24}$$

where $\|\cdot\|_2$ denotes here the Euclidean norm. For SEFDM, this is equivalent to the square root of the energy of the respective SEFDM base function [52].

Next, u_2 is calculated by subtracting from v_2 its projection onto u_1 and then normalising over the norm of the resulting vector as

$$u_2^{'} = v_2 - \langle v_2, u_1 \rangle u_1,$$
$$u_2 = \frac{u_2^{'}}{\|u_2^{'}\|_2}.\tag{3.25}$$

The same process is then reiterated until all N orthonormal vectors are generated. The Nth vector is given by

$$u_N^{'} = v_N - \sum_{i=1}^{N-1} \langle v_N, u_i \rangle u_i,$$
$$u_N = \frac{u_N^{'}}{\|u_N^{'}\|_2}.\tag{3.26}$$

Table 3.1 provides the algorithmic steps of the CGS as used in this thesis for the generation of the SEFDM receiver orthonormal base.

It must be stated that in CGS the number of the generated non zero orthonormal vectors is equal to the number of the linear independent vectors of

60

Orthonormalisation algorithm I: CGS	
01: $v[1:N] \leftarrow g[1:N]$	initialisation step
02: for m from 1 to N	
03: $u_m \leftarrow \frac{1}{\sqrt{\xi_m}} \left[v_m - \sum_{i=1}^{m-1} \langle v_m, u_i \rangle \right]$	orthonormalise m^{th} vector
04: end m loop	
05: $b[1:N] \leftarrow u[1:N]$	set SEFDM base

Table 3.1: CGS Orthonormalisation Algorithm.

the initial set [52]. In addition, the CGS orthonormal base is not unique since its outcome depends on the selection of the first vector v_1. Therefore, for each permutation of the vectors of the initial base, CGS results into a different orthonormal base. In any case, the produced set of vectors shares the same span with the initial base. A proof is derived below. Following [53] the span of the orthonormal vectors $u_1, u_2, \ldots, u_N$ is the set of all their linear combinations. Consequently, it is given by

$$\text{span}\{u_1, u_2, ..., u_n\} = \left\{ \sum_{i=1}^{N} \kappa_i u_i \, : \, \kappa_i \in C \right\}, \qquad (3.27)$$

where C is the set of complex numbers. Thanks to GS orthonormalisation each of u_i is deduced to a linear combination of the vectors of the initial base. Hence,

$$u_i = \left\{ \sum_{j=1}^{N} \lambda_j v_j \, : \, \lambda_j \in C \right\}. \qquad (3.28)$$

From Eqs (3.27) and (3.28), the orthonormal base span is given by

$$\text{span}\{u_1, u_2, ..., u_n\} = \left\{ \sum_{i=1}^{N} \kappa_i \left(\sum_{j=1}^{N} \lambda_j v_j \right) \, : \, \kappa_i, \lambda_j \in C \right\}. \qquad (3.29)$$

Apparently, the term $\sum_{i=1}^{N} \kappa_i$ is equal to a new complex number, call it c. Consequently, Eq. (3.29) becomes

$$\text{span}\{u_1, u_2, ..., u_n\} = \left\{ c \sum_{j=1}^{N} \lambda_j v_j = \sum_{j=1}^{N} c\lambda_j v_j \, : \, c, \lambda_j \in C \right\}. \qquad (3.30)$$

Orthonormalisation Algorithm II: MGS	
01: $v[1:N] \leftarrow g[1:N]$	initialisation step
02: for m from 1 to N	
03: $u_m \leftarrow \frac{1}{\sqrt{\xi_m}} \left[v_m - \sum_{i=1}^{m-1} \langle v_m, u_i \rangle \right]$	orthonormalise m^{th} vector
04: for n from $m+1$ to N	re-orthonormalise $m+1 \rightarrow n$ vectors
05: $v_n \leftarrow \frac{1}{\sqrt{\xi_n}} \left[v_n - \sum_{i=1}^{n-1} \langle v_m, u_i \rangle \right]$	
06: end of n loop	
07: end m loop	
08: $b[1:N] \leftarrow u[1:N]$	set SEFDM base

Table 3.2: MGS Orthonormalisation Algorithm.

Finally, setting $c\lambda_j = \mu_j$, Eq. (3.30) reduces to

$$\text{span}\{u_1, u_2, ..., u_n\} = \left\{ \sum_{j=1}^{N} \mu_j v_j \ : \ \mu_j \in C \right\}. \tag{3.31}$$

The latter is equivalent to the span of the initial base vectors $v_1, v_2, \ldots, v_N$.

3.5.2 Modified Gram Schmidt (MGS) orthonormalisation

Although CGS is widely used because of its simplicity, it suffers from a relatively large numerical error in the derivation of the vectors projections [53]. Consequently, the orthonormalisation process fails for larger dimensions of the initial vectors set. To improve the orthonormalisation result, the application of the modified Gram Schmidt (MGS) method is proposed. According to well established literature, whilst MGS is mathematically equivalent to CGS it has a superior computational performance because of its iterative nature [61], [53]. A short description of the MGS algorithm is given in Table 3.2

It becomes apparent that the main difference between CGS and MGS is the following: in CGS an orthonormal vector is generated at each step and the initial base of vectors remain unchanged for the rest of the calculations. In

Orthonormalisation Algorithm III: IMGS	
01: $v[1:N] \leftarrow g[1:N]$	initialisation step
02: for k from 1 to K	repeat MGS for K times
03: for m from 1 to N	implement MGS
04: $u_m \leftarrow \frac{1}{\sqrt{\xi_m}} \left[v_m - \sum_{i=1}^{m-1} \langle v_m, u_i \rangle \right]$	
05: for n from $m+1$ to N	
06: $v_n \leftarrow \frac{1}{\sqrt{\xi_n}} \left[v_n - \sum_{i=1}^{n-1} \langle v_m, u_i \rangle \right]$	
07: end of n loop	
08: end m loop	end of MGS
09: end k loop	end of K iterations
10: $b[1:N] \leftarrow u[1:N]$	set SEFDM base

Table 3.3: IMGS Orthonormalisation Algorithm.

contrast, in MGS the initial base is updated at each step after the reorthonormalisation of some of its vectors.

3.5.3 Iterative Modified Gram Schmidt (IMGS) orthonormalisation

In the iterative variant of MGS the orthonormalisation process is repeated for a predefined K number of steps. The orthonormal base generated at each step is set as an initial input to the orthonormalisation process of the next step [62]. It has been shown that a small number ($K = 2$) of iterations is enough to further improve the MGS orthonormalisation accuracy [54], [63]. A simple implementation of IMGS is given in Table 3.3

In order to confirm the superior performance of IMGS, relative to CGS and MGS, simulations were performed for SEFDM signals with different number of carriers $N = \{4 \longrightarrow 256\}$. For the sake of comparison, the orthonormalisation

error E of each method was measured. E is defined as

$$E = \left\| \mathbf{I} - \mathbf{U}\mathbf{U}^H \right\|_F^2, \tag{3.32}$$

where $\|\cdot\|_F$ denotes the Frobenius norm of a matrix, $\mathbf{I}$ is the $N \times N$ identity matrix and $\mathbf{U}$ is the matrix of the orthonormal base vectors.

Figs 3.7 (a) and 3.7 (b) demonstrate the orthonormalisation error E normalised over the MATLAB machine precision ($\approx 2.2204 \times 10^{-16}$). It is clear and expected that CGS and MGS performance degrade with the increase in N and/or the decrease in α. This observation implies that both techniques are not efficient for the orthonormalisation of the set of the initial SEFDM carriers when the sub-bands overlap and consequently the system inherent interference are considerably high. In particular, simulation results show that CGS and MGS work inadequately for ($N > 8, \alpha = 0.5$) and ($N > 16, \alpha = 0.5$) settings, respectively. Notwithstanding, IMGS is superior as opposed to MGS and CGS and achieves a pretty low orthonormalisation error even for large dimensional SEFDM signals, e.g. $N = 256$. In addition, as seen in Fig. 3.7 (b), E seems to be independent from α. Finally, it appears that $K = 2$ is sufficient for good IMGS performance and that a higher K number of iterations, e.g. $K = 6$, offers nothing but a trivial improvement in the IMGS orthonormalisation.

3.5.4 Löwdin orthonormalisation

Gram Schmidt procedure and its variants are non symmetric orthonormalisation methods in the sense that their outcome strongly depends on the initial seed - vector. Therefore, the set of orthonormal vectors is different for any permutation of the initial SEFDM carriers set. Löwdin introduced, in work associated with quantum chemistry and a different orthonormalisation method that is not sequence dependent [64], [65] and further exhibits the attractive property of generating vectors that resemble the most to the primal ones in the least squares sense [66], [67].

(a) IMGS vs MGS and CGS.

(b) IMGS.
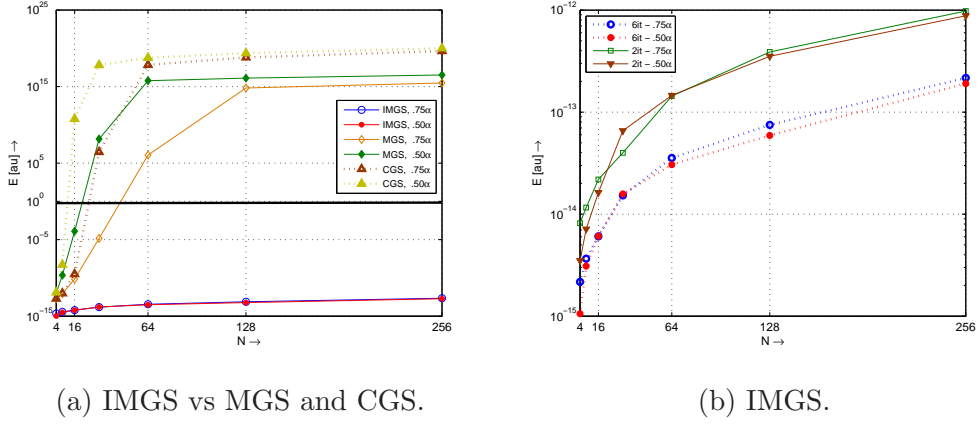
Figure 3.7: Orthonormalisation error E for different orthonormalisations.

Considering $\mathbf{V}$ is the matrix of the linear independent but non orthonormal vectors $[v_1, v_2, ..., v_n]$, Löwdin method generates the respective orthonormal base $\mathbf{U} = [u_1, u_2, ..., u_n]$ as follows: first, a transformation matrix $\mathbf{M}$ is derived,

$$\mathbf{U} = \mathbf{M}\mathbf{V}. \tag{3.33}$$

Under the assumption that $\mathbf{U}$ matrix is orthonormal,

$$\mathbf{U}\mathbf{U}^H = \mathbf{I}_N \Leftrightarrow (\mathbf{M}\mathbf{V})(\mathbf{M}\mathbf{V})^H = \mathbf{I}_N \Leftrightarrow \mathbf{M}(\mathbf{V}\mathbf{V}^H)\mathbf{M} = \mathbf{I}_N. \tag{3.34}$$

It is obvious that the matrix $\mathbf{V}\mathbf{V}^H$ is equal to the Grammian matrix of the initial set of vectors that is Hermitian [68]. Replacing $\mathbf{V}\mathbf{V}^H$ with $\boldsymbol{\Delta}$, Eq. (3.33) reduces to

$$\mathbf{M}\boldsymbol{\Delta}\mathbf{M}^H = \mathbf{I}_N \Leftrightarrow \boldsymbol{\Delta}^{-1} = \mathbf{M}^H\mathbf{M}. \tag{3.35}$$

A solution for the above equation is $\mathbf{M} = \boldsymbol{\Delta}^{-1/2}$. In order to calculate the inverse of its square root, $\boldsymbol{\Delta}$ is diagonalised [69] using its eigenvectors matrix $\mathbf{E}$ as

$$\boldsymbol{\Delta} = \mathbf{E}\mathbf{D}\mathbf{E}^{-1}, \tag{3.36}$$

where $\mathbf{D}$ is a diagonal matrix whose diagonal elements are $\boldsymbol{\Delta}$ eigenvalues. Con-

---

Orthonormalisation Algorithm IV: Löwdin

01: $v[1:N] \leftarrow g[1:N]$ initialisation step

02: $(\delta[1:N], e[1:N]) \leftarrow \mathrm{eig}\{v[1:N]^H v[1:N]\}$ eigenvalue decomposition of $\mathbf{V}^H \mathbf{V}$

03: $\mathbf{M} \leftarrow e[1:N]\mathrm{Diag}\{\delta[1:N]^{-\frac{1}{2}}\}e[1:N]^{-1}$ calculation of Löwdin $\mathbf{M}$

04: $u[1:N] \leftarrow \mathbf{M}v[1:N]$ orthonormalisation

05: $b[1:N] \leftarrow u[1:N]$ set SEFDM base

Table 3.4: Löwdin Orthonormalisation Algorithm.

sequently, $\mathbf{\Delta}^{-1/2}$ is given by

$$\mathbf{\Delta}^{-1/2} = \mathbf{E}\mathbf{D}^{-1/2}\mathbf{E}^{-1}. \tag{3.37}$$

Next, the new orthonormal base is generated according to

$$\mathbf{U} = \mathbf{\Delta}^{-1/2}\mathbf{V}, \tag{3.38}$$

where $\mathbf{\Delta}$ is given in Eq. (3.37). A description of the Löwdin orthormalisation method is given in Table 3.4. The symbols $\delta[1:N]$ and $e[1:N]$ correspond to the eigenvalues and eigenvectors of a matrix, respectively. The function $\mathrm{eig}\{\cdot\}$ generates the eigenvalues and eigenvectors matrices δ and e, respectively, while the function $\mathrm{Diag}\{\cdot\}$ creates a square diagonal matrix whose diagonal comprises of the elements of the argument vector.

Finally, as already mentioned, the Löwdin method generates orthogonal vectors that resemble the most the initial vectors in the least squares sense, i.e. the generated carriers have the property of minimising the following norm

$$\mathrm{min.}\ \|\mathbf{V} - \mathbf{U}\|_F^2 = \mathrm{min.}\ \mathrm{Tr}((\mathbf{V} - \mathbf{U})(\mathbf{V} - \mathbf{U})^H), \tag{3.39}$$

where $\mathrm{Tr}\{\cdot\}$ denotes the trace of the matrix.

3.5.5 Projections matrix properties

The properties of the projections matrix $\mathbf{M}$ are important since they determine the distribution of the system inherent interference at the output of the demod-

ulator correlators. Upon the orthonormalisation method the matrix shape and properties vary. This section shows either by mathematical analysis and/or simulation results some important properties of $\mathbf{M}$.

Proposition 1: *The SEFDM projections matrix is upper triangular when the GS method is applied for the generation of the receiver orthonormal base.*

Proof: The GS method is by construction a QR decomposition method of the initial set $\mathbf{V}$ of SEFDM carriers, i.e.

$$\mathbf{V} = \mathbf{QR} \Longleftrightarrow \mathbf{Q}^H \mathbf{V} = \mathbf{R}, \tag{3.40}$$

where $\mathbf{Q}$ is an orthonormal matrix and $\mathbf{R}$ an upper triangular matrix. It is apparent from the RHS of Eq. (3.40) that $\mathbf{M} = \mathbf{R}$.

Proposition 2: *The sum of the squares of the elements of each column of the SEFDM GS projections matrix is equal to unity.*

Proof: from Eq. (3.40) the Grammian $\mathbf{M}^H \mathbf{M}$ is

$$\mathbf{M}^H \mathbf{M} = (\mathbf{Q}^H \mathbf{V})^H \mathbf{Q}^H \mathbf{V} = (\mathbf{V})^H \mathbf{Q} \mathbf{Q}^H \mathbf{V}. \tag{3.41}$$

Since $\mathbf{Q}$ is unitary, it is clear that

$$\mathbf{M}^H \mathbf{M} = \mathbf{V}^H \mathbf{V}. \tag{3.42}$$

It has been shown in the transmitters sections 3.4 that $\mathbf{V}^H \mathbf{V} = \mathbf{F}_\alpha^{-1} \mathbf{F}_\alpha = \mathbf{\Phi}$ where $\mathbf{F}_\alpha$ is the fractional fourier matrix. In addition, from proposition (1) $\mathbf{L} = \mathbf{M}^H$ is a lower triangular matrix. Apparently, $\mathbf{L}$ is the Cholesky decomposition matrix of $\mathbf{\Phi}$, i.e.

$$\mathbf{\Phi} = \mathbf{L}\mathbf{L}^H = \mathbf{M}^H \mathbf{M}. \tag{3.43}$$

From [70] the diagonal elements l_{ii}, $i = 1, \ldots, N$, of $\mathbf{L}$ are given by

$$l_{ii} = m_{ii} = \sqrt{\phi_{ii} - \sum_{k=1}^{i-1} l_{ik} l_{ik}^*} \Longrightarrow m_{ii} = \sqrt{\phi_{ii} - \sum_{k=1}^{i-1} m_{ki} m_{ki}^*}. \tag{3.44}$$

The diagonal elements ϕ_{ii} of the FrFT Grammian matrix $\mathbf{\Phi}$ are equal to

$$\phi_{ii} = \frac{1}{N} \sum_{l=1}^{i-1} e^{\frac{j 2\pi (i-1)(l-1)\alpha}{N}} e^{\frac{-j 2\pi (l-1)(i-1)\alpha}{N}} = \frac{1}{N} \sum_{l=1}^{i-1} 1 = 1. \tag{3.45}$$

From Eqs (3.44) and (3.45) it is derived that m_{ii} is equal to

$$m_{ii} = \sqrt{1 - \sum_{k=1}^{i-1} m_{ki} m_{ki}^*} \Rightarrow m_{ii}^2 = 1 - \sum_{k=1}^{i-1} m_{ki}^2. \tag{3.46}$$

The LHS of Eq. (3.46) reduces to

$$\sum_{k=1}^{i} m_{ki}^2 = 1. \tag{3.47}$$

It is notable that m_{ki} determine the contribution of the transmit symbol S_k at the output of the ith correlator. Consequently, proposition (2) could be interpreted as follows: the overall energy of the ith symbol is preserved yet redistributed by the GS projections matrix according to Eq. (3.47). From Eq. (3.46) is also clear that

$$m_{11} = 1 \text{ and } m_{ii} < 1 \text{ for } i \neq 1. \tag{3.48}$$
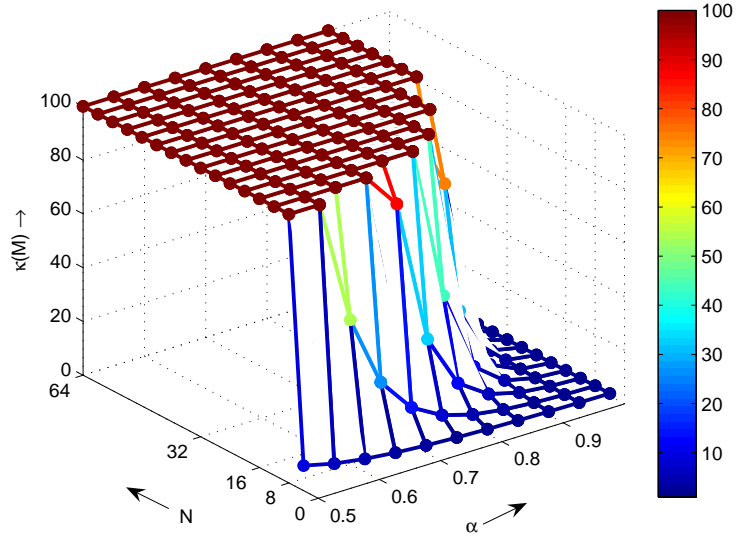
Figure 3.8: The condition number κ of IMGS matrix $\mathbf{M}$ for $N \in \{4, 8, 16, 32, 64\}$ and α ranging from 1 to 0.5

Proposition 3: *The condition of the SEFDM GS projections matrix is overly worsening with the increase in N and/or decrease in α.*

Simulation results have shown that the diagonal elements, i.e. the eigenvalues, of the triangular matrix $\mathbf{M}$ decay very fast towards zero as N increases and/or α decreases. Consequently, the condition of $\mathbf{M}$ also deteriorates under the same conditions since [70]

$$\kappa\{\mathbf{M}\} = \frac{\lambda_{max}}{\lambda_{min}}, \tag{3.49}$$

where $\kappa\{\cdot\}$ denotes the condition number of a matrix, and λ_{max} and λ_{min} the minimum and maximum eigenvalues of $\mathbf{M}$. From Eq. (3.48) it is obvious that $\lambda_{max} = m_{11} = 1$. Consequently, as $\lambda_{min} \to 0$, $k\{\mathbf{M}\} \to \infty$.

Fig. 3.8 shows the condition number $\kappa\{\cdot\}$ of $\mathbf{M}$ generated by IMGS, versus N and α. For the sake of illustration, all the big values $\kappa\{\mathbf{M}\} \geq 10^2$ of the condition number are set to be equal to 10^2.

Assuming that 10^2 is a lower bound for the matrix bad condition, it is clear that for $N > 16$ and or $\alpha \leq 0.8$ the projections matrix $\mathbf{M}$ gradually becomes severely ill conditioned and tends to be numerically singular.

Proposition 4: *The size of the cluster of the small singular values of the SEFDM GS projections matrix is equal to $(1 - \alpha)N$.*

In order to verify the above proposition, the matrix was singular valued decomposed using the standard MATLAB SVD function. Fig. 3.9 (a) and (b) shows $\mathbf{M}$ singular values for N ranging from 8 to 64 and α from 0.5 to 1. In all cases $(1 - \alpha)N$ singular values of matrix $\mathbf{M}$ gradually decay to zero.

Proposition 5: *The SEFDM projections matrix is Hermitian when the Löwdin method is applied for the generation of the receiver orthonormal base.*

Proof: The projections matrix $\mathbf{M}$ is by definition the inner product of the matrices of the initial and the orthonormal base, $\mathbf{V}$ and $\mathbf{U}$, respectively

$$\mathbf{M} = \mathbf{V}\mathbf{U}^H. \tag{3.50}$$

After replacing $\mathbf{U}$ from Eq. (3.38) and $\boldsymbol{\Delta}$ with $\mathbf{V}\mathbf{V}^{\mathbf{H}}$, (3.50) reduces to

$$\mathbf{M} = \mathbf{V}\left(\left(\mathbf{V}\mathbf{V}^H\right)^{-1/2}\mathbf{V}\right)^H = \mathbf{V}\mathbf{V}^H\left(\left(\mathbf{V}\mathbf{V}^H\right)^{-1/2}\right)^H = \boldsymbol{\Delta}\left(\boldsymbol{\Delta}^{-1/2}\right)^H. \tag{3.51}$$

(a) $\mathbf{M}$ singular values; $N = 16$.

(b) $\mathbf{M}$ singular values; $N = 32$.
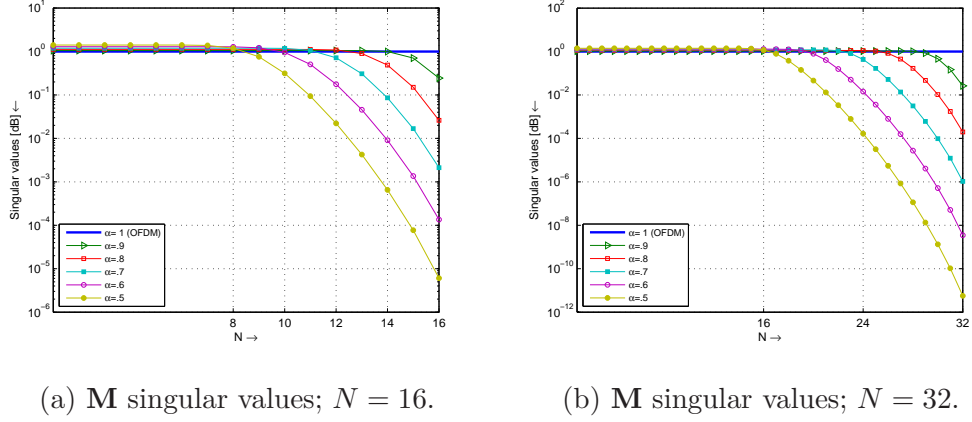
Figure 3.9: SVD of SEFDM IMGS projections matrix $\mathbf{M}$ with $\alpha \in \{0.5, 0.8, 1\}$.

It is clear that $(\mathbf{\Delta})^{-1/2}$ is also symmetric since $\mathbf{\Delta}$ is a Grammian positive semidefinite Hermitian matrix. To show the product of two Hermitian matrices $\mathbf{A}$ and $\mathbf{B}$ is also Hermitian, it is enough to show $\mathbf{AB} = \mathbf{BA}$ or equivalently that $(\mathbf{AB})(\mathbf{BA})^{-1} = \mathbf{I}$ [53]. Consequently, following (3.51) it must be shown that

$$\left(\mathbf{\Delta}^{-1/2}\right)^{H} \mathbf{\Delta} \left(\mathbf{\Delta}\left(\mathbf{\Delta}^{-1/2}\right)^{H}\right)^{-1} = \mathbf{I}$$

$$\Leftrightarrow \left(\mathbf{\Delta}^{-1/2}\right)^{H} \mathbf{\Delta} \left((\mathbf{\Delta}^{-1/2})^{H}\right)^{-1} \mathbf{\Delta}^{-1} = \mathbf{I}, \qquad (3.52)$$

and because $\mathbf{\Delta}^{-1/2} = (\mathbf{\Delta}^{-1/2})^{H}$, since $\mathbf{\Delta}$ is Hermitian, it is sufficient to show

$$\mathbf{\Delta}^{-1/2}\mathbf{\Delta}(\mathbf{\Delta}^{-1/2})^{-1}\mathbf{\Delta}^{-1} = (\mathbf{\Delta}^{-1/2}\mathbf{\Delta})(\mathbf{\Delta}^{-1/2}\mathbf{\Delta})^{-1} = \mathbf{I}$$

$$\Rightarrow \mathbf{M} = \mathbf{\Delta}(\mathbf{\Delta}^{-1/2})^{H} \in \mathbf{S}^{N}, \qquad (3.53)$$

where $\mathbf{S}^{N}$ denotes the set of the square Hermitian matrices of N dimension.

Proposition 6: *The sum of the interfering terms is smaller in a Löwdin than in a GS based SEFDM system.*

The Frobenius norm $\|\mathbf{M}\|_{F}^{2}$ is equal to

$$\|\mathbf{M}\|_{F}^{2} = \sum_{i=1}^{N}\sum_{j=1}^{N} |m_{i,j}|^{2} = \mathrm{Tr}\left(\mathbf{MM}^{H}\right) =$$

$$\mathrm{Tr}\left(\mathbf{VU}^{H}(\mathbf{VU}^{H})^{H}\right) = \mathrm{Tr}\left(\mathbf{VUU}^{H}\mathbf{V}^{H}\right) = \mathrm{Tr}(\mathbf{VV}^{H}) = \|\mathbf{V}\|_{F}^{2} =$$

70

$$\sum_{i=1}^{N}\sum_{j=1}^{L}|v_{i,j}|^2 \;=\; \sum_{i=1}NE_i = N, \tag{3.54}$$

where E_i is the energy of the ith vector, here normalised to unity.

It was also found by simulation that the sum of the squares of the $\mathbf{M}$ diagonal elements, $|m_{i,i}|^2$, is larger in Löwdin than in IMGS. In addition, it is clear from Eq. (3.54) that since $\|\mathbf{M}\|_F^2$ is constant, the sum of the squares of the non-diagonal elements is smaller in Löwdin than in IMGS

$$\sum_{i=1}^{N}|m_{i,i}|^2_{\text{(Löwdin)}} \;>\; \sum_{i=1}^{N}|m_{i,i}|^2_{(MGS)} \;\stackrel{(3.54)}{\Rightarrow}$$

$$\sum_{i=1}^{N}\sum_{j=1}^{N}|m_{i,j}|^2_{\text{(Löwdin)}} \;<\; \sum_{i=1}^{N}\sum_{j=1}^{N}|m_{i,j}|^2_{(MGS)}. \tag{3.55}$$

From an energy point of view, this indicates that in Löwdin orthonormalisation the output of the correlators suffers from less interference since a smaller amount of the signal energy is transferred to the interfering terms. Fig. 3.10 provides a comparison between the Löwdin and the IMGS orthonormalisation methods in terms of size of the norm of the diagonal elements of the respective correlation matrices $\mathbf{M}$. Simulations were performed for different numbers of SEFDM carriers with various values of the normalised frequency separation α.

3.6 Noise properties after projection

From Eqs (3.3) and (3.4), it is apparent that the output of the receiver k^{th} correlator includes a noise component n_k given by

$$n_k = \int_0^T n(t)b_k^*(t)dt, \quad k = 0, 1, ..., N-1, \tag{3.56}$$

where b_k is the kth orthonormal base function generated by IMGS and $n(t)$ represents the channel AWGN with zero mean and variance σ^2.

The expected value $\mathrm{E}\{\cdot\}$ of each of the noise components will be

$$\mathrm{E}\{n_k\} = \mathrm{E}\left\{\int_0^T n(t)b_k^*(t)dt\right\}. \tag{3.57}$$
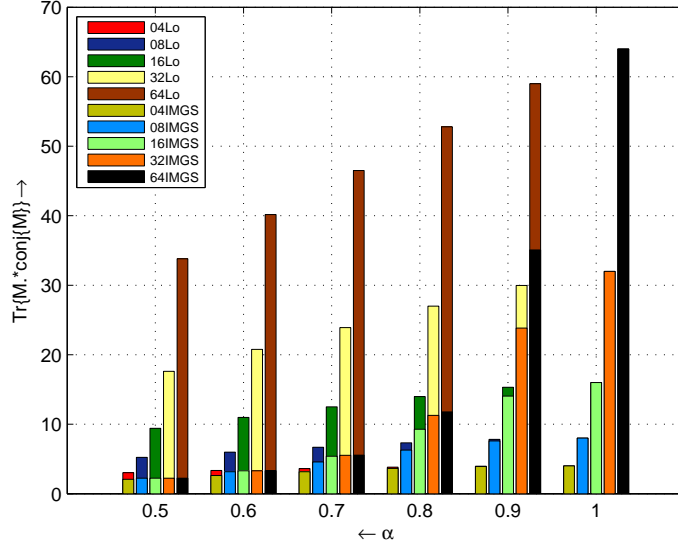
Figure 3.10: Comparison between Löwdin and IMGS methods. conj{·} and .∗ denote the conjugate and the element by element multiplication, respectively.

It can be shown that

$$E\{n_k\} = \int_0^T E\{n(t)\} b_k^*(t)dt. \tag{3.58}$$

Yet, assuming the channel noise has zero mean, i.e. $E\{n(t)\} = 0$, it follows that

$$E\{n_k\} = 0. \tag{3.59}$$

In addition, the covariance $C_{n_i n_j}$ of any two of the noise components n_i and n_j, with $i, j \in \{0, 1, ..., N - 1\}$, is given by

$$C_{n_i n_j} = E\{(n_i - E\{n_i\})(n_j^* - E\{n_i\})\}. \tag{3.60}$$

Following Eq. (3.59) Eq. (3.60) reduces to

$$
\begin{aligned}
C_{n_i n_j} &= E(n_i - 0)(n_j^* - 0) = E\left\{n_i n_j^*\right\} = \\
C_{n_i n_j} &= E\left\{\int_0^T n(t)b_i^*(t)dt \int_0^T n^*(\tau)b_i(\tau)d\tau\right\} = \\
C_{n_i n_j} &= \int_0^T \int_0^T E\{n(t)n^*(\tau)\} b_i^*(t)b_j(\tau)dtd\tau.
\end{aligned} \tag{3.61}
$$

72

The autocorrelation function $\mathrm{E}\left\{n(t)n^*(\tau)\right\}$ is equal to $\sigma^2\delta(t-\tau)$ because of the assumed white nature of noise $n(t)$. Consequently, Eq. (3.61) reduces to the following

$$
\begin{aligned}
C_{n_i n_j} &= \int_0^T \int_0^T \sigma^2\delta(t-\tau)b_i^*(t)b_j(\tau)dtd\tau \iff \\
C_{n_i n_j} &= \sigma^2 \int_0^T b_i^*(t)b_j(t)dt.
\end{aligned}
\tag{3.62}
$$

The orthogonality property of the GS or Löwdin base functions b_i ensures that the covariance of the noise components is equal to

$$
C_{n_i n_j} = \begin{cases} \sigma^2 & i=j \\ 0 & i\neq j \end{cases}.
\tag{3.63}
$$

Consequently, in matrix representation, the vector $\mathbf{N}$ of the noise at the correlators outputs (see Eq. (3.5)) will be comprised of N uncorrelated (since their covariance is zero [71]) noise variables, $[n_0, n_1, ..., n_{N-1}]$, with zero mean (see Eq. (3.58)) and covariance matrix equal to $\sigma^2\mathbf{I}$ (see Eq. (3.63)), where $\mathbf{I}$ is the $N \times N$ identity matrix.

3.7 SEFDM optimal detector

The front end of the SEFDM system is a detector that makes use of the demodulator sufficient statistics to recover the transmitted data symbols. This section provides the mathematical analysis of the MAP detection which is optimal in the sense that it minimises the probability of erroneous decisions [52]. The analysis initially accounts the assumption that the signal is affected by AWGN only. Consequently, due to the projection of the received signal onto an orthonormal base the noise variables at the correlators' outputs will exhibit the properties shown in section 3.6.

According to Bayes theorem [71] the a 'posteriori' probability can be expressed as

$$
p(\mathbf{S}_m|\mathbf{R}) = \frac{p(\mathbf{R}|\mathbf{S}_m) \times p(\mathbf{S}_m)}{p(\mathbf{R})}.
\tag{3.64}
$$

The probabilities $p(\mathbf{S}_m)$ of transmitted SEFDM symbols are called a 'priori'. To facilitate the analysis it is further assumed that at all transmitted symbols are Independent and Identical Distributed (IID). Hence, since the same constellation is used for the modulation of all carriers, $p(\mathbf{S}_m) = 1/M^N$ and Eq. (3.64) reduces to

$$p(\mathbf{S}_m|\mathbf{R}) = \frac{1}{M^N} \times \frac{p(\mathbf{R}|\mathbf{S}_m)}{p(\mathbf{R})}. \qquad (3.65)$$

It is apparent that the a 'posteriori' probability depends only on the likelihood function $p(\mathbf{R}|\mathbf{S}_m)$ that offers a measure of closeness of the receiver statistics vector $\mathbf{R}$ to the transmitted waveform $\mathbf{S}_m$. Hence, it is sufficient to maximise the likelihood function $p(\mathbf{R}|\mathbf{S}_m)$.

In order to further reduce the problem of the likelihood function optimisation, $p(\mathbf{R}|\mathbf{S}_m)$ is derived. First, the probability distribution function for each of the correlators outputs (receiver statistics) is calculated. In particular, each of the statistics follows a Gaussian distribution with mean $S'_{m,k} = M_k \mathbf{S}_m$ and variance equal to σ^2 [52] (see section 3.6 above), where M_k is the kth row of the $\mathbf{M}$ matrix. So, their probability distribution functions are

$$p(R_k|\mathbf{S}_m) = \frac{1}{\sqrt{2\pi}\sqrt{N_0/2}} e^{\left\{-\frac{(R_k - S'_{m,k})^2}{N_0}\right\}}, \quad k = 1, \ldots, N. \qquad (3.66)$$

The probability distribution of the signal/vector $\mathbf{R} = [R_1, R_2, ..., R_N]$ is given by the joint distribution of the statistics variables as

$$p(\mathbf{R}|\mathbf{S}_m) = p(R_1, R_2 \ldots, R_N|\mathbf{S}_m). \qquad (3.67)$$

Furthermore, thanks to the statistical independence of $R_k|\mathbf{S}_m$ (guaranteed by the correlations with an orthonormal base) their joint likelihood probability of $p(\mathbf{R}|\mathbf{S}_m)$ (see(3.65)) is equal to the product of the individual ones,

$$p(\mathbf{R}|\mathbf{S}_m) = \prod_{k=1}^{N} p(R_k|\mathbf{S}_m). \qquad (3.68)$$

Following Eq. (3.66) Eq. (3.68) reduces to

$$p(\mathbf{R}|\mathbf{S}_m) = \frac{1}{(\pi N_0)^{N/2}} e^{\left\{ -\sum_{k=1}^{N} \frac{(R_k - S'_{m,k})^2}{N_0} \right\}}. \tag{3.69}$$

The maximisation of the likelihood function is equivalent to the minimisation of the exponent term in Eq. (3.68). Consequently, the ML detection reduces to the following Least Squares (LS) optimisation problem, i.e. the minimisation of a sum of squares,

$$\begin{aligned} \text{min.} \quad & \sum_{k=1}^{N} (R_k - S'_{m,k})^2 = \|\mathbf{R} - \mathbf{S}'_m\|_2^2 = \|\mathbf{R} - \mathbf{M}\mathbf{S}_m\|_2^2, \\ \text{s.t.} \quad & \mathbf{S}_m \in Q^N, \end{aligned} \tag{3.70}$$

where Q^N is the set of all the possible SEFDM symbols $\mathbf{S}_m$ and $\mathbf{S}'_m = [S'_{m,1}, S'_{m,2}, ..., S'_{m,N}]$ corresponds to the symbols $\mathbf{S}_m$ after transformation by the projections matrix $\mathbf{M}$ SEFDM.

In order to investigate the error performance of ML detection, a simple detector is implemented in MATLAB following an exhaustive enumeration method. In particular, the cost function of Eq. (3.70) is calculated over the entire set Q^N. Then, the vector $\mathbf{S}_m$ that achieves the minimum value in (3.69) is picked up as the optimal estimate $\hat{\mathbf{S}}_m$.

A set of preliminary simulations were performed for small dimensions only, $N \in \{2, 4, 8\}$, of BPSK and QPSK modulated SEFDM carriers due to the overly complexity of the applied brute force method. Figs 3.11 and 3.12 demonstrate the SEFDM optimal detection bit error rate (BER) curves versus α ranging from 1 to 0.3. It is notable that optimal BPSK SEFDM detection achieves the OFDM (i.e. SEFDM with $\alpha = 1$) error rate for $\Delta fT \geq 0.5$. However, in QPSK case the signal detection gradually degrades for $\Delta fT \leq 0.8$. Consequently, ML detection performance approximates the error performance of an equivalent OFDM system under specific constraints that are related to the kind of the transmitted data (e.g. BPSK, QPSK) as well as the projections matrix $\mathbf{M}$

properties. The latter depends on the signal dimension N and the frequency separation Δf of the SEFDM subcarriers.
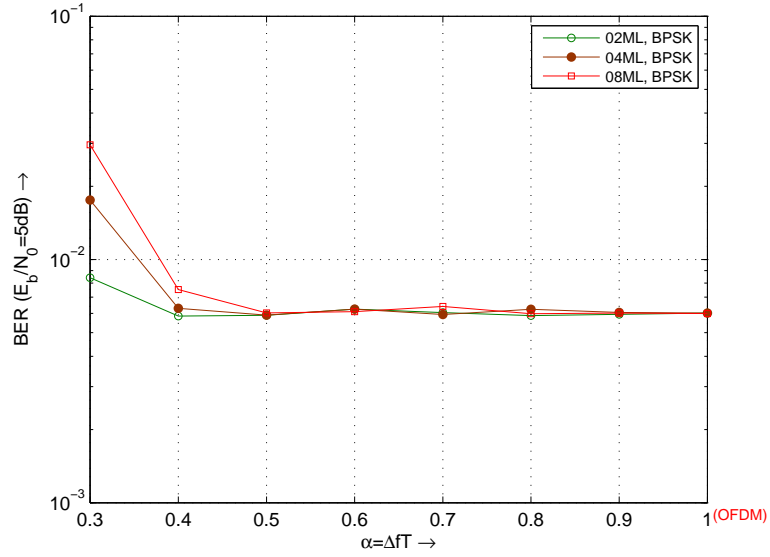
Figure 3.11: ML detection error performance versus α for BPSK SEFDM.
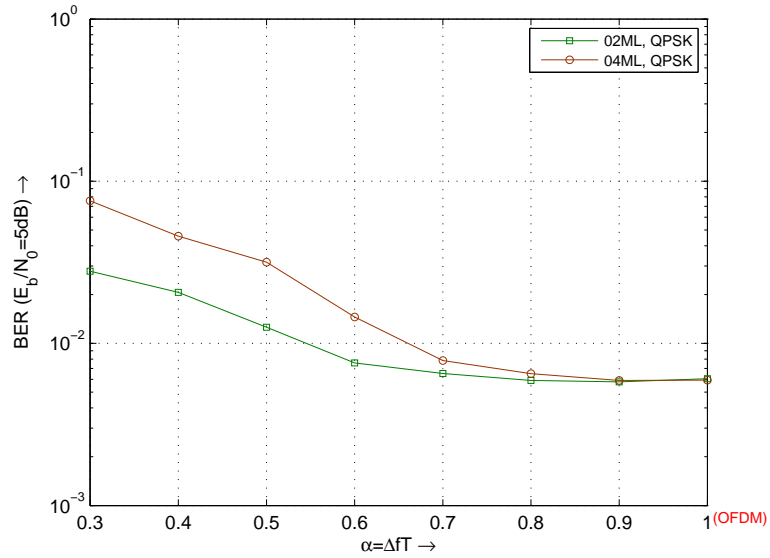
Figure 3.12: ML detection error performance versus α for QPSK SEFDM.
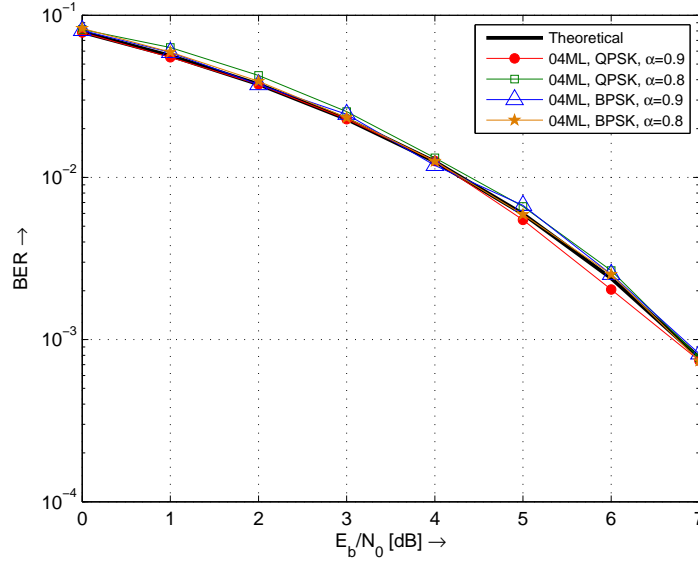
Figure 3.13: ML detection error performance versus E_b/N_0 for BPSK and QPSK SEFDM with $N = 2 \rightarrow 4$ carriers. α was set to 0.9 and 0.8.

It must be noticed that the brute force ML detection is not tangible for SEFDM signals with $\left| Q^N \right| > 2^{16}$, with $|\cdot|$ denoting the set cardinality. In this work modelling the number of carriers N was constrained due to simulation time reasons, to 8 for BPSK and 4 for QPSK SEFDM, respectively.

3.8 Comments on the SEFDM system complexity

A possible digital implementation of the SEFDM system is illustrated in Fig. 3.14. It is apparent that the main SEFDM transceiver is broken down into three main parts: the transmit signal generator, the demodulator and the detector.

As shown in section 3.4 the complexity of a fractional FT needed for the SEFDM samples generation is $O(N \log N)$ [57]. Consequently, from a computational effort view point, the transmitter does not constitute a real constraint for the SEFDM system design.

Regarding the demodulator, the computational cost is twofold: first, the
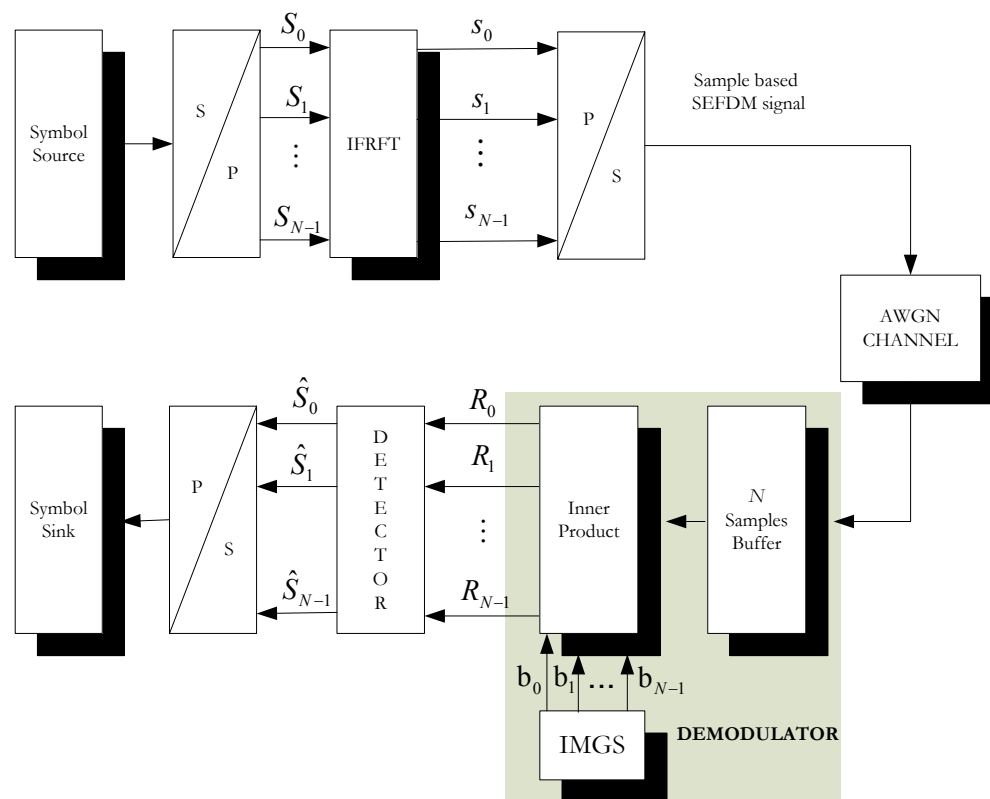
Figure 3.14: General block diagram of a computationally feasible SEFDM system [73].

generation of a GS orthonormal base is $O(N^3)$ [53]. However, the orthonormalisation can be precomputed offline and therefore does not affect the system overall complexity. Second, a straightforward implementation of the projections requires N multiplications between two $N \times 1$ vectors. That is $O(N^2)$ and may prove to be a practical limitation for very large dimensional SEFDM systems.

Finally, as far as the detector is concerned, it has been shown that the SEFDM optimal detection reduces to a combinatorial least squares problem. Such a problem has been proved to be non polynomial hard [72]. In addition, the complexity of its solution following an exhaustive enumeration over all the possible hypotheses is $O(M^N)$. As a result, a 'real time' SEFDM detection is limited to 4-QAM systems with $N < 8$. Hence, it is apparent that the detection is the main bottleneck for the SEFDM system performance, which is the focus of what follows in this thesis.

3.9 Conclusions and discussion

This chapter gives a detailed general description of the SEFDM model initially proposed by Rodrigues and Darwazeh in [29]. The most significant SEFDM benefits were presented in terms of bandwidth reduction and spectral efficiency gain when compared to equivalent data rate OFDM system. It was shown by mathematical derivations and simulations that SEFDM offers a spectral gain of $\frac{1-\alpha}{\alpha}$ and is closer than OFDM and single carrier schemes to the ideal channel capacity bound derived by Shannon.

In addition, the main design challenges of an SEFDM system were identified. First, a short description of possible implementations of a practical SEFDM digital transmitter is given. In analogy to the standard use of IFFT in OFDM systems, a generalised fourier transformation could be applied for the generation of the time domain samples of the SEFDM symbols. The so called FrFT can be implemented by fast algorithms that require $20N \log N$ floating

operations only. Apart from FrFT, recent research efforts based on typical DFTs [59], [60] have also been cited. These proposals achieve the generation of the SEFDM signal at the expense of a small increase in complexity of an equal sized OFDM systems, yet offer compatibility with the FFT techniques used in the modern communication systems.

Furthermore, this chapter dealt with the receiver design issues. It was shown by simulations that the classic Gram Schmidt (GS) method, as in [29] initially proposed for the generation of the receiver orthonormal base, suffers from a severe rounding error even for medium sized SEFDM signals. Consequently, other variants of GS are proposed. It was concluded that an iterative modified GS (IMGS) technique performs sufficiently well for large SEFDM signals. In addition, the Löwdin method, well known in the field of quantum chemistry, was examined because of its interesting property of generating orthonormal functions that resemble the most the initial SEFDM carriers.

The chapter reports a detailed study of the SEFDM linear model matrix $\mathbf{M}$. By construction, $\mathbf{M}$ includes the correlation coefficients between the transmit SEFDM carriers and the receiver orthonormal base. It was proved that the shape of $\mathbf{M}$ depends on the orthonormalisation method and that for all the GS variants and the Löwdin method $\mathbf{M}$ is upper triangular or Hermitian, respectively. Moreover, it was mathematically shown that the energy of each transmitted symbol is preserved but redistributed to the correlators outputs through the projections process. Finally, it was demonstrated by simulation that the condition of $\mathbf{M}$ is overly worsening with the SEFDM inherent intercarriers interference; and it was found that the number of 'corrupted' $\mathbf{M}$ singular values is equal to αN.

In addition, considering that the receiver base is orthonormal by the IMGS application, it was proved that the noise variables at the output of the demodulator are uncorrelated with zero mean and covariance equal to $\sigma^2 \mathbf{I}$. Following this, the last section of this chapter introduced the detection issue that is the

main motivation of this work. Based on the derived noise properties, the optimal, in terms of decision errors, maximum a posteriori detector was reduced to a maximum likelihood detector that solves a combinatorial least squares optimisation problem. Some preliminary simulations were run by applying a brute force solver to the problem. Results complied with [34], [32], [33] and demonstrated that optimal 4-QAM SEFDM detection can perform similarly to OFDM when $\alpha \geq 0.8$. However, it was seen that as α decreases below this bound and N increases the optimal SEFDM detection results in error penalties when compared to single carrier and OFDM schemes. In addition, results were limited to SEFDM with $N \leq 8$ since the complexity of the ML detector increases exponentially with the number of the carriers and the modulation size. Upon these observations, it is concluded that the main gap in the research area of the SEFDM systems is the creation of a practical detector for medium and large SEFDM signals that could trade-off sufficiently computational cost for error penalty. The following chapters present this work findings, including descriptions and simulation results, for various detection algorithms that approach a solution to the problem under different conditions.

Chapter 4

Linear and iterative detectors

4.1 Introduction

The previous chapter presented the main challenges in the design of an SEFDM system; efficient signal generation, the generation of sufficient statistics at the receiver and finally the reliable detection of the transmitted SEFDM symbols. In all three, the computational complexity is a major prerequisite for real practical systems. In [73] and more recently in [60], it has been shown that efficient signal generation could be achieved using either IFrFT or a combination of parallel IFFTs with the same order of complexity of an OFDM transmitter, i.e. $O(NlogN)$ where N is the number of the signal sub-carriers. As far as the statistics generation is concerned, [29] proposed the projection of the received signal onto a Gram Schmidt (GS) generated orthonormal base that has the same span of the transmitted SEFDM signal. CGS, MGS and its iterative versions are $O(N^3)$ [53], yet they do not actually encumber the system computational effort since they need to be implemented only once offline [73]. In addition, assuming no oversampling, the projections computation complexity is also $O(N^2)$ since a single projection requires no more than N complex multiplications and $N - 1$ additions.

However, the SEFDM detection appears to be significantly more complex.

The internal ICI, due to the squeeze in the frequency separation Δf of SEFDM carriers, prohibits a simple OFDM-like approach. SEFDM optimal ML detection is a non polynomial hard combinatorial problem (see section 3.7). Hence, its solution relies on an exhaustive search over the set of all possible hypotheses, i.e. the set of the SEFDM transmitted symbols, that increases exponentially with N and with the constellation cardinality M. Consequently, the NP hard nature of the ML detection constitutes a significant bottleneck for the system overall performance and complexity.

In this chapter, a first attempt to deal with this problem is made by investigating suboptimal linear detection techniques like ZF and MMSE. First, ZF implementations are examined based on either the inversion of the projections matrix $\mathbf{M}$ or an iterative process that takes advantage of the triangular shape of $\mathbf{M}$. In addition, encouraged by the properties of the Lowdin orthonormalisation as discussed in section 3.5.4, a heuristic approach that combines the projection of the received signal on a Lowdin orthonormal base with an iterative cancellation process is proposed. Then, the Tikhonov regularisation of the ML problem is described and the effect of the regularisation is demonstrated by simulation. In addition, the linear MMSE detector is derived and it is shown that it constitutes a special regularised ML solver. Finally, a combined MMSE-ML method is designed in order to improve performance over a standalone MMSE detector.

4.2 ZF SEFDM detection

The received SEFDM is described by the linear statistical model [29]

$$\mathbf{R} = \mathbf{MS} + \mathbf{N}, \tag{4.1}$$

where $\mathbf{R}$ is the $N \times 1$ statistics vector, $\mathbf{S}$ is the $N \times 1$ vector of the transmit symbols that take values in a discrete alphabet Q^N, $\mathbf{M}$ is the $N \times N$ matrix of the projections of the SEFDM sub-carriers onto an orthonormal base, and $\mathbf{N}$ is the $N \times 1$ vector of the noise variables at the output of the receiver correlators.

Thanks to the noise vector properties (see Chapter 3), the SEFDM ML detection reduces to a LS minimisation problem

$$\text{min.} \quad \|\mathbf{R} - \mathbf{MS}\|_2^2,$$
$$\text{s.t.} \quad \mathbf{S} \in Q^N. \tag{4.2}$$

With no loss of the generality, Q^N could be further constrained to include integers only. Hence, the ZF solution of the Integer LS (ILS) problem involves two steps: First, the problem is relaxed, by omitting the input constraint

$$\text{min.} \|\mathbf{R} - \mathbf{MS}\|_2^2 \Leftrightarrow \mathbf{R} = \mathbf{MS}, \tag{4.3}$$

then, from Eqs (4.1) and (4.3) the solution $\tilde{\mathbf{S}}$ of the unconstrained problem is

$$\tilde{\mathbf{S}} = \mathbf{M}^{-1}\mathbf{R} = \mathbf{M}^{-1}(\mathbf{MS} + \mathbf{N}) = \mathbf{S} + \mathbf{M}^{-1}\mathbf{N}, \text{ with } \tilde{\mathbf{S}} \in R^N, \tag{4.4}$$

where R^N is the set of all the possible real N-tuples. Finally, $\tilde{\mathbf{S}}$ is rounded to the closest integer so that a solution $\hat{\mathbf{S}}$ of the original problem of Eq. (4.2) is derived. The ZF, also known as Babai estimate [74], $\hat{\mathbf{S}}$ is given by

$$\hat{\mathbf{S}} = \left\lfloor \tilde{\mathbf{S}} \right\rceil = \left\lfloor \mathbf{M}^{-1}\mathbf{R} \right\rceil, \ \hat{\mathbf{S}} \in Z^N, \tag{4.5}$$

where Z^N is the set of the integer N-tuples and $\lfloor \cdot \rceil$ denotes the slice operator.

Despite its polynomial complexity, mainly determined by $\mathbf{M}$ inversion that is $O(N^3)$, ZF error performance is suboptimal. While ZF eliminates interference, as it renders $\mathbf{M}$ to the identity matrix, it multiplies the noise vector with the inverse of the projections matrix $\mathbf{M}^{-1}$. As a result, the noise effect could be overly increased depending on $\mathbf{M}$ properties. In particular, as $\mathbf{M}$ eigenvalues, or equivalently its determinant, become very small the noise is expected to grow and the performance of the detection scheme deteriorates.

Finally, another limitation of this technique is the inversion requirement for the matrix $\mathbf{M}$ that for SEFDM tends to be one numerically singular and consequently non-invertible, as the number of the carriers increases and/or their frequency separation decreases.

4.3   Iterative Cancellation (IC)

For the GS based SEFDM system, Eq. (4.1) is analytically written as

$$
\begin{bmatrix} R_1 \\ \vdots \\ R_{N-1} \\ R_N \end{bmatrix} = \begin{bmatrix} m_{11} & \cdots & m_{1N-1} & m_{1N} \\ \vdots & \ddots & \vdots & \vdots \\ 0 & \cdots & m_{N-1N-1} & m_{N-1N} \\ 0 & \cdots & 0 & m_{NN} \end{bmatrix} \begin{bmatrix} S_1 \\ \vdots \\ S_{N-1} \\ S_N \end{bmatrix} + \begin{bmatrix} n_1 \\ \vdots \\ n_{N-1} \\ n_N \end{bmatrix}.
$$
(4.6)

Noticing $\mathbf{M}$ is triangular (see section 3.5.5), an iterative detector could be applied. Starting from the Nth element, the estimate $\hat{S}_N$ of the Nth transmit symbol is

$$
\hat{S}_N = \left\lfloor \frac{R_N}{m_{NN}} \right\rceil.
$$
(4.7)

Then, the estimate $\hat{S}_{N-1}$ of the $N-1$ symbol is calculated from Eq. (4.6) after the subtraction of the interference due to S_N as

$$
\hat{S}_{N-1} = \left\lfloor \frac{1}{m_{N-1N-1}} \left(R_{N-1} - m_{N-1N}\hat{S}_N \right) \right\rceil.
$$
(4.8)

The same process is repeated backwards until the first element. The estimate of the ith element, $i = 1, \ldots, N$, is given by the recursive formula

$$
\hat{S}_i = \left\lfloor \frac{1}{m_{ii}} \left(R_i - \sum_{j=i+1}^{N} m_{ij}\hat{S}_j \right) \right\rceil.
$$
(4.9)

For a first order estimation of the complexity we take the simple assumption that division, multiplication, addition or subtraction count for one flop (i.e. floating operation) each. Hence, the calculation of the $\hat{S}_i$ element requires $2(N-i)+1$ flops. The total number I of flops performed for the detection of an SEFDM symbol is

$$
\begin{aligned}
\mathrm{I} &= \sum_{i=1}^{N} (2(N-i)+1) = \sum_{i=1}^{N} (2N+1) - 2\sum_{i=1}^{N} i \Leftrightarrow \\
\mathrm{I} &= 2N^2 + N - 2\frac{N(N+1)}{2} = N^2 - N.
\end{aligned}
$$
(4.10)

Consequently, the complexity of this iterative method is quadratic, i.e. $O(N^2)$, that is lower than the cubic complexity of ZF.

4.4   IC using a Lowdin base (IC-Lo)

In Chapter 3, it was shown that the Lowdin orthonormalisation generates a set of vectors that resemble mostly to the SEFDM carriers in the least square sense. It was also demonstrated by simulations, that the result of this similarity is that the size of the squares of the diagonal elements m_{ii}, $i = 1, \ldots, N$, of the projections matrix $\mathbf{M}$ is larger than in a GS based SEFDM. Hence, it appears that more energy is assigned to the useful terms and less to the interfering products. Driven by this observation, the following heuristic is proposed and tested:

- First, project the received signal onto a Lowdin generated base. Consequently, a Hermitian $\mathbf{M}$ is generated;

- Set $m_{ij} = 0$ for $i > j$, i.e. cancel all the interfering terms that are due to the $\mathbf{M}$ elements that lie below its diagonal;

- Apply the IC method described in section 4.3.

To clarify the concept, the following simple numerical example is given: for an SEFDM system with $N = 4$ and $\alpha = 0.8$, the algorithm generates first the projections matrix following the Lowdin method. As a result, $\mathbf{M}$ is

$$
\mathbf{M} = \begin{bmatrix} 0.98 & -0.1 + 0.07i & -0.03 + 0.10i & 0.02 + 0.07i \\ \text{-0.1-0.07i} & 0.97 & -0.1 + 0.07i & -0.03 + 0.1i \\ \text{-0.03-0.1i} & \text{-0.1-0.07i} & 0.97 & -0.1 + 0.07i \\ \text{0.02-0.07i} & \text{-0.03-0.1i} & \text{-0.1-0.07i} & 0.98 \end{bmatrix}.
$$

Then, the shadowed part of the matrix will be forced to zero resulting into

$$
\mathbf{M} = \begin{bmatrix} 0.98 & -0.1 + 0.07i & -0.03 + 0.1i & 0.02 + 0.07i \\ 0 & 0.97 & -0.1 + 0.07i & -0.03 + 0.1i \\ 0 & 0 & 0.97 & -0.1 + 0.07i \\ 0 & 0 & 0 & 0.98 \end{bmatrix}.
$$

Finally, the iterative process of section 4.3 is applied. For example, if $\mathbf{S}$ and $\mathbf{R}$ are respectively

$$\mathbf{S} = \begin{bmatrix} -1 \\ +1 \\ -1 \\ -1 \end{bmatrix} \text{ and } \mathbf{R} = \begin{bmatrix} 0.45 - 0.61i \\ 0.19 + 1.37i \\ 0.79 - 0.95i \\ 0.09 - 1.03i \end{bmatrix},$$

the estimate of the last transmit symbol will be

$$\hat{S}_4 = \left\lfloor \frac{R_4}{m_{44}} \right\rceil = \left\lfloor \frac{0.09 - 1.03i}{0.98} \right\rceil = \lfloor 0.0926 - 1.0483i \rceil = -1.$$

The process is iterated for the remaining of $\hat{S}_i$. It is notable that uniform and close to unity values of the diagonal correlation coefficients are generated by the projections of the SEFDM carriers onto the Lowdin base.

4.5   Numerical Results

A set of initial simulations were run in order to test the error performance of the linear detection techniques described in the previous paragraphs. In particular, the bit error rate (BER) of ZF, IC and IC-Lo are measured for SEFDM signals with N varying from 8 to 32 and modulated by BPSK or QPSK symbols. Results are taken for different values of the normalised sub-carriers frequency separation $\alpha = \Delta fT$, ranging from 1, i.e. OFDM, to 0.5, i.e. FOFDM. The power of the additive noise in the SEFDM system is varied by setting E_b/N_0 from 0 to 7 dB. All the results are averaged over at least 10000 random generations of SEFDM symbols. Finally, IMGS is used as an orthonormalisation method for ZF and IC methods while the Lowdin method is used only for IC.

Figs 4.1 and 4.2 demonstrate BER curves versus α for BPSK and QPSK SEFDM, respectively, for a fixed value of $E_b/N_0 = 5$dB. The SEFDM ML error rate result is taken as the upper bound of the SEFDM detectors performance.
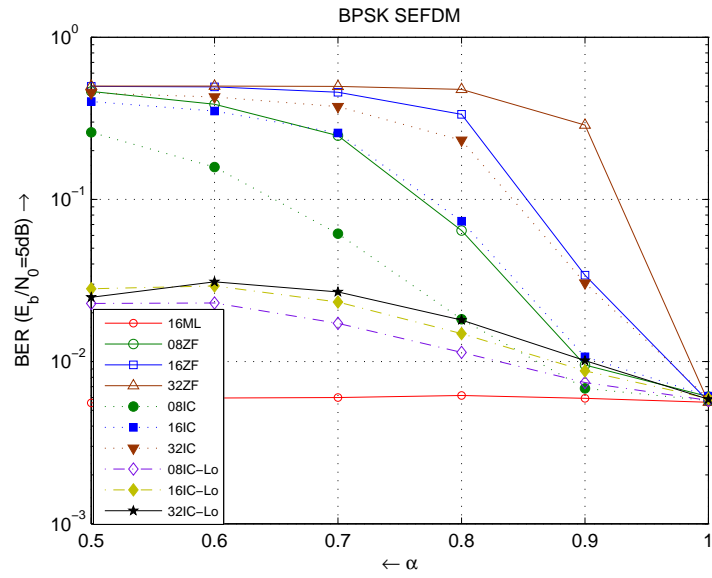
Figure 4.1: Linear detections error performance versus α for BPSK modulated $8 \rightarrow 32$ SEFDM carriers.
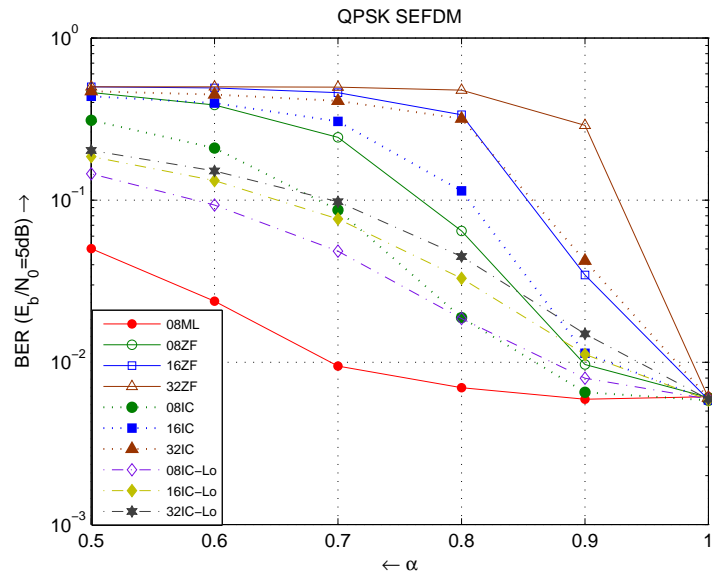
Figure 4.2: Linear detections error performance versus α for QPSK modulated $8 \rightarrow 32$ SEFDM carriers.

It is obvious that for both modulations the performance of all three methods is inferior as opposed to the ML detection. ZF is completely inefficient even for a small $N = 8$ due to the large noise enhancement. The condition of the projections matrix $\mathbf{M}$ deteriorates with the increase of N and/or α reduction, the ZF error rate overly degrades. IC method appears to perform quite better than ZF for $N = 8, 16$. This is attributed to the avoidance of $\mathbf{M}$ inversion that suffers from numerical inaccuracies (see section 3.5.5). However, for a larger, $N = 32$, signal dimension and $\alpha < 0.8$ performs similarly to ZF. This is because according to Eq. (4.7) the pre-slice estimates involve a high noise amplification if the $\mathbf{M}$ diagonal elements are very small. In addition, due to its iterative nature, IC suffers the effect of propagation of errors. Thus, an erroneous decision at the first symbol additively encumbers the detection of the remaining data symbols.

Finally, it is notable that the proposed IC-Lo heuristic has superior performance to ZF and IC, especially in the BPSK SEFDM detection. Nevertheless, IC-Lo results significantly deviate from the optimal detection curve, too.

Figs. 4.3 and 4.4 illustrate BER curves versus E_b/N_0, for $\alpha = 0.8$ corresponding to the dual Mazo limit (see Chapters 2, 3). The theoretical BER curves of single carrier (SC) BPSK and QPSK detections were used as a measure of comparison. It appears again that IC-Lo prevails among the examined linear detections. Nevertheless, all three methods introduce significant error penalties relative to the ideal case even for a small, $N = 16$, SEFDM signal.

4.6   Least Squares (LS) problems Regularisations

Noticing that the singular values of the SEFDM matrix $\mathbf{M}$ are decreasing gradually (see section 3.5.5), the unconstrained detection problem of Eq. (4.3) is
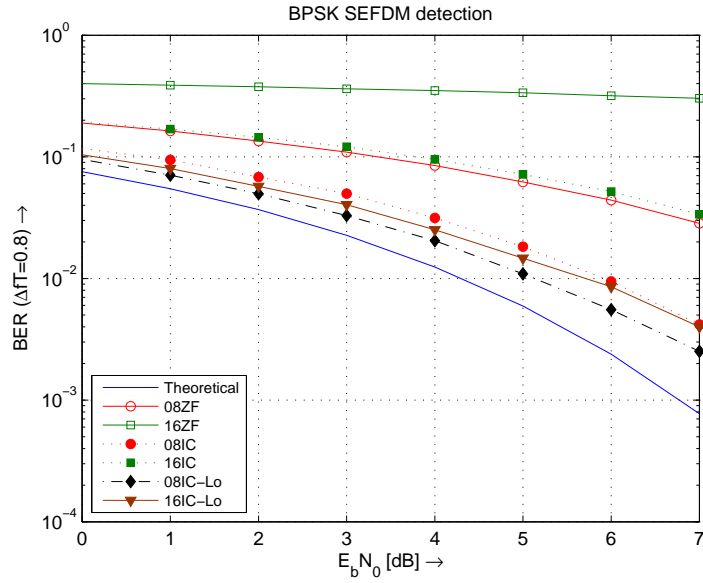
Figure 4.3: Linear detections error performance versus E_b/N_0 for BPSK modulated 8 and 16 SEFDM carriers. α was equal to 0.8.
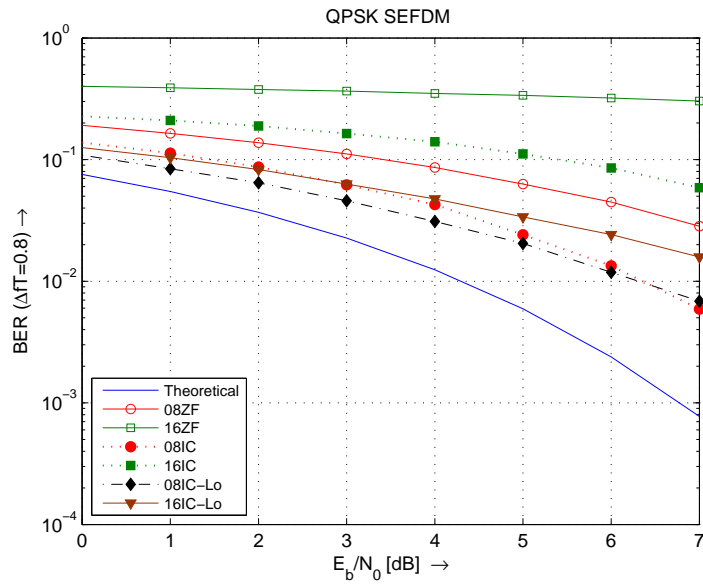
Figure 4.4: Linear detections error performance versus E_b/N_0 for QPSK modulated 8 and 16 SEFDM carriers. α was equal to 0.8.

identified as an ill-posed LS problem [1]. A tool for studying and solving such problems is the Singular Value Decomposition (SVD) of the coefficients matrix of the respective linear model [75]. The ordinary SVD of $\mathbf{M}$ is

$$\mathbf{M} = \mathbf{U\Sigma V}^H. \tag{4.11}$$

where $\mathbf{U} = [\mathbf{u}_1 \; \mathbf{u}_2 \ldots \mathbf{u_N}]$ and $\mathbf{V} = [\mathbf{v}_1 \; \mathbf{v}_2 \ldots \mathbf{v}_N]$ are the left and right singular vectors matrices, respectively, and $\mathbf{\Sigma}$ is a diagonal matrix containing the singular values σ_i of $\mathbf{M}$.

The inverse of $\mathbf{M}$ can be derived by SVD in the following

$$\mathbf{M}^{-1} = \left(\mathbf{U\Sigma V}^H\right)^{-1} = \mathbf{V\Sigma}^{-1}\mathbf{U}^H = \sum_{i=1}^{N} \frac{\mathbf{v}_i \mathbf{u}_i{}^H}{\sigma_i}. \tag{4.12}$$

Then, the solution of the unconstrained SEFDM problem given in Eq. 4.4 is written in terms of SVD as

$$\tilde{\mathbf{S}} = \mathbf{M}^{-1}\mathbf{R} = \sum_{i=1}^{N} \frac{\mathbf{v}_i \mathbf{R} \mathbf{u}_i{}^H}{\sigma_i}. \tag{4.13}$$

Eq. (4.13) shows that $\tilde{\mathbf{S}}$ is a linear combination of $\mathbf{M}$ singular vectors weighted by its singular values. As these values decay rapidly to zero, any perturbation (noise in terms of AWGN or numerical inaccuracies) of the statistics vector $\mathbf{R}$ from the transmit symbol $\mathbf{S}$ will be overly enhanced and the solution $\tilde{\mathbf{S}}$ will be extremely large. As a result, the slice operator will introduce a significant error in the SEFDM detection hard decisions.

Notwithstanding, an improvement could be achieved by applying suitable regularisation techniques [75]. The following sections examine Tikhonov regularisation that is the most well known and most commonly used.

---

[1] Most of LS problems with ill conditioned matrices belong to two main classes: rank-deficient problems that are characterised by coefficients matrices with a well identified cluster of very small singular values; and discrete ill-posed problems where the singular values of the coefficients matrix decay gradually to zero. Simulation results in section 3.5.5 demonstrate that the unconstrained SEFDM detection exhibits the properties of an ill posed problem [75].

4.6.1 Tikhonov Regularisation

By Tikhonov, the LS problem of Eq. (4.3) is regularised by adding in the cost function a penalty term that provides some further information about $\tilde{\mathbf{S}}$. The general Tikhonov LS problem formulation is

$$\text{min. } \|\mathbf{R} - \mathbf{M}\mathbf{S}\|_2^2 + \epsilon\mathbf{\Omega}^2(\mathbf{S}). \tag{4.14}$$

where ϵ is called the regulator and $\mathbf{\Omega}^2(\mathbf{S})$ is called the smoothing norm. The latter is usually given as $\|\mathbf{L}\mathbf{S}\|_2^2$ where $\mathbf{L}$ is the regulator matrix. For simplicity, $\mathbf{L}$ is assumed to be equal to the identity matrix $\mathbf{I}$. Thus, the Tikhonov regularisation reduces to

$$\text{min. } \|\mathbf{R} - \mathbf{M}\mathbf{S}\|_2^2 + \epsilon\|\mathbf{S}\|_2^2. \tag{4.15}$$

The solution of Eq. (4.15) is [75]

$$\tilde{\mathbf{S}} = (\mathbf{M}^H\mathbf{M} + \epsilon\mathbf{I})^{-1}\mathbf{M}^H\mathbf{R}. \tag{4.16}$$

or in SVD form,

$$\begin{aligned}
\tilde{\mathbf{S}} &= \sum_{i=1}^{N} f_i \frac{v_i \mathbf{R} u_i{}^H}{\sigma_i}, \\
f_i &= \frac{\sigma_i^2}{\sigma_i^2 + \epsilon}.
\end{aligned} \tag{4.17}$$

Hence, the matrix $(\mathbf{M}^H\mathbf{M} + \epsilon\mathbf{I})^{-1}\mathbf{M}^H$ will be the regularised inverse. From Eqs (4.16), (4.18) two conclusions could be deduced: first, the regularised inverse is never singular; second, the impact of $\mathbf{M}$ small singular values could be mitigated by picking the proper regulator value, i.e. small singular values σ_i could be redeemed if the filtering factors f_i are conveniently set.

On the other hand, despite the mitigation of the noise effect, a large regulator also increases the cost norm $\left\|\mathbf{R} - \mathbf{M}\tilde{\mathbf{S}}\right\|_2^2$ by adding the regularisation term. In other words the regularisation introduces a kind of error to the initial LS problem. Thus, a proper choice of the regulator value should take into account

the trade off between the regularisation noise introduced in the system and the mitigation of the noise amplification that already exists in the system.

The literature is rich of methods (e.g., L-curve, min norm product, U-curve and others) determining the optimum regulator in the unconstrained LS problem Eq. (4.3), i.e. where the solution can be any real number [75], [76], [77], [78]. However, to the author's knowledge there is no such a method for applications that solve the integer LS (ILS) problem such as the SEFDM detection. The section below describes the regulator effect on the linear detection.

4.6.2 Linear detection and the regulator effect

In order to investigate the effect of the regularisation process, simulations are performed for noiseless ($E_b/N_0 = \infty$) and noisy ($E_b/N_0 = 5$dB) SEFDM systems. The constellations of the transmitted symbols and the solutions (ZF and regularised) of the unconstrained LS problem, i.e. before the slice operator, are compared. In addition, small and large values of the regulator ϵ are applied in order to observe the result of weak and strong regularisations, respectively. Finally, the constellation of the outputs of the receiver correlators are used to study the internal interference of the system.

Fig. 4.5 illustrates a comparison between a noiseless OFDM signal of 32 carriers and an equivalent, in terms of symbol rate and carriers, SEFDM that suffers from relatively small orthogonality violation at $\alpha = 0.9$. It is easily deduced that in the ideal OFDM case the projections matrix reduces to an N-dimensional identity matrix, $\mathbf{I}$. Consequently, the correlators recover the transmitted symbols exactly. However, when the regularisation is applied to the ideal matrix it can be seen that the larger the regulator, the more the solution points are biased towards the center of the constellation diagram.

This could be explained simply by considering Eq. (4.16) after setting $\mathbf{M} = \mathbf{I}_N$

$$\tilde{\mathbf{S}} \quad = \quad (\mathbf{I}^H\mathbf{I}_N + \epsilon\mathbf{I})^{-1}\mathbf{I}^H\mathbf{R}, \qquad (4.18)$$
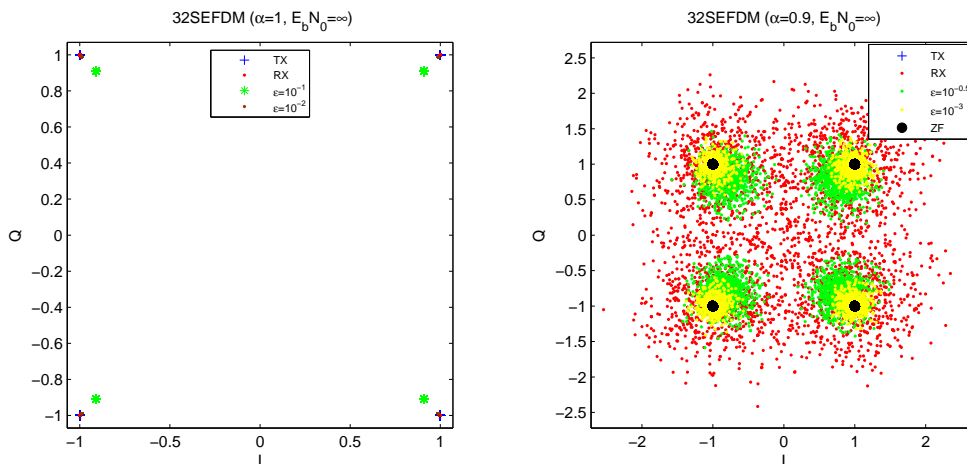
(a) Noiseless OFDM.

(b) Noiseless SEFDM ($\alpha = 0.9$).

Figure 4.5: Constellation diagram for a noiseless 32 SEFDM signal for an orthogonal ($\alpha = 1$) separation of carriers (left) and a small violation ($\alpha = 0.9$) of orthogonality (right).

$$\tilde{S}_i \;\; = \;\; \frac{S_i}{1 + \epsilon}, \; i = 1, \ldots, N.$$

However, from Fig. 4.5 (a), it is clear that for a small loss of orthogonality even in the ideal channel (i.e. without noise and fading), the correlators outputs (red points) deviate from the transmit constellation points due to system internal interference. Notwithstanding, the matrix is invertible and ZF detection that achieves the exact solution (black points) can be implemented. As far as the regularised solution is concerned, it seems that it works better with a small regulator (yellow-light points) since a large regularisation (green-dark points) decreases the decision area of the slice operator.

Simulations were repeated for a matrix with worse properties $\alpha = 0.75$. Fig. 4.6 depicts results that certify that the system interference increases with the deterioration of matrix **M** properties. Nevertheless, the exact solution can be still achieved by the inversion of the matrix which is still computationally
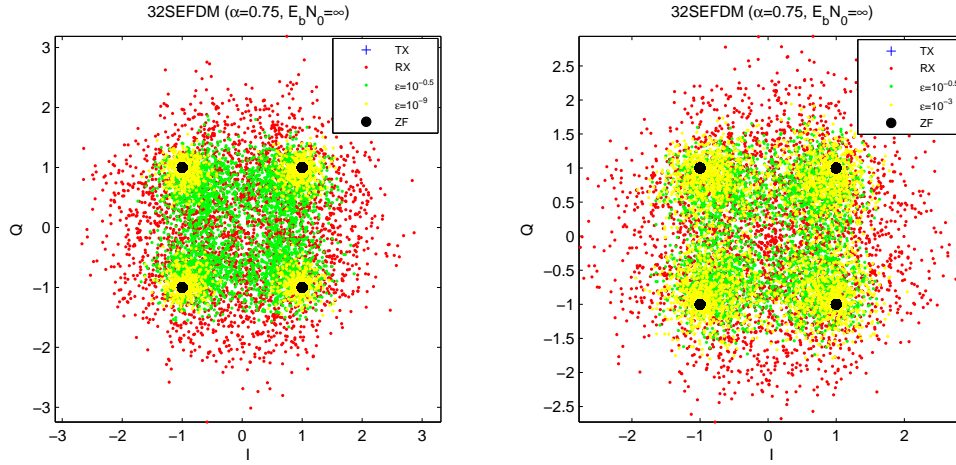
(a) Small regulator - $\epsilon = 10^{-9}$.

(b) Large regulator - $\epsilon = 10^{-3}$.

Figure 4.6: Constellations for a noiseless 32SEFDM with $\alpha = 0.75$. A small ($\epsilon = 10^{-9}$) or a large ($\epsilon = 10^{-3}$) regulator is applied. ϵ is also set to $10^{0.5}$, corresponding to the $\frac{1}{E_b/N_0}$ value for $E_b/N_0 = 5$ dB.

manageable. In addition, it appears that the regularised solution points are more concentrated around the ideal constellations when the regulator is small. This is logical since for $\epsilon \to \infty$ this process reduces to the ZF detection.

Consequently, it could be concluded that in a noiseless environment the exact solution could be achieved by ZF detection as long as the projections matrix is numerically invertible. Furthermore, a regularised solution appears to be better when the regulator is small because its points are better distributed in the constellation diagram. On the contrary, when the regularisation becomes stronger the points are moved towards the diagram center reducing consequently the effective decision area.

It is interesting to investigate whether these results are repeated in case of a noisy ($E_b/N_0 = 5$ dB) SEFDM signal. Fig. 4.7 shows that in the OFDM case the regularised and ZF solutions are similar. A great change is observed though when the orthogonality principle is violated, i.e. $\alpha = 0.9$. It is clear that

(a) OFDM.

(b) SEFDM-$\alpha = 0.9$.
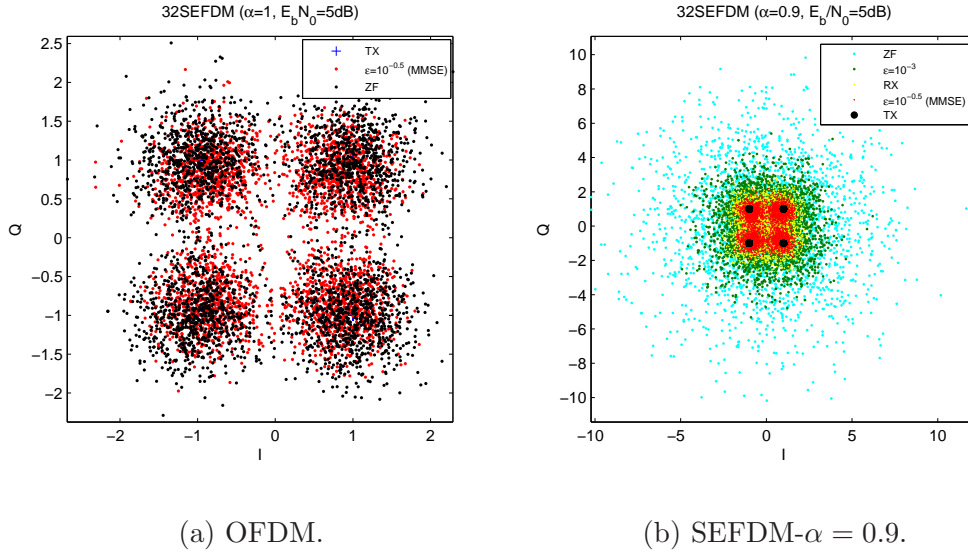
Figure 4.7: Constellation diagram for a 32SEFDM signal for an orthogonal ($\alpha = 1$) separation of carriers (left) and a small violation ($\alpha = 0.9$) of orthogonality (right) in presence of noise, $E_b/N_0 = 5$ dB.

the noise is overly amplified in ZF due to the bad conditioning of **M** matrix. On the contrary, the regularised solution appears to work better with a large regulator. This is expected since as the regularisation grows the condition the regularised inverse is improved. Consecutively, the noise enhancement is less.

To resume, it became clear that a weak regulator should be preferred in case of a noiseless environment since it does not bias significantly the exact solution. On the other hand, a large regulator appears to be better for the detection of noisy SEFDM signals since the points of the regularised solution appear to be less spread. Thus, a slice operator would probably generate less wrong decisions.

4.7 MMSE SEFDM detection

In order to mitigate the complexity of ML and reduce the noise enhancement in ZF, the performance of the Linear MMSE detection is further investigated.

Such comprises the following optimisation problem

$$
\begin{aligned}
\text{min.} \quad & \mathrm{E}\left\{\left(\mathbf{S}-\hat{\mathbf{S}}\right)^{2}\right\}, \\
\text{s.t.} \quad & \mathbf{S} \in Q^{N},
\end{aligned} \tag{4.19}
$$

where $\hat{\mathbf{S}}$ is the MMSE estimate and $\mathrm{E}\left\{\cdot\right\}$ denotes the expected (or mean) value. Ignoring the constraint of $\mathbf{S} \in Q^{N}$, Eq. (4.19) reduces to

$$
\text{min. } \mathrm{E}\left\{\left(\mathbf{S}-\tilde{\mathbf{S}}\right)^{2}\right\}, \tag{4.20}
$$

where $\tilde{\mathbf{S}}$ is the solution of the unconstrained MMSE problem. Assuming further that $\tilde{\mathbf{S}}$ is generated after multiplying (equivalent to filtering) the statistics vector $\mathbf{R}$ with a matrix $\mathbf{G}$, Eq. (4.19) is reduced to

$$
\text{min. } \mathrm{E}\left\{(\mathbf{S}-\mathbf{G R})^{2}\right\}. \tag{4.21}
$$

According to the orthogonality principle [35], the error of the unconstrained linear MMSE estimation is uncorrelated with the observation vector $\mathbf{R}$. Therefore, the following condition must be met [71]

$$
\mathrm{E}\left\{\mathbf{R}(\mathbf{S}-\tilde{\mathbf{S}})^{H}\right\}=0 \Longleftrightarrow \mathrm{E}\left\{\mathbf{R R}^{H}\right\} \mathbf{G}=\mathrm{E}\left\{\mathbf{R S}^{H}\right\}. \tag{4.22}
$$

Replacing $\mathbf{R}$ with $\mathbf{M S}+\mathbf{N}$, according to the linear statistical model, the mean terms of the RHS and LHS of Eq. (4.22) are reduced to

$$
\begin{aligned}
\mathrm{E}\left\{\mathbf{R R}^{H}\right\}=\mathrm{E}\left\{\mathbf{M S S}^{H}\mathbf{M}^{H}\right\} \quad &+\quad \mathrm{E}\left\{\mathbf{N N}^{H}\right\}+\mathrm{E}\left\{\mathbf{M S N}^{H}\right\}+\mathrm{E}\left\{\mathbf{N S}^{H}\mathbf{M}^{H}\right\}, \\
\mathrm{E}\left\{\mathbf{R S}^{H}\right\} \quad &=\quad \mathrm{E}\left\{\mathbf{M S S}^{H}\right\}+\mathrm{E}\left\{\mathbf{N S}^{H}\right\}.
\end{aligned} \tag{4.23}
$$

$\mathbf{M}$ is deterministic; assuming the noise mean value $\mathrm{E}\left\{\mathbf{N}\right\}$ is zero and the noise and the signal covariance matrices $\mathrm{E}\left\{\mathbf{N N}^{H}\right\}$ and $\mathrm{E}\left\{\mathbf{S S}^{H}\right\}$ are equal to $\sigma^{2}\mathbf{I}$ and $\sigma_{s}^{2}\mathbf{I}$, respectively, it is concluded that

$$
\begin{aligned}
\mathrm{E}\left\{\mathbf{R R}^{H}\right\} \quad &=\quad \mathbf{M M}^{H}+\frac{\sigma^{2}}{\sigma_{s}^{2}}\mathbf{I}, \\
\mathrm{E}\left\{\mathbf{R S}^{H}\right\} \quad &=\quad \mathbf{M},
\end{aligned} \tag{4.24}
$$

where σ^2 and σ_s^2 are the noise and the signal power, respectively. From Eqs (4.22) and (4.24), the MMSE matrix $\mathbf{G}$ is derived as

$$\mathbf{G} = \mathbf{M}^H \left(\mathbf{MM}^H + \frac{\sigma^2}{\sigma_s^2}\mathbf{I} \right)^{-1}. \tag{4.25}$$

Consequently, $\tilde{\mathbf{S}}$ is given by

$$\tilde{\mathbf{S}} = \mathbf{M}^H \left(\mathbf{MM}^H + \frac{\sigma^2}{\sigma_s^2}\mathbf{I} \right)^{-1} \mathbf{R}, \tag{4.26}$$

where the ratio $\frac{\sigma^2}{\sigma_s^2}$ represents the inverse of the Signal to Noise Power ratio (SNR) [79], [80].

Finally, to recover the solution of the initial SEFDM constrained problem of Eq. (4.19) a slicing operator is applied on the outcome of Eq. (4.26), i.e.

$$\hat{\mathbf{S}} = \left\lfloor \mathbf{M}^H \left(\mathbf{MM}^H + \frac{\sigma^2}{\sigma_s^2}\mathbf{I} \right)^{-1} \mathbf{R} \right\rceil. \tag{4.27}$$

It is clear that in case of zero noise in the system, MMSE reduces to the ZF detection since the term $\mathbf{M}^H \left(\mathbf{MM}^H \right)^{-1}$ is equal to the Moore - Penrose pseudoinverse [53] of matrix $\mathbf{M}$. However, in case of noise presence the MMSE detection constitutes a special case of Tikhonov regularisation where the regularisation term, $\frac{\sigma^2}{\sigma_s^2}\mathbf{I}$, dynamically adapts to the noise level. Consequently, the overall BER performance of MMSE detection is expected to be better than ZF because the noise is less amplified as shown in section 4.6.2. In addition, the MMSE matrix is never singular and consequently MMSE detection is not limited by the singularity of the projections matrix like the ZF method.

Figs 4.8 and 4.9 show simulation results for MMSE detection as opposed to ML and ZF cases. The theoretical BPSK single carrier result [52] serves as a lower bound for the BER vs the E_b/N_0 performance. It is obvious that MMSE appears to be a compromise between ML overly complexity and ZF bad error performance. However, it still performs inefficiently as the number of the carriers increases and/or their frequency separation decreases.
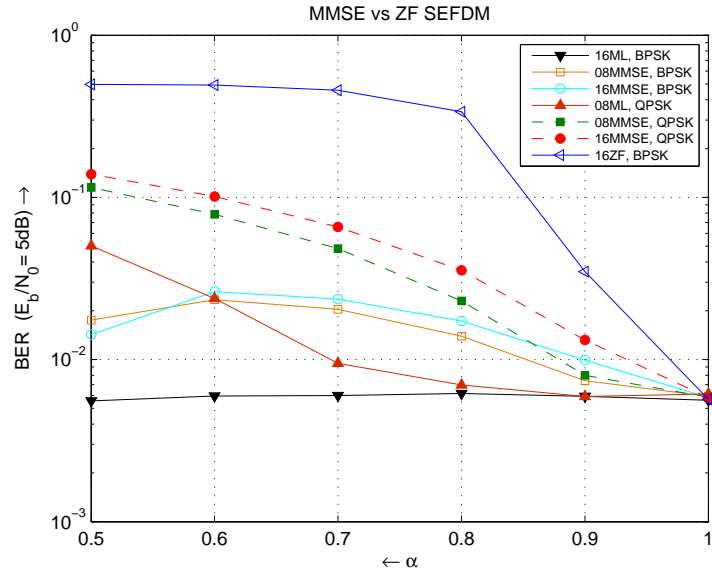
Figure 4.8: MMSE detection BER versus α for BPSK and QPSK modulated $4 \rightarrow 16$ FDM carriers.
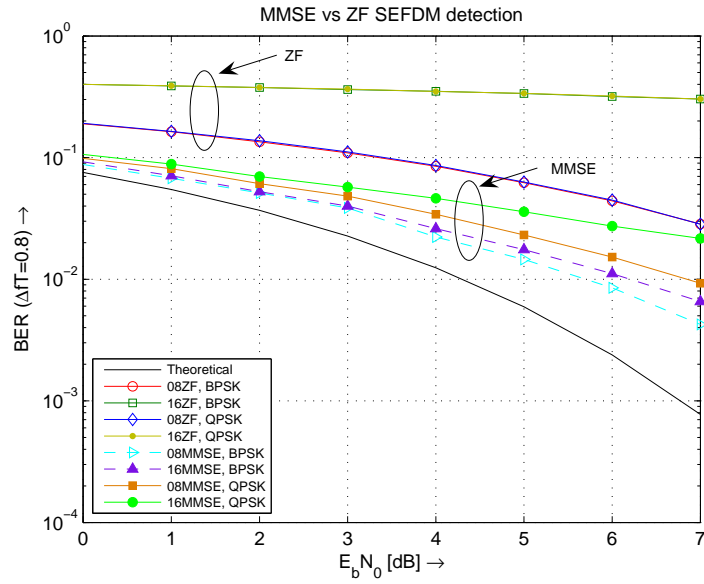
Figure 4.9: MMSE detection BER versus E_b/N_0 for BPSK and QPSK modulated $4 \rightarrow 16$ SEFDM carriers.

4.8 A combination of MMSE and ML

Linear detection techniques are superior to ML in terms of algorithmic complexity at the expense of sub-optimal detection error rates. Motivated by relevant studies in the area of MIMO systems [81], [82] the combination of linear MMSE and brute force ML is proposed as a compromise between them. In particular, the detector of the receiver makes use of the correlators outputs to determine a first estimate $\hat{\mathbf{S}}$ of the SEFDM symbol based on the MMSE criterion and then it applies ML in a small subset of the possible transmitted SEFDM symbols that are close enough to the MMSE estimator. We can define the SEFDM symbols subset as a neighborhood D of the $\tilde{\mathbf{S}}$ vector. In particular, $\mathbf{D}$ is composed from the SEFDM symbols $\mathbf{S_i}$ that meet the following condition

$$\mathbf{S_i} \in D \; if \; d_H(\mathbf{S_i'}, \; \hat{\mathbf{S}}') \leq P,$$
$$P = 0, \ldots, N \log_2 M, \tag{4.28}$$

where d_H is the Hamming distance between the binary version of the SEFDM symbols $\mathbf{S}_i'$ and the binary version of the MMSE estimate $\hat{\mathbf{S}}'$. Consequently, the introduced MMSE-ML detection solves by exhaustive enumeration the following optimisation problem

$$\text{min.} \quad \|\mathbf{R} - \mathbf{MS}\|_2^2,$$
$$\text{s.t.} \quad \mathbf{S} \in D \subset Q^N. \tag{4.29}$$

The algorithmic complexity of the proposed method depends on the number of calculations of both the MMSE and the ML parts of the algorithm. The former has a complexity of polynomial order $O(N^3)$ over the number of carriers N. To determine the complexity of the latter, it is calculated the size of the MMSE neighborhood D, since this is equal to the number of the executed ML comparisons. The length of the expanded binary SEFDM symbols is equal to $N \times \log_2 M$. Consequently, the size of D will be equal to the sum of all possible
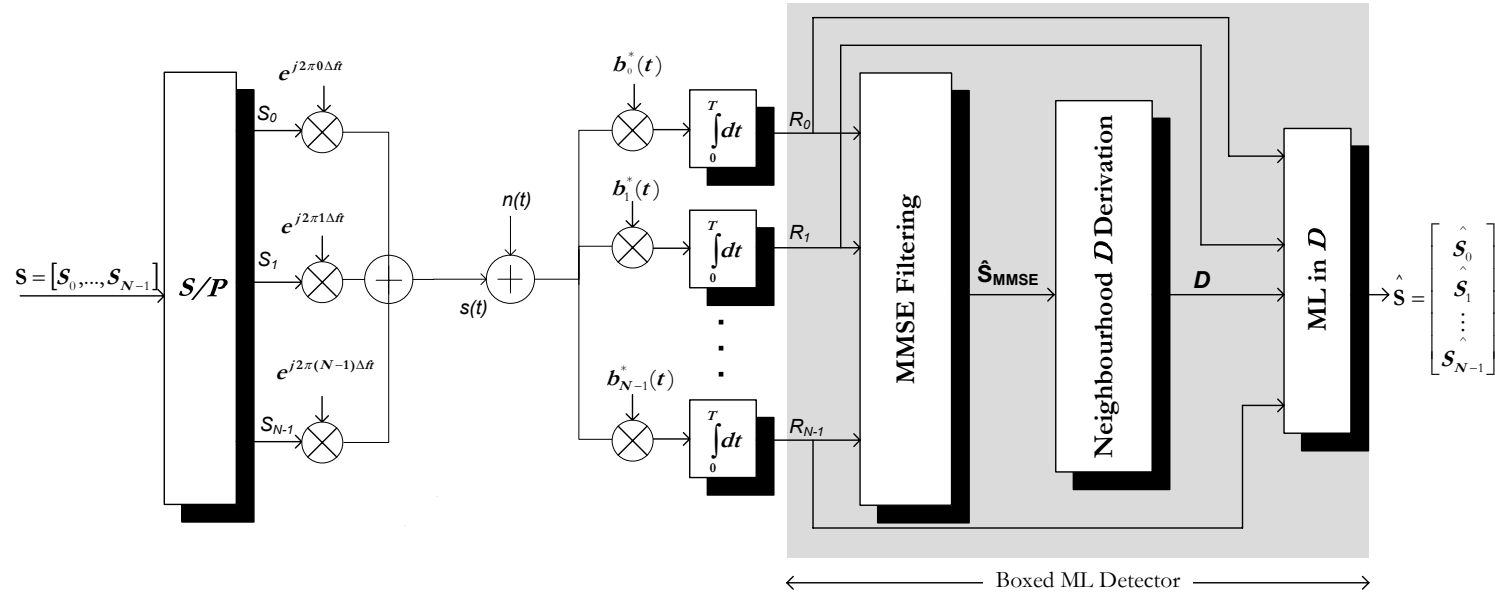
Figure 4.10: The combined MMSE-ML SEFDM System Architecture.

combinations of $N \times \log_2 M$ bits taken d_H at a time with d_H taking values from 1 to P (see Eq. (4.28))

$$size(D) = \sum_{i=1}^{d_H} \binom{N \log_2 M}{i} =$$

$$\sum_{i=1}^{d_H} \frac{(N \log_2 M)!}{(N \log_2 M - i)! i!}, \quad d_H = 1, \dots, P. \tag{4.30}$$

Each of the ML comparisons requires $O(N^2)$ calculations. Thus, the total number of flops required by the local search will be approximately given by

$$N^2 \sum_{i=1}^{d_H} \frac{(N \log_2 M)!}{(N \log_2 M - i)! i!}, \tag{4.31}$$

where $d_H = 1, \dots, P$. It is clear that the order of complexity of the ML part of the combined MMSE-ML will be $O(N^{2+d_H})$. Consequently, the order of complexity of the entire algorithm will be

$$\begin{cases} O(N^3) \text{ for } d_H = 0 \vee d_H = 1 \\ O(N^{2+d_H}), \text{ otherwise.} \end{cases} \tag{4.32}$$

It is apparent that for d_H equal to zero the introduced scheme reduces to MMSE. For d_H equal to unity, the number of necessary comparisons is $N \log_2 M$, as opposed to the M^N comparisons required for the ML implementation over the entire group of SEFDM symbols. Table 4.1 provides the ratio γ of the number of ML over MMSE-ML comparisons for various SEFDM signal dimensions. Simulation tests were performed using MATLAB in order to confirm the theoretical analysis. This work modelling assumed perfect knowledge of the GS basis and that the only channel effect is AWGN. Bit Error Rate (BER) simulations were performed for the proposed MMSE-ML scheme for up to $N = 48$ SEFDM carriers with minimum frequency separation equal to 0.3 of the inverse of the SEFDM symbol period, $\Delta f = \frac{0.3}{T}$, and a fixed value of Energy Per Bit to Noise Density Ratio (E_b/N_0) equal to 5 dB. Carriers were modulated either by real BPSK or complex QPSK symbols. In all simulations, ML and/or ZF detection curves were used as reference points.

	BPSK	BPSK	QPSK	QPSK
Carriers	$\gamma, d_H = 1$	$\gamma, d_H = 2$	$\gamma, d_H = 1$	$\gamma, d_H = 2$
2	2	1.33	4	1.6
4	4	1.60	32	7.11
8	32	7.11	4096	481.88
16	4096	481.88	$> 10^{10}$	$> 8 \times 10^6$

Table 4.1: Ratio γ of ML over the MMSE-ML Comparisons
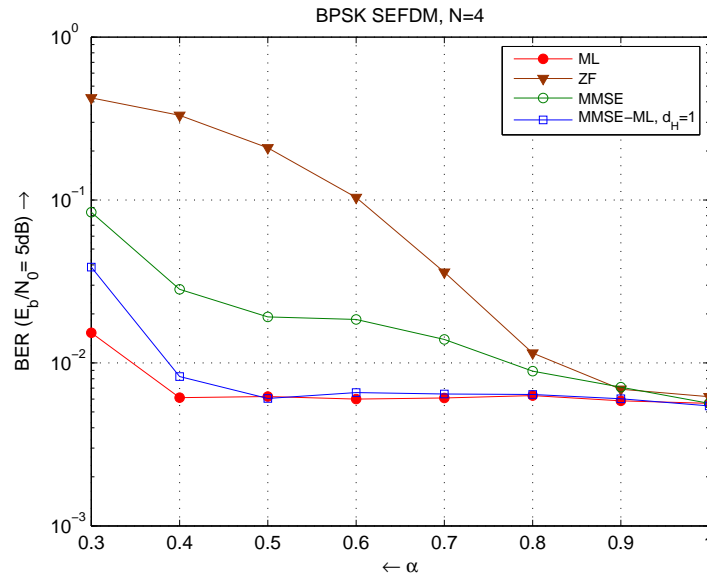
Figure 4.11: BER of MMSE and MMSE-ML detection versus $\alpha = \Delta fT$ for $N = 4$ BPSK SEFDM. E_b/N_0 is 5 dB and $d_H = 1$.

Figs 4.11 and 4.12 show BER versus the carrier distance that is described as a fraction of the inverse of the SEFDM symbol period, ΔfT. Simulations were performed for a small number ($N = 4$) of BPSK and QPSK SEFDM carriers. MMSE-ML measurements were taken with Hamming distance $d_H = 1$ for BPSK carriers and $d_H = \{1, 2\}$ for QPSK carriers.
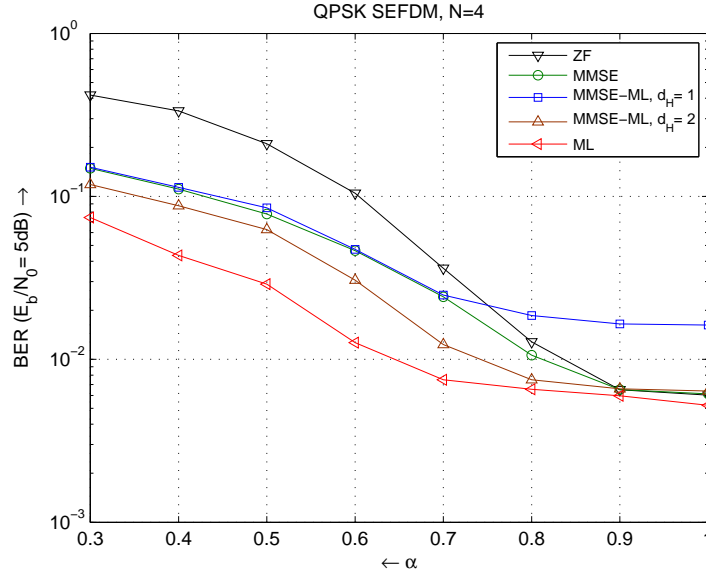
Figure 4.12: BER of MMSE and MMSE-ML detection versus $\alpha = \Delta fT$ for $N = 4$ QPSK SEFDM. E_b/N_0 is 5 dB and $d_H = \{1, 2\}$.

Both figures show that MMSE is superior to ZF but inferior to ML for BPSK and QPSK SEFDM signals. MMSE-ML performs close to ML for BPSK SEFDM carriers. However, the BER in QPSK case depends on the selected Hamming distance.

Further studies were performed for a larger number of BPSK carriers $N = 4, 8, 24, 36, 48$ and an MMSE neighborhood of $2 \times N$ size as derived from Eq. (4.28) with $d_H = 1$. Fig. 4.13 shows that concatenating MMSE-ML detection introduces only a small error penalty as the number of BPSK SEFDM carriers increases.

In addition, BER measurements were taken for various E_b/N_0 values, for a fixed $\Delta fT = 0.75$. Fig. 4.14 shows that BPSK performance almost matches the ML case. On the contrary, Fig. 4.15 shows that in the QPSK case the error performance depends on the length of the selected Hamming distance. For $d_H = 1$, it appears that the proposed heuristic suffers local minima. As a result, MMSE-ML performs worse than MMSE even for a small number of
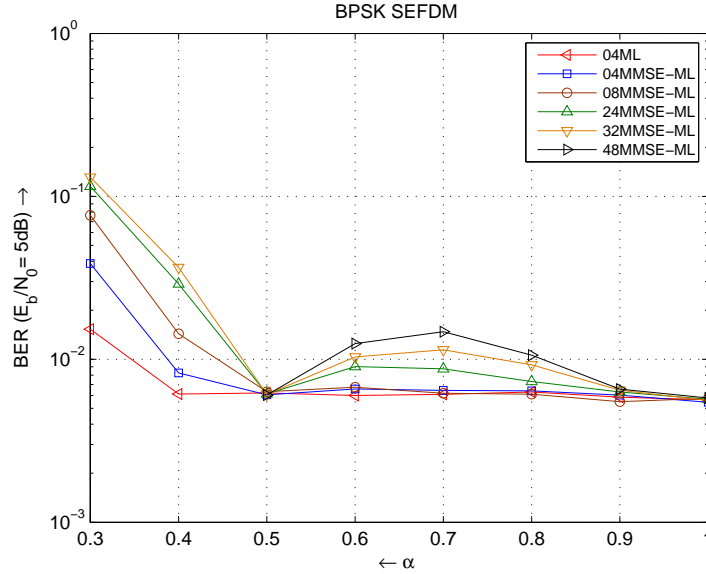
Figure 4.13: BER of MMSE-ML detection versus $\alpha = \Delta fT$ for $N = \{4, 8, 24, 32, 48\}$ SEFDM. E_b/N_0 is 5 dB and $d_H = 1$.

carriers. As the latter increases a larger Hamming distance $(d_H \geq 2)$ is required to improve the single MMSE detection.

To estimate the computational complexity of the proposed methods, the CPU (Pentium (R)4 3GHz) execution time was measured in different simulations scenarios. All simulations implemented the detection of 1000 SEFDM symbols for $E_b/N_0 = 5$ dB and $\Delta fT = 0.75$. In addition, MMSE-ML was evaluated for Hamming distances $d_H = \{1, 2, 3\}$.

Figs 4.16 and 4.17 illustrate a comparison of indicative CPU times between ZF, MMSE and MMSE - ML detection. It is clear that ZF and MMSE require less computational effort. MMSE - ML with d_H equal to unity has simulation time comparable to that of MMSE. However, the order of its complexity increases with the size of the MMSE neighborhood.
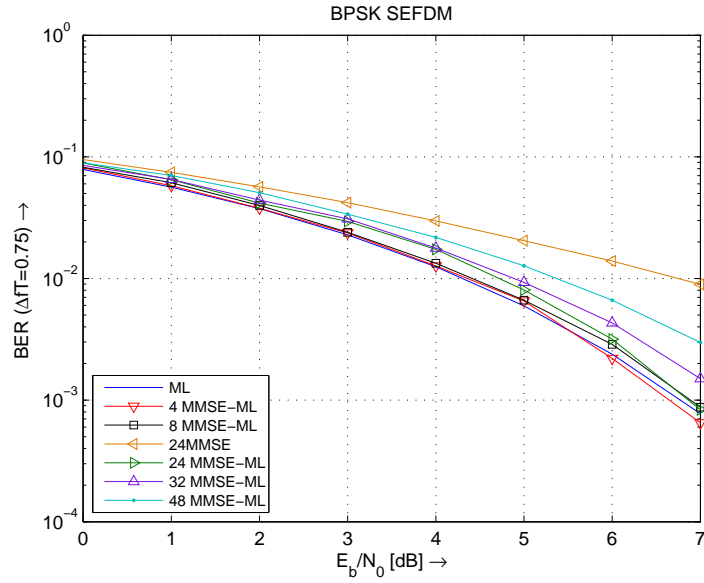
Figure 4.14: BER of MMSE and MMSE-ML detection versus E_b/N_0 for $N = \{4, 8, 24, 36, 48\}$ BPSK SEFDM. $\Delta fT = \frac{0.75}{T}$ and $d_H = 1$.
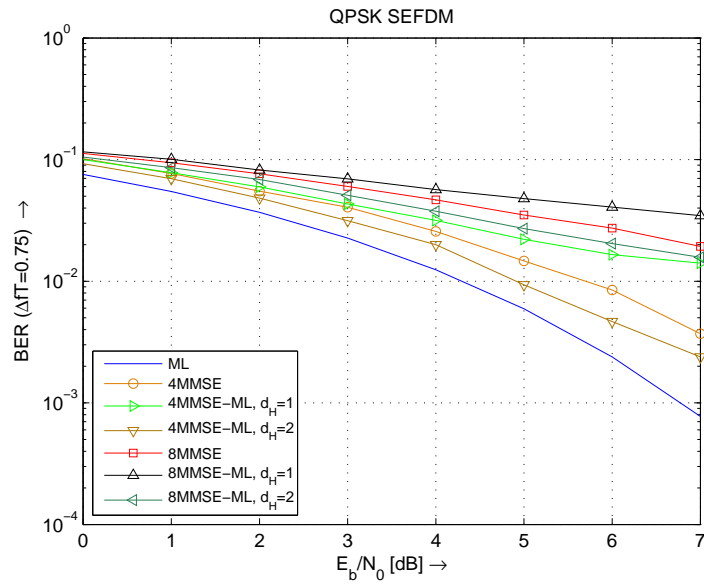
Figure 4.15: BER of MMSE and MMSE-ML detection versus E_b/N_0 for $N = \{2, 4, 8\}$ QPSK SEFDM. $\Delta fT = \frac{0.75}{T}$ and $d_H = \{1, 2\}$.
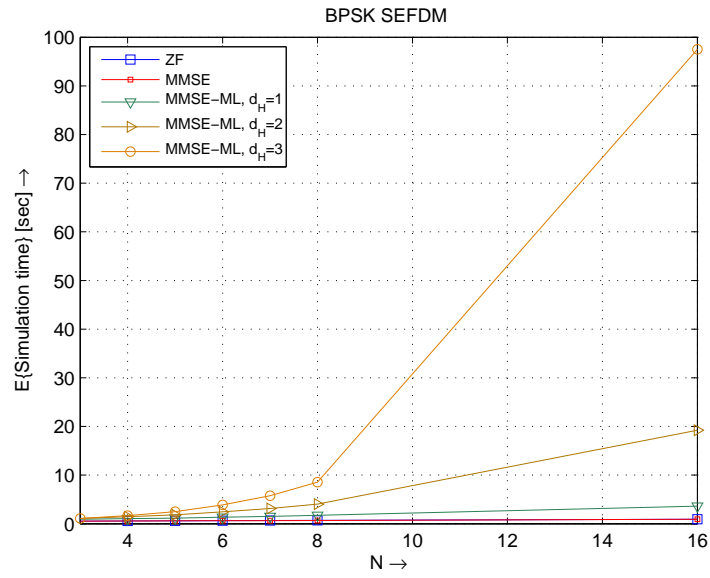
Figure 4.16: CPU execution times for ZF, MMSE, and MMSE-ML detection for BPSK SEFDM symbols of $N = 2$ to 16 carriers. ΔfT set to 0.75.
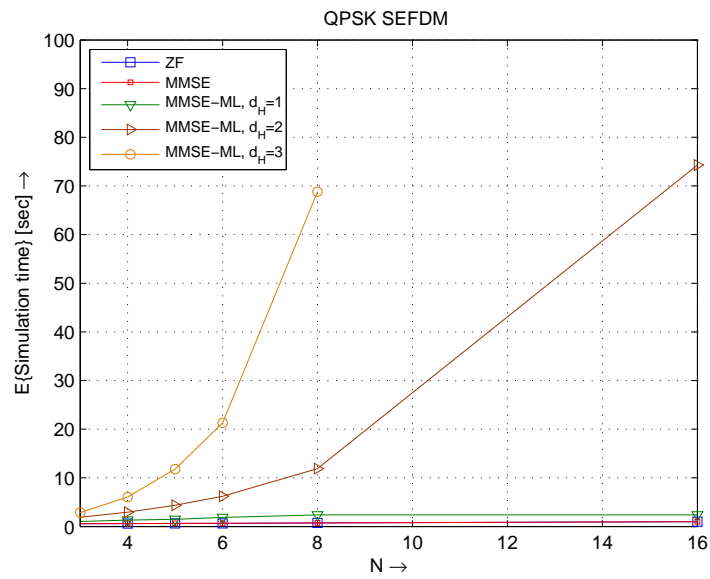
Figure 4.17: CPU execution times for ZF, MMSE, and MMSE-ML detection for QPSK SEFDM symbols of $N = 2$ to 16 carriers. ΔfT set to 0.75.

4.9 Summary and Discussion

In this chapter the error performance of the SEFDM linear detection, using techniques like zero forcing (ZF), as well as iterative cancellation (IC) methods were investigated. Although these methods exhibit a reasonable complexity for medium size SEFDM, they result in a big degradation in their error performance due to either $\mathbf{M}$ ill - conditioning and/or the error in the cancellation process, respectively. Therefore, regularisation techniques that could partially amend $\mathbf{M}$ condition were considered and consecutively a minimum mean squared error (MMSE) detection was applied. The latter technique appears to be significantly superior, in terms of error performance, to ZF.

However, the MMSE detection error rate still degrades with the increase in N and/or the decrease in Δf. Consequently, a combination of MMSE with brute force ML was proposed as a sufficient compromise between ML error performance and MMSE algorithmic cost efficiency. This new method performs a local search around a first MMSE estimate $\hat{\mathbf{S}}$. The extent of this search depends on a predefined parameter that constrains the Hamming distance between $\hat{\mathbf{S}}$ and the vectors - hypotheses that should be enumerated. Although MMSE-ML was expected to be sub-optimal since it suffers from local minima, it appeared to perform reliably and with affordable complexity for BPSK SEFDM with up to $N = 48$ carries. Notwithstanding, for higher constellations, e.g. 4-QAM, the method seemed to be computationally inefficient due to the larger number of enumerations that was required for a good error performance.

Chapter 5

Sphere decoders

5.1 Introduction

As already seen in the previous Chapters 3 and 4, the detection of the SEFDM signals in the system proposed in [29] reduces to an optimisation problem with discrete inputs. Moreover, if the information symbols have integer inphase (I) and/or quadrature (Q) components, the SEFDM detection becomes an Integer Least Squares problem that is well known to be NP hard to solve by applying an exhaustive search over the entire feasible set [86]. Consequently, approaches other than a brute force ML must be followed so that a practically fast detection for the SEFDM is met. Chapter 4 investigated linear detection techniques like ZF and MMSE that are based on the constraints' relaxation of the ML optimisation problem. It has been shown that although such methods offer solutions of fixed and polynomially bounded complexity, they suffer from the introduction of a severe error penalty. Consequently, they are inappropriate for the SEFDM detection since their error performance considerably degrades with the increase of the deliberate overlapping of the transmitted signal sub-bands.

This chapter is concerned with developing a new approach to address the complexity - error rate issue discussed above, but from a different perspective; the initial SEFDM ML detection program is not relaxed but it is attempted

to be solved optimally by splitting the problem of the overlapped SEFDM carriers detection into a number of separate sequential steps. In particular, the dynamic programming algorithm that is called SD is examined. The SD was first proposed by Fichke and Pohst in 1985 [87] to solve the problem of finding the shortest vectors in a given lattice. Extensive research has taken place on the application of SD in diverse areas of communications such as the Lattice Code Decoding [88], [89], the MIMO systems [90], [91], [92], the Multi-User detection of Multi-Carrier CDMA (MC-CDMA) systems [93] and even the reduction of the Peak to Average Power Ratio (PAPR) of OFDM systems [94], [95].

The following sections entail a detailed description of the concept of this well known algorithm and discuss its most important issues like the radius calculation, the reordering strategies and its algorithmic complexity. As far as the latter topic is concerned, this work mainly refers to the initial SD paper [87] as well as the work published by Hassibi and Vikalo [86], [74], [96] and Jalden and Ottersten [97], [98].

In parallel, the chapter investigates the application and performance of diverse SD versions to the SEFDM detection problem. These SD versions are based either on the real decomposition [99] or the complex SD [100]. Various comparisons are demonstrated in terms of computational effort and error rates for different SEFDM systems. In addition, these comparative studies identify the limitations of the SD detection due to the particularities of the SEFDM model, and overcome the effect of the SEFDM projections matrix ill conditioning and its potential numerical singularity by applying regularisation techniques like the Tikhonov variant proposed by Cui and Tellambura in [101]. Finally, this work findings are summarised and the conclusions regarding the use of SDs for a feasible real time SEFDM detection are discussed. Possible areas of further research of SD algorithm with regard to the properties of the investigated SEFDM system, are also underlined. The starting point of this chapter is based on the block diagram of the SEFDM system proposed in [29],

110

combined with a SD as illustrated in Fig. 5.1 below.
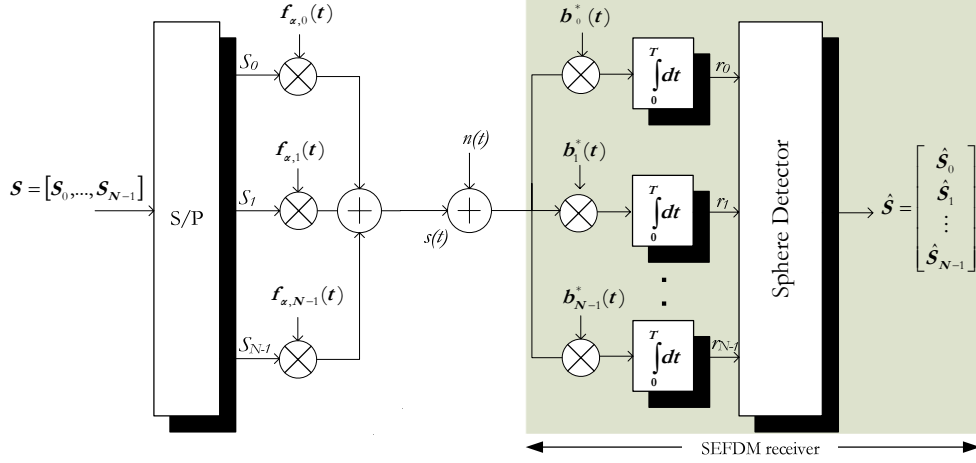
Figure 5.1: A general block diagram of an SEFDM system combined with a Sphere detector.

5.2 SD for the SEFDM detection

The Sphere decoder was first proposed by Fichke and Pohst [87] as a computationally efficient method of finding the shortest - in terms of the Euclidean norm $\|\cdot\|_2$ - vector $\mathbf{X}$ in a given lattice Λ [1], i.e. the solution of the following optimisation problem

$$\text{min.} \quad \|\mathbf{MX}\|_2^2, \tag{5.1}$$
$$\text{s.t.} \quad \mathbf{X} \in \mathbb{Z}^N,$$

where $\mathbf{M}$ is the generator matrix of the lattice Λ.

In order to formulate the SEFDM detection as a Shortest Vector (SV) problem, it is considered that the linear transformation $\mathbf{MS}$ of the transmitted data symbols, $\mathbf{S} = [S_1, S_2, \ldots, S_N]$, constitutes a lattice Λ whose generator matrix

---

[1]A Lattice in this context is a mathematical representation of vectors in a Euclidean space. A brief introduction to Lattice theory is in Appendix B

$\mathbf{M}$ is the matrix of the projections of the SEFDM carriers onto the GS orthonormal base (see Section 3.2). Furthermore, the following assumptions are made: First, S_i take values over a discrete alphabet Q^N of elements with integer in-phase (I) and/or quadrature (Q) components (i.e. the modulation scheme can be either M-PAM or M-QAM). Second, $\mathbf{M}$ is non singular and therefore its square Grammian matrix $\mathbf{M}^H\mathbf{M}$ is positive definite. It is also assumed that Λ is translated so that it is centered around the statistics vector $\mathbf{R}$. As a result, the optimal SEFDM detection decision reduces to the following SV problem

$$
\begin{aligned}
&\text{min.} \|\mathbf{R} - \mathbf{M}\mathbf{S}\|_2^2, \\
&\text{s.t. } \mathbf{S} \in Q^N \subset \mathbb{Z}^N
\end{aligned}
\quad \Leftrightarrow \quad
\begin{aligned}
&\text{min.} \|\mathbf{W}\|_2^2, \\
&\text{s.t. } \mathbf{W} \in \mathbf{R} - \Lambda
\end{aligned}
\tag{5.2}
$$

where $\mathbf{W}$ are the vectors of the translated by $\mathbf{R}$ lattice Λ.

From an optimisation point of view, SD solves exactly the LS problem of the ML detection as described in Section 3.7 but subject to an extra constraint; the value of the cost function (i.e. the square of the Euclidean norm $\|\mathbf{R} - \mathbf{M}\mathbf{S}\|_2$) of the ML problem must be less than a predefined or precalculated real value C. Consequently, Eq. (5.2) reduces to

$$
\begin{aligned}
\text{min.} \quad & \|\mathbf{R} - \mathbf{M}\mathbf{S}\|_2^2, \\
\text{s.t.} \quad & \|\mathbf{R} - \mathbf{M}\mathbf{S}\|_2^2 \le C, \\
& \mathbf{S} \in Q^N.
\end{aligned}
\tag{5.3}
$$

It is apparent that geometrically the constraint implies that SD investigates only the lattice points $\mathbf{M}\mathbf{S}$ that lie within an N-dimensional hypersphere whose center and radius are the statistics vector $\mathbf{R}$ and the parameter C, respectively (see Fig. 5.2). Hence, depending on the proper selection of an efficient radius, SD avoids an exhaustive search, thereby it is more computationally efficient and achieves the optimal solution faster than brute force ML.

Before proceeding with the detailed description of the SD steps, it must be noticed that the SD algorithm introduced in [87] solves the problem in the real
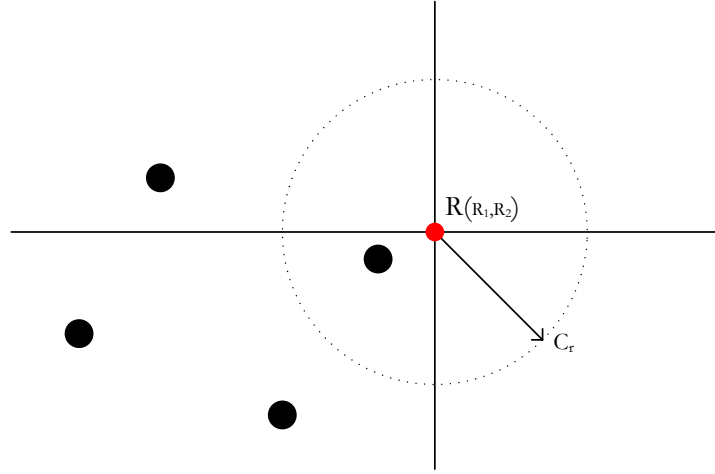
Figure 5.2: Sphere search in a 2-dimensional Lattice.

space, i.e. all the vectors and matrices of the linear model have elements that are real. However, due to the baseband representation of the SEFDM signal in this model, the cross correlations matrix $\mathbf{M}$ as well as the data symbols vector $\mathbf{S}$ are complex. In order to overcome this model inconsistency, we apply a technique widely used that proposes the expansion of all the matrices in the model using a kind of real decomposition [99], [92], [91] as

$$\mathbf{R}' = \left[\begin{array}{c} \text{Re}\{\mathbf{R}\} \\ \text{Im}\{\mathbf{R}\} \end{array} \right], \quad \mathbf{M}' = \left[\begin{array}{cc} \text{Re}\{\mathbf{M}\} & \text{Im}\{\mathbf{M}\} \\ -\text{Im}\{\mathbf{M}\} & \text{Re}\{\mathbf{M}\} \end{array} \right],$$

$$\mathbf{S}' = \left[\begin{array}{c} \text{Re}\{\mathbf{S}\} \\ \text{Im}\{\mathbf{S}\} \end{array} \right], \quad \mathbf{N}' = \left[\begin{array}{c} \text{Re}\{\mathbf{N}\} \\ \text{Im}\{\mathbf{N}\} \end{array} \right]. \tag{5.4}$$

where the $\text{Re}\{\cdot\}$ and $\text{Im}\{\cdot\}$ operators denote the real and imaginary parts of the argument matrix, respectively. This decomposition expands $\mathbf{M}$ matrix and $\mathbf{S}$, and $\mathbf{R}$ vectors respectively into $\mathbf{M}'$, $\mathbf{S}'$, and $\mathbf{R}'$ of $2N \times 2N$, $2N \times 1$ and $2N \times 1$ dimension, respectively. It should be noticed that the decomposition process doubles the dimension of the problem from N to $2N$.

Hence, the constraint of the Eq. (5.3) is converted to

$$\|\mathbf{R}' - \mathbf{M}'\mathbf{S}'\|_2^2 \leq C \Longrightarrow$$

$$(\rho' - \mathbf{S}')^T \mathbf{M}'^T \mathbf{M}'(\rho' - \mathbf{S}') \leq C, \tag{5.5}$$

where ρ' is the expanded $2N \times 1$ vector of the unconstrained ML estimate $\mathbf{M}^{-1}\mathbf{R}$. Note that the Left Hand Side (LHS) of the inequality of the second line represents the equation of an ellipsoid that is centered at the ZF estimate and whose generator matrix is the Grammian matrix $\mathbf{M}'^T \mathbf{M}'$.

Assuming that $\mathbf{M}'$ is non singular, $\mathbf{M}'^T \mathbf{M}'$ is positive definite. Consequently, the latter can be decomposed using Cholesky method and it can be written as a product of an upper triangular matrix $\mathbf{L}$ and its transpose $\mathbf{L}^T$ such as $\mathbf{M}'^T \mathbf{M}' = \mathbf{L}^T \mathbf{L}$. Thus, Eq. (5.5) reduces to

$$\|\mathbf{L}(\rho' - \mathbf{S}')\|_2^2 \leq C, \tag{5.6}$$

Thanks to the triangular form of $\mathbf{L}$, the detection problem can be split in a number of $2N$ consecutive steps corresponding to each of the dimensions of the SEFDM signal. Developing the Euclidean norm, Eq. (5.6) reduces to

$$C \geq (l_{2N,2N}(\rho'_{2N} - S'_{2N}))^2 +$$

$$(l_{2N-1,2N-1}(\rho'_{2N-1} - S'_{2N-1}) + l_{2N-1,2N}(\rho'_{2N} - S'_{2N}))^2$$

$$+ \ldots, \tag{5.7}$$

where $l_{i,j}$, S'_i, and ρ'_i ($i = 1, \ldots 2N$ and $j = 1, \ldots 2N$) are the elements of the L, S' and ρ' vectors, respectively. By examining each of the square terms in separate step, the search in the $2N$-dimension hypersphere is reduced into $2N$ consecutive 1-dimensional spheres, i.e. linear intervals, searches. According to the LHS of Eq. (5.7), the following inequality stands for the $2N^{th}$ term

$$l_{2N,2N}^2(\rho'_{2N} - S'_{2N})^2 \leq C_{2N} = C, \tag{5.8}$$

Developing Eq. (5.8) the following lower and upper bound (LB and UB, respectively) are derived for the search interval of the $2N$-dimension

$$\text{LB} = \left\lceil -\frac{\sqrt{C_{2N}}}{l_{2N,2N}} + \rho'_{2N} \right\rceil \leq S'_{2N} \leq \left\lfloor \frac{\sqrt{C_{2N}}}{l_{2N,2N}} + \rho'_{2N} \right\rfloor = \text{UB}, \qquad (5.9)$$

where the operators $\lceil \cdot \rceil$ and $\lfloor \cdot \rfloor$ denote rounding, respectively, to the nearest larger or smaller integer that span a single dimension of the lattice (this is equivalent to the integer values of the I and Q components of the modulation scheme). The possible values of the data symbols within the $2N^{th}$ linear interval are enumerated. Then, the first point, i.e. the lower bound, is considered. Following (5.7) the radius is updated according to

$$C_{2N-1} = C_{2N} - l_{2N,2N}^2 (\rho'_{2N} - S'_{2N})^2, \qquad (5.10)$$

and the following inequality is solved

$$(l_{2N-1,2N-1}(\rho'_{2N-1} - S'_{2N-1}) + l_{2N-1,2N}(\rho'_{2N} - S'_{2N}))^2 \leq C_{2N-1}. \qquad (5.11)$$

Replacing ρ'_{2N-1} with ξ'_{2N-1} given by

$$\xi'_{2N-1} = \rho'_{2N-1} + \frac{l_{2N-1,2N}}{l_{2N-1,2N-1}}(\rho'_{2N} - S'_{2N}), \qquad (5.12)$$

the inequality (5.11) reduces to

$$l_{2N-1,2N-1}^2 (\xi'_{2N-1} - S'_{2N-1})^2 \leq C_{2N-1}. \qquad (5.13)$$

Then, the algorithm proceeds with the enumeration of the points in the $(2N-1)^{th}$ dimension applying (5.9) similarly to the first step. The same process is iterated until the last dimension. For the ith dimension the following iterative formulas are used

$$C_i = C - \sum_{l=i+1}^{2N} \sum_{j=l}^{2N} l_{ij}^2 (\rho'_j - S'_j)^2, \qquad (5.14)$$

$$\xi_i = \rho'_i + \sum_{j=i+1}^{2N} \frac{l_{ij}}{l_{ii}}(\rho'_j - S'_j). \qquad (5.15)$$

In addition, the radius C_i is linked to C_{i-1} according to

$$C_{i-1} = C_i - l_{ii}^2 (\rho'_i - S'_i)^2. \qquad (5.16)$$

When, SD reaches the last level, i.e. $i = 1$, a candidate vector $\mathbf{M'S'}$ is identified as a point within the sphere when the value of the respective Euclidean norm $\|\mathbf{R'} - \mathbf{M'S'}\|_2^2$ is smaller than the initial radius C. The condition to be met is that can also be written as

$$\|\mathbf{R'} - \mathbf{M'S'}\|_2^2 = \sum_{i=1}^{2N} \sum_{j=i}^{2N} \left(l_{ij}(\rho_j' - S_j') \right)^2 < C. \tag{5.17}$$

Setting $i = 0$ and $i = 1$ in Eqs (5.14) and (5.16), respectively, we have that

$$C_0 = C_{2N} - \sum_{l=1}^{2N} \sum_{j=l}^{2N} l_{ij}^2 (\rho_j' - S_j')^2, \tag{5.18}$$

$$C_0 = C_1 - l_{11}^2 (\rho_1' - S_1')^2. \tag{5.19}$$

Equating the RHS of both equations, we conclude that

$$\sum_{l=1}^{2N} \sum_{j=l}^{2N} l_{ij}^2 (\rho_j' - S_j')^2 = C_{2N} - C_1 + l_{11}^2 (\rho_1' - S_1')^2. \tag{5.20}$$

Consequently, from (5.20) Eq. (5.17) reduces to

$$C_{2N} - C_1 + l_{1,1}^2 (\rho_1' - S_1')^2 < C. \tag{5.21}$$

From a spanning tree view point, SD traces in depth a tree of $N + 1$ levels. The number of the branches of each node is equal to the size of the modulation alphabet, e.g. for BPSK this is 2, as seen in Fig. 5.3. The transition from a 'parent' $i + 1$ to a 'child' i tree node determines the decision about the ith transmitted data symbol. The overall dimension of the search space (i.e. the number of tree nodes) is $M^N + 1$, where M is the constellation cardinality and N is the number of carriers. Every time a complete path is found, a point within the sphere is enumerated. Note that in the real decomposition based SD, the tree has double depth, i.e. $2N + 1$ levels.

A flow chart illustrating the SD algorithm is drawn in Fig. 5.4.

5.2.1 SD radius derivation

The computational efficiency of SD algorithm depends on whether the number of the candidate points that lie within the hypersphere is sufficiently small.
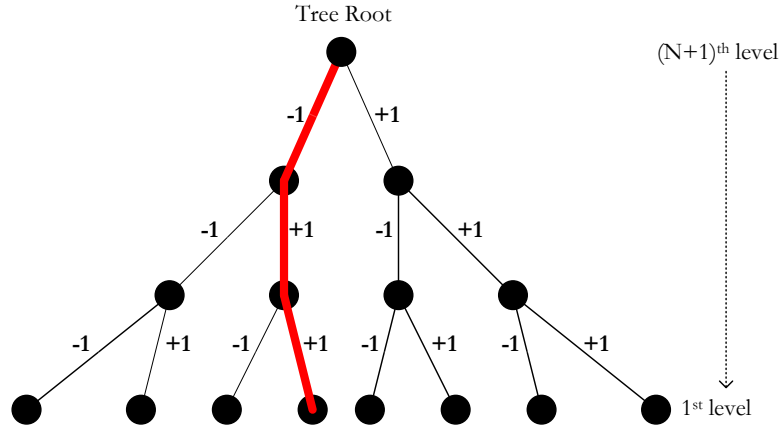
Figure 5.3: Spanning tree of a typical Sphere Decoder.

Apparently if the radius of the sphere is too big, all the lattice points will be investigated and SD will reduce to a brute force ML with exponential complexity over the size of the lattice. On the other hand, if the radius is too small there is a strong likelihood that no point is found and the execution of the algorithm proves to be fruitless. Consequently, the proper definition of the initial radius is decisive for the achievement of a practical detection.

In the literature, many different proposals regarding the radius precalculation have come to the light. As mentioned in [89] and [74], an obvious candidate should be the lattice covering radius (see Appendix B) since it guarantees the existence of at least one point within the sphere. Notwithstanding, its derivation is also an NP hard problem [74].

Another typical approach is to set the initial radius to be equal to the distance from the sphere centre (i.e. the statistics vector $\mathbf{R}$) to a pre-calculated first estimate like ZF or MMSE estimates [102], [93], i.e.

$$C = \left\| \mathbf{R} - \mathbf{M}\tilde{\mathbf{S}} \right\|_2^2, \tag{5.22}$$

where $\tilde{\mathbf{S}}$ is the value of the first estimate. The main disadvantage of this approach is that in case the initial estimation deviates significantly from the optimal point, for example due to the matrix $\mathbf{M}$ bad conditioning or low SNR,

117
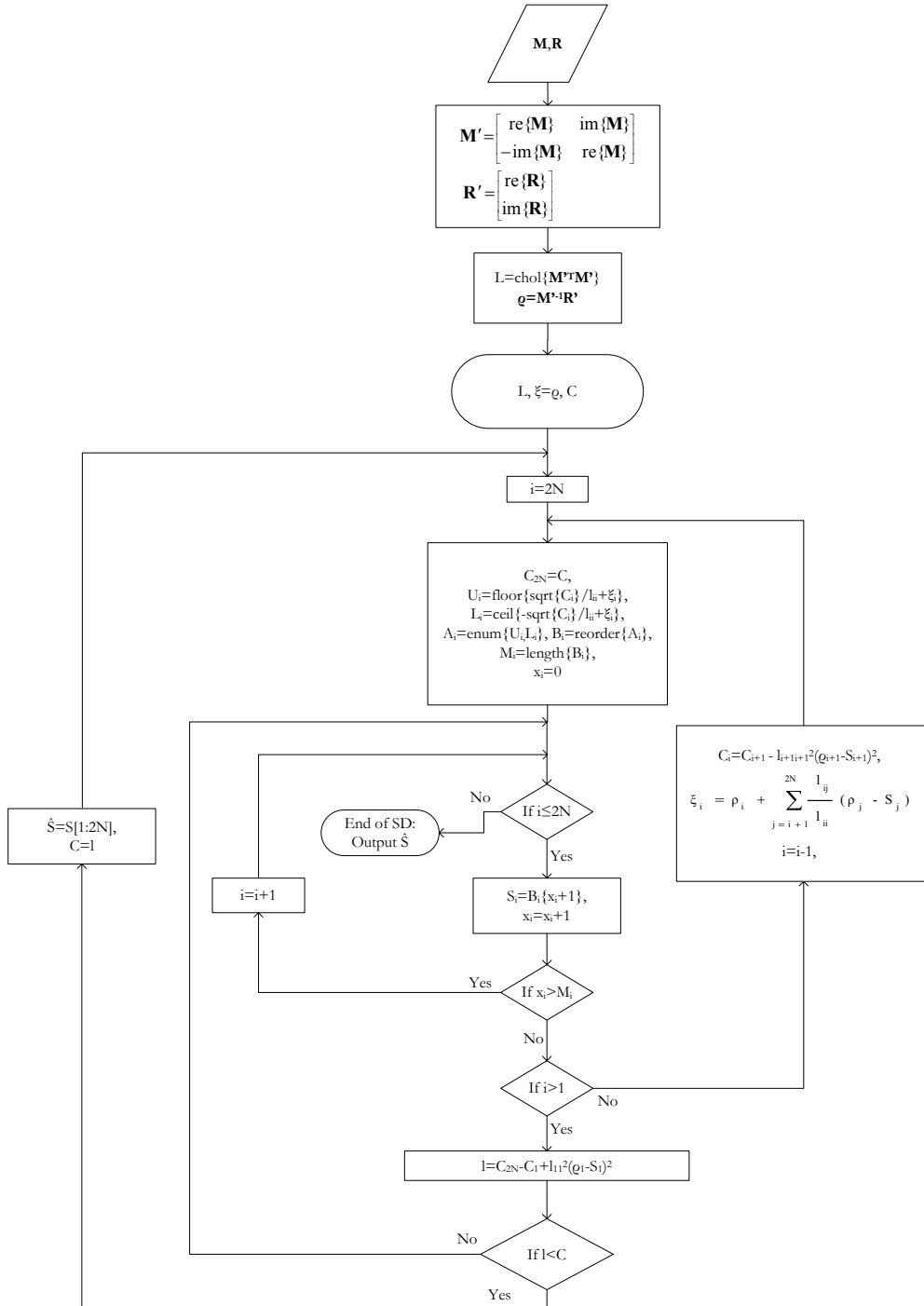
Figure 5.4: Flow chart of a Sphere Decoder based on real decomposition (RSD).

the complexity can be extremely high.

A more practical choice of C is suggested in [89]. In particular, it is proposed to derive the radius according to the noise variance σ^2. In [100] and [74] a more thorough description of this technique is given. According to the linear statistical model the cost function of the SD problem is equal to the norm of the noise variables at the output of the correlators, i.e.

$$\frac{1}{\sigma^2}\|\mathbf{R} - \mathbf{MS}\|_2^2 = \frac{1}{\sigma^2}\|\mathbf{N}\|_2^2. \tag{5.23}$$

The term $\|\mathbf{N}\|_2^2$ in the Right Hand Side (RHS) of (5.23) comprises the sum of the squares of $2N$ standard independent Gaussian variables with variances σ^2. Consequently, it represents a χ^2 random variable U [71] with $2N$ degrees of freedom. The probability of such a variable being smaller than a value C/σ^2 is given by

$$P\{U \leq C\} = \int_0^C \frac{U^{N-1}}{2^N \Gamma(N)} e^{-U/2} dU, \tag{5.24}$$

where $\Gamma(\cdot)$ stands for the well known Gamma function.

C could be set to be equal to a scaled, by a real $k > 1$, variance of the noise vector, i.e.

$$C = k2N\sigma^2, \tag{5.25}$$

and then calculate k so that the probability of Eq. (5.24) is very high, e.g. $P\{U \leq 2kN\sigma^2\} = 0.99$. The disadvantage of this method is that there is always a likelihood of a detection failure (i.e. no point found in the sphere). In this case, the above probability and consequently the radius of the sphere should be increased until a solution is achieved. In order to overcome this limitation, the idea of reordering the enumerated points at each step of the algorithm has been applied [91], [103], [90]. The following paragraph describes a reordering strategy called Schnorr-Euchner (SE) enumeration, as proposed in [102]. SE enables setting initial sphere radius equal to very large values so that the probability of no point being found in the sphere approaches zero.

5.2.2 Schnorr-Euchner (SE) enumeration

While in the original Fichke-Pohst (FP) enumeration [87] the search starts from the point closer to the lower bound defined in eq. (5.9) and then moves towards the upper bound, in SE strategy the points at each level are reordered so that the search starts from the candidate that is closest to the center of the SD one dimensional spheres. According to Eqs (5.9) and (5.15) the middle point is given by

$$\xi_i = \rho_i' + \sum_{i+1}^{2N} \frac{l_{i,j}}{l_{i,i}} \left(\rho_j' - S_j' \right).$$ (5.26)

Then, the enumeration of points at the i level takes place from the left to the right in the following order

$$\lfloor \xi_i \rceil, \lfloor \xi_i \rceil + \beta, \lfloor \xi_i \rceil - \beta, \lfloor \xi_i \rceil + 2\beta, \lfloor \xi_i \rceil - 2\beta, \ldots,$$ (5.27)

where $\lfloor \cdot \rceil$ the denotes the rounding operator that rounds to the nearest integer. The step β depends on the modulation alphabet that is used, e.g. for $Q^N = \{\pm 1, \pm 3, \ldots\}^N$, $\beta = 2$.

Fig. 5.5 shows the difference between SE and a typical FP enumeration. Instead of the so called natural spanning of typical FP, in SE the points are spanned in a 'zig-zag' order from the interval center ξ_i.

The main advantage of the method is that there is no need for a precise definition of the initial radius. It is enough to set C to a sufficiently large value, depending on the dimension of the problem and the SNR, that can be even ∞ [103], [91]. Thus, the probability of a detection failure (in terms of no point found at the end of the algorithm execution) becomes zero.

It is also clear from Eq. (5.9) that the first point that is enumerated corresponds to the real decomposed version of the ZF estimate, $\hat{\mathbf{S}}_{\mathbf{ZF}}'$. Consequently, at the first step of the SE SD variant the radius of the hypersphere is reduced to the distance from this estimate that is equal to $\left| \mathbf{R}' - \mathbf{M}' \hat{\mathbf{S}}_{\mathbf{ZF}}' \right|_2^2$. The smaller this quantity is the faster the search of the tree. Therefore, in the ideal case
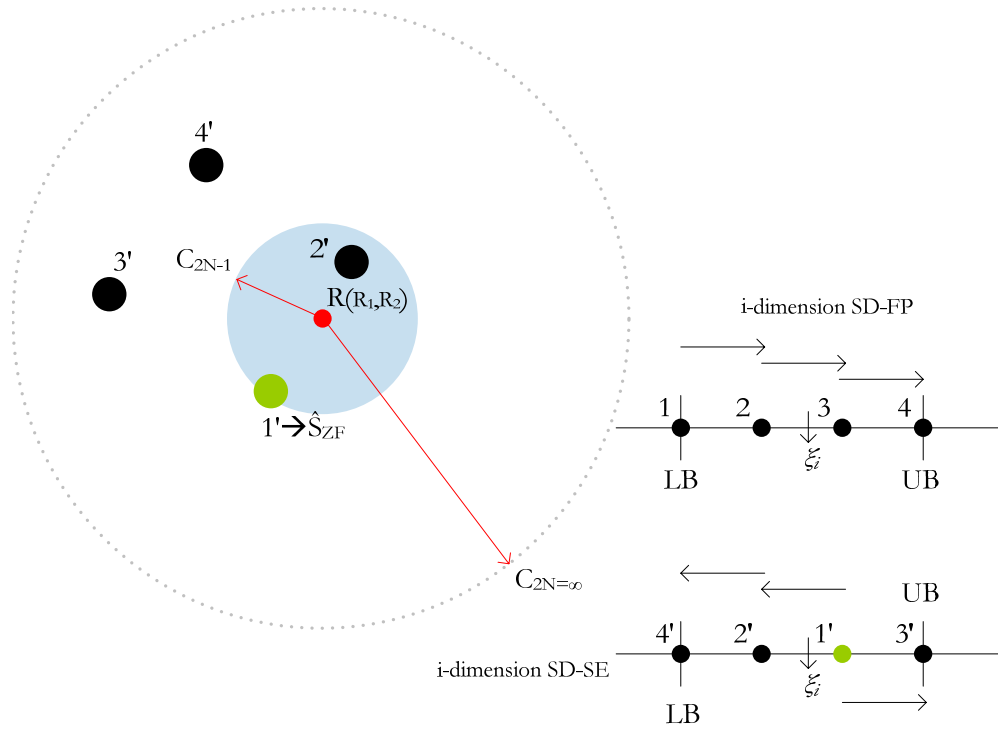
Figure 5.5: Intervals spanning in typical FP and SE enumeration strategies. The spanning takes place in a numerical order from number 1 to number 4.

of no noise the calculational effort is minimum since the lattice point corresponding to the $\hat{\mathbf{S}}'_{\mathbf{ZF}}$ coincides with the sphere center and the SD detection is accomplished after the execution of the first step only. In this case, SD complexity is upper bounded by the pre-calculation of the ZF estimate, where the complexity is of cubic order due to the required inversion of $\mathbf{M}'$.

5.2.3 SD Complexity

From the previous paragraphs, it has become apparent that the main issue in the SD implementation is not its error performance, since if the radius has been chosen properly the optimum solution is achieved, but its computational efficiency. The latter obviously depends on the number of the lattice points that are investigated and consequently on the size of the SD spanning tree.

121

This is equal to the total number of tree nodes given by

$$\sum_{i=0}^{N} M^i, \tag{5.28}$$

where M is the constellation cardinality and N is the dimension of the problem. As a consequence, the author conjectures that the complexity will depend not only on the problem size but it will also be data dependent since larger data modulation alphabets compose larger SD trees.

In [87] a first analysis about the SD complexity was given. In particular, the main result was the derivation of an upper bound for the number of arithmetic operations required by the algorithm to converge, that is given by [87],

$$\frac{1}{6}(2(2N)^3 + 3(2N)^2 - 10N) + \frac{1}{2}((2N)^2 + 24N - 7)$$
$$\times \left((2 \left\lfloor \sqrt{Cl_{min}} \right\rfloor + 1) \binom{\lfloor 4Cl_{min}+2N-1 \rfloor}{\lfloor 4Cl_{min} \rfloor} + 1 \right), \tag{5.29}$$

where l_{min}^{-1} is the lower bound for the eigenvalues of the Grammian $\mathbf{M'^T M'}$, which in SEFDM case (see Section 3.5.5) tends to zero as the number of the carriers increases and/or their frequency separation decreases. Although this complexity bound has been reported as an extremely loose one [74], the above formula indicates that the complexity of the SD SEFDM detection will inevitably increase in these two cases.

In [86] and [74], Hassibi and Vikalo observed that the problem solved by SD is a random integer LS problem. Based on this, they derived formulae for the expected complexity in two different scenarios. Firstly, they considered that there is no knowledge about the statistics vector, i.e. it is an arbitrary point. They stated the expected number of points visited in SD will be at least equal to the expected number of points P visited in an arbitrary i-dimensional sphere, $i = 1, \ldots, 2N$ of radius C. This is proportional to the sphere volume given in Eq. (11) and found to meet the following bound [74],

$$P \geq \frac{\pi^{\frac{k}{2}}}{\Gamma\left(\frac{k}{2}+1\right)} C^K \tag{5.30}$$

Developing this inequality under the assumption that at least a point is found, they concluded that

$$P \geq \frac{1}{\sqrt{\pi}} \delta^{\frac{2N}{2\delta} + \frac{1}{2}} (2N)^{\frac{1}{2\delta} - \frac{1}{2}} , \qquad (5.31)$$

where $\delta = 2N/k$. For a fixed δ it appears that when the received point is arbitrary, the SD expected complexity increases exponentially in N.

Secondly, in SEFDM detection in presence of AWGN, as in most of the communications cases where SD is applied, the statistics vector is a point of the lattice **MS** disturbed by additive Gaussian noise with known variances σ^2 (also see Section 5.2.1. Based on this and the assumption that **M** is also random , in [74] and [96] it was shown that in a such a system the expected complexity could be polynomial for specific SNRs and problem dimensions. The last conclusion is also consistent with results given by Jalden and Ottersten in [97] that prove that SD expected complexity is $O(M^{\beta N})$, where $\beta \in [0, 1]$ and depends on the SNR. Furthermore, for large SNR values $\beta << 1$ implying that for moderate N the complexity is dominated by polynomial terms.

Motivated by the last conclusions, the following investigate the performance of different variants of SD adapted to the properties of our SEFDM system and identify the possible SNR areas for which a real-time detection for a moderate size SEFDM signal can be achieved. For the discussion below, the following SEDFDM particularities should be underlined:

- First, the generator matrix **M** is not a matrix with independent random entries but it is a deterministic matrix whose elements values depend only on the number of SEFDM carriers and their frequency separation;

- The SEFDM-SD detection modelling involves techniques like SE reordering and radius update that have not been taken into account in the literature and above derivations. Although published closed formulae do not stand for this case, the expected complexity of such SD variants is no greater than the one calculated in [96].
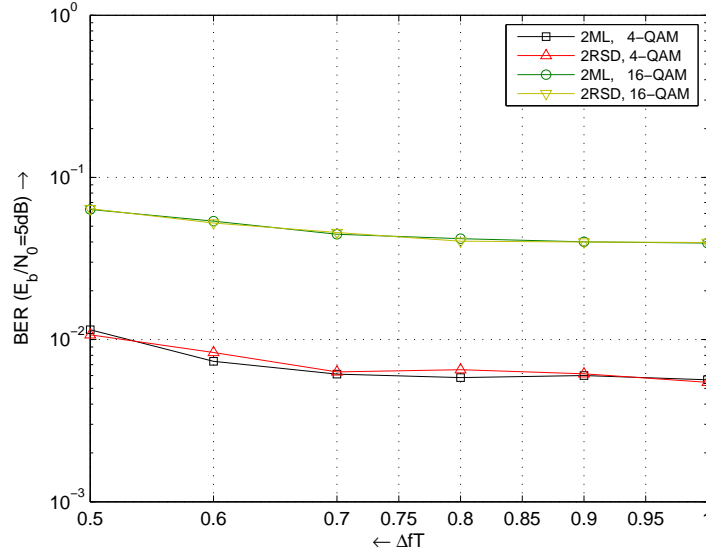
Figure 5.6: BER versus ΔfT comparison between ML and RSD 4-QAM and 16-QAM SEFDM detection with $N = 2$ carriers.

5.2.4 Real SD (RSD) Numerical Results

In this work the initial design of the SD detector is based on the real decomposition technique. In addition, the SE enumeration strategy was followed and arbitrarily set the initial radius to a very large value. Moreover, perfect knowledge of the IMGS base at the receiver side was assumed and that the only channel impairment is AWGN. A pseudocode of the real decomposed SD (RSD) implementation based on Python symbolics [104] is shown in Fig. 5.7.

BER measurements were taken for up to $N = 24$ carriers with minimum frequency separation $\Delta f = \frac{1}{2T}$. In addition, carriers were modulated either by 4-QAM or 16-QAM baseband symbols. In all simulations, MMSE curves were used as a performance reference.

Fig. 5.6 provides a brief comparison of ML and SD detection methods for the smallest ($N = 2$) dimensional SEFDM signals. The result confirms the theoretical expectations since both schemes have identical performance.

Figs 5.8 and 5.9 show the evaluation of the error performance of the SD

```
def  SD (M, R, N, C, lattice_points)
         R’=decomp{R}, M’=decomp{M}
         L = cholesky(M’ᵀM’)
         ϱ = M’⁻¹R’
         i=2N,  Cᵢ= C,  ξᵢ=ϱᵢ
         LBᵢ = ceil{-√(Cᵢ/lᵢ,ᵢ²)+ξᵢ}
         UBᵢ = floor{√(Cᵢ/lᵢ,ᵢ²)+ξᵢ
         Aᵢ = enum{lattice_points, LBᵢ, UBᵢ}
         Bᵢ = sortSE{Aᵢ, ξᵢ}
         Mᵢ = length{Bᵢ}, xᵢ=0
         while i<=2N:
                 Sᵢ= Bᵢ,ₓ
                 xᵢ+=1
                 if nodes_counter_level> Mᵢ:
                         i+=1
                         continue
                 elif i>1:
                         i-=1
                         Cᵢ = Cᵢ₊₁ - lᵢ₊₁,ᵢ₊₁²(ξᵢ₊₁ - Sᵢ₊₁)²
                         ξᵢ=ϱᵢ + lᵢ, ₍ᵢ₊₁₎:₂N/lᵢ,ᵢ x (ϱᵢ₊₁:₂N - Sᵢ₊₁:₂N)
                         LBᵢ = ceil{-√(Cᵢ/lᵢ,ᵢ²)+ξᵢ}
                         UBᵢ = floor{√(Cᵢ/lᵢ,ᵢ²)+ξᵢ}
                         Aᵢ = enum{lattice_points, LBᵢ, UBᵢ }
                         Bᵢ = sortSE{Aᵢ, ξᵢ}
                         Mᵢ = length{Bᵢ}, xᵢ = 0
                 elif C_{N-1} − C₁+l₁,₁²(ξ₁-S₁)² < C:
                         C = C_{N-1} − C₁+l₁,₁²(ξ₁ - S₁)²
                         C_{N-1} = C_{N-1} − C₀+l₁,₁²(ξ₁ - S₁)²
                         Ŝ  = S, i = 2N
                         LBᵢ = ceil{-√(Cᵢ/lᵢ,ᵢ²)+ξᵢ}
                         UBᵢ = floor{√(Cᵢ/lᵢ,ᵢ²)+ξᵢ}
                         Aᵢ = enum{lattice_points, LBᵢ, UBᵢ }
                         Bᵢ = sortSE{Aᵢ, ξᵢ}
                         Mᵢ = length{Bᵢ}, xᵢ = 0
         Solution = recomp{Ŝ}
return [Solution]
```

Figure 5.7: SD pseudocode based on a Python implementation.

125

detection versus the normalised carriers frequency separation of the FDM signal, ΔfT. Simulations were performed for 4-QAM SEFDM SD detection with $N = 2, 4, 8, 16$ carriers and 16-QAM SEFDM SD detection with $N = 2, 4, 8$ carriers. All measurements were taken for a fixed value of Energy Per Bit to Noise Power Spectral Density Ratio (E_b/N_0) equal to 5 dB. From both figures it is apparent, for both 4-QAM and 16-QAM SEFDM, as the distance between the carriers decreases there is an error penalty as opposed to the single carrier error rate. Nevertheless, SD appears to be considerably superior to MMSE for all frequency separation points. Moreover, for 4-QAM modulation case SD achieves the OFDM, or equivalently the single carrier, performance (BER $\leq 10^{-2}$) for $\Delta fT \geq 0.8$. Some useful insight about this observation is given in [32], [33]. According to the authors, the Euclidean distance between the transmitted 4-QAM SEFDM symbols does not shrink until this ΔfT point. Consequently, the effect of the noise and the respective BER in the SEFDM systems are expected to remain the same with those in the OFDM case.
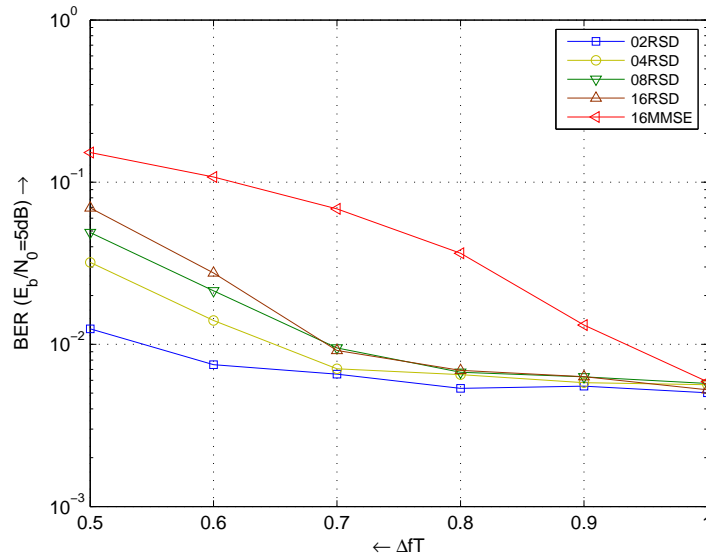
Figure 5.8: BER versus ΔfT of 4-QAM SEFDM RSD detection for $N = \{2, 4, 8, 16\}$ carriers.
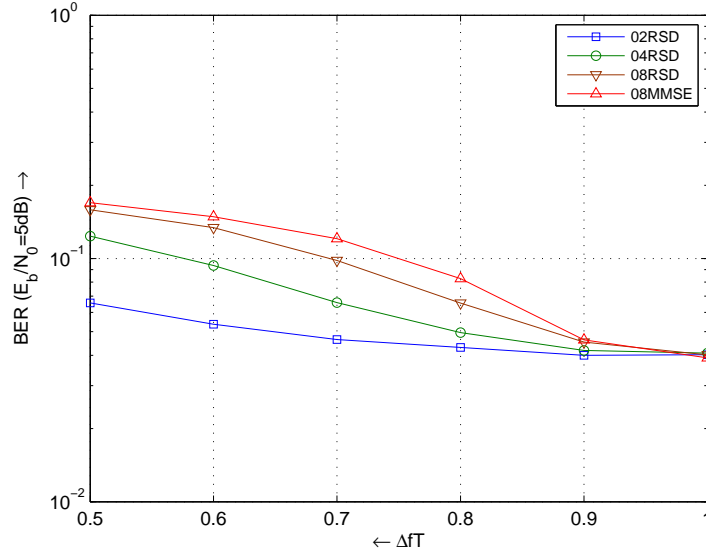
Figure 5.9: BER versus ΔfT of 16-QAM SEFDM RSD detection for $N = \{2, 4, 8\}$ carriers.

Simulations for different E_b/N_0 values for a fixed 0.75 ΔfT frequency separation. In particular, Figs 5.10 and 5.11 illustrate the system BER performance versus E_b/N_0. It is interesting that in 4-QAM case, the lack of orthogonality introduces a small error penalty (≤ 0.5 dB) for up to 24 carriers. It must be mentioned that the 24 carriers case result was based on the simulation of only 100 SEFDM symbols, due to the long simulation time, and therefore it can be only indicative. In 16-QAM the error grows rapidly with the number of the carriers and introduces an approximate 2 dB penalty. However, SD still performs better than the MMSE detector.

In addition to the error performance, evaluation has come out for the computational complexity of the SD method measuring the number H of the visits to the nodes of the SD spanning tree. All simulations were based on the detection of 100 SEFDM symbols for $E_b/N_0=5$ and 8 dB, and for $\Delta fT = 1, 0.75$. Fig. 5.12 depicts the results for $N = \{4, 8, 16\}$ 4-QAM SEFDM carriers. It is clear that the calculation complexity is not fixed but dependent on the pro-

127
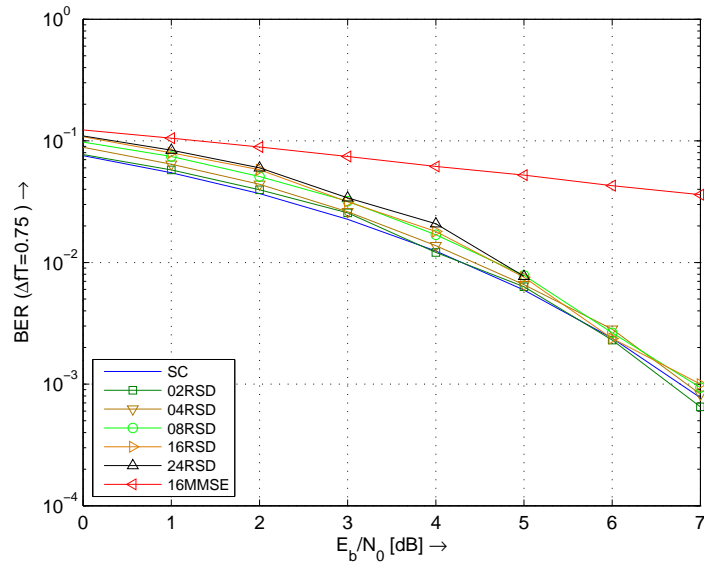
Figure 5.10: BER versus E_b/N_0 of 4-QAM SEFDM RSD detection for $N = \{2, 4, 8, 16\}$ and $N = 24$ carriers over 10^4 and 10^2 SEFDM symbols, respectively.
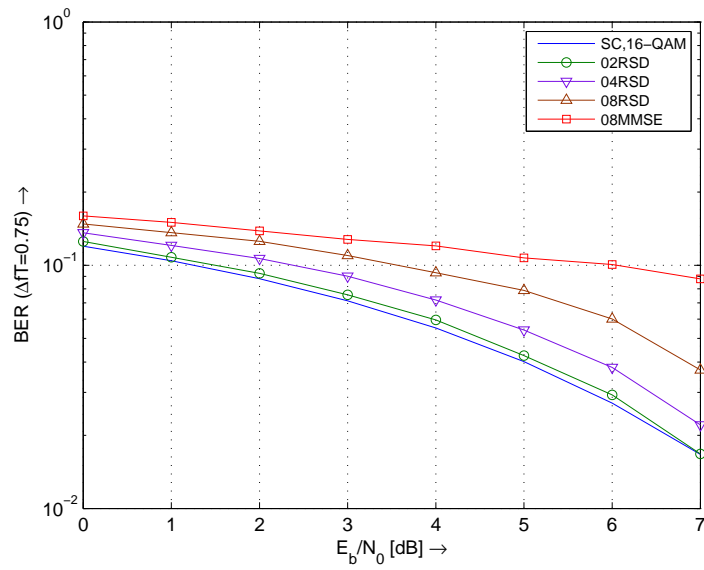
Figure 5.11: BER versus E_b/N_0 of 16-QAM SEFDM RSD detection for $N = \{2, 4, 8\}$ carriers.

jections matrix properties and the noise in the system. As far as the former is concerned, it can be observed that the complexity vastly increases with the number of carriers and/or as the reduction of the frequency separation. Regarding the latter, it can be seen that SD computational effort is also influenced by the SNR level. It can be clearly seen that the high noise system ($E_b/N_0 = 5$ dB) requires almost double the number of operations to achieve the optimal solution. Fig. 5.13 illustrates similar results for 16-QAM. It is obvious that there is a further degradation of the detection complexity due to the higher modulation level scheme.
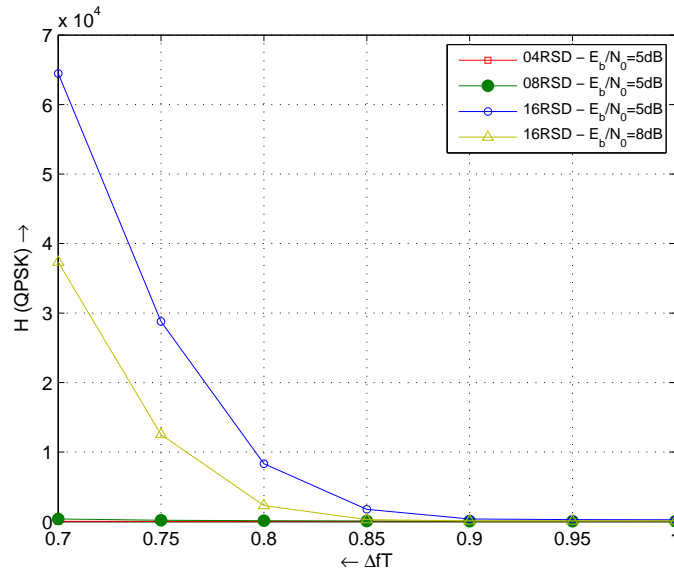
Figure 5.12: Visits to the SD tree nodes for 4-QAM RSD detection.

5.3 Complex Sphere Decoding (CSD)

As already mentioned, one of the main factors that affects the SD complexity is the dimension of the problem which in the SEFDM detection is equal to the number N of the SEFDM carriers. However, the real version of SD (RSD) requires the real decomposition of the matrices of the SEFDM model due to the
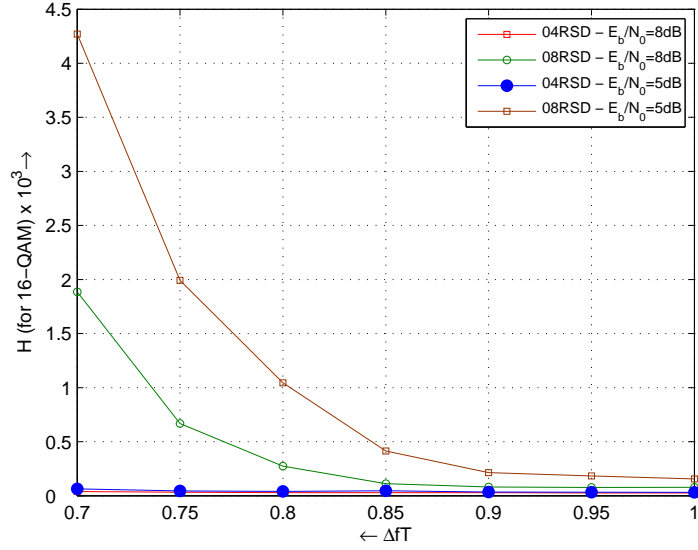
Figure 5.13: Visits to the SD tree nodes for 16-QAM RSD detection.

complex nature of the projections matrix $\mathbf{M}$, before applying the SD algorithm (Fig. 5.7). Consequently, the dimension of the model matrices and of the detection problem is doubled. As a result, SD searches for the optimum solution in a spanning tree which has a number of levels that is double that number of the carriers. In order to avoid the aforementioned doubling of the problem dimension a Complex version of SD (CSD) [100], [93] [105] could be applied.

The analysis in the following sub-sections examines, for simplicity reasons, the application of CSD for the detection of SEFDM modulated only by M-PSK symbols though this is not an actual constraint [100].

5.3.1 CSD Description

It is assumed that at any SEFDM dimension the lattice points lie exactly on the diameter of a circle of a fixed radius $r = 1$. Hence, each of the transmitted symbols S_i can be written as

$$S_i = re^{j\theta_i} \ \left| \theta_i \in \mathrm{A} = \left\{0, \frac{2\pi}{2^M}, \ldots, (2^{M-1})\frac{2\pi}{2^M}\right\}, \ i = 1, \ldots, N, \right. \qquad (5.32)$$

130

where θ_i is the phase corresponding to the ith carrier M-PSK symbol and A is the set of possible phases of the M-PSK symbols.

Then, each of the SEFDM symbols $\mathbf{S} = [S_1, S_2, \ldots, S_N]$ can be represented by a vector of phases $\boldsymbol{\Theta} = [\theta_1, \theta_2, \ldots, \theta_N]$. Thus, the SD program described in Eq. (5.3) can be transformed into the following equivalent problem

$$\text{min.} \quad \left\| \mathbf{M}(\hat{\mathbf{S}}'_{\mathbf{ZF}} - e^{j\boldsymbol{\Theta}}) \right\|^2, \tag{5.33}$$
$$\text{s.t.} \quad \left\| \mathbf{M}(\hat{\mathbf{S}}'_{\mathbf{ZF}} - e^{j\boldsymbol{\Theta}}) \right\|^2 \leq C,$$
$$\boldsymbol{\Theta} \in \mathrm{A}^N,$$

where $\hat{\mathbf{S}}'_{\mathbf{ZF}} = [\hat{S}'_{ZF,1}, \hat{S}'_{ZF,2}, \ldots, \hat{S}'_{ZF,N}]$ is the vector of the signal ZF estimator $\hat{\mathbf{S}}_{\mathbf{ZF}} = \mathbf{M}^{-1}\mathbf{R}$ whose elements are expressed in spherical coordinates $(\hat{r}_{ZF,i}, \theta_{ZF,i})$ such as

$$\hat{S}'_{ZF,i} = \hat{r}_{ZF,i}e^{j\hat{\theta}_{ZF,i}}, \; i = 1, \ldots, N. \tag{5.34}$$

It should be mentioned that complex SD fits better the introduced SEFDM model since thanks to the triangular shape of the matrix $\mathbf{M}$, the Cholesky decomposition step at the initialisation stage of the SD algorithm can be neglected. Consequently, the problem is directly decomposed into a number of steps equal to the number of the SEFDM carriers. After developing the norm of Eq. (5.34) the following inequality must be met for the Nth dimension (corresponding to the first SD step)

$$\left(\hat{S}_{ZF,N} - S_N\right)^2 \leq \frac{C_N}{m_{N,N}^2}, \tag{5.35}$$

where C_N is the sphere radius at the first SD step. The transformation of S_N and $\hat{S}_{ZF,N}$ according to Eqs (5.32) and (5.34) leads to

$$\left(\hat{r}_{ZF,N}e^{j\hat{\theta}_N} - re^{j\theta_N}\right)^2 \leq \frac{C_N}{m_{N,N}^2} \Rightarrow$$
$$\hat{r}_{ZF,N}^2 + r^2 - 2\hat{r}_{ZF,N}r\cos(\hat{\theta}_{ZF,N} - \theta_N) \leq \frac{C_N}{m_{N,N}^2}, \tag{5.36}$$

where $m_{N,N}$ is the Nth diagonal element of the projections matrix. Solving (5.36) with respect to θ_N results in

$$-\cos^{-1}(k) + \hat{\theta}_{ZF,N} \leq \theta_N \leq \cos^{-1}(k) + \hat{\theta}_{ZF,N}, \qquad (5.37)$$

where

$$k = \frac{1}{2\hat{r}_{ZF,N}r}\left(\hat{r}_{ZF,N}^2 + r^2 - \frac{C}{m_{N,N}^2}\right). \qquad (5.38)$$

Multiplying both sides of (5.37) by $\frac{2^M}{2\pi}$ and rounding to the nearest integer leads to the following

$$\left\lceil \frac{2^M}{2\pi}\left(\hat{\theta}_{ZF,N} - \cos^{-1}(k)\right)\right\rceil \leq \lambda_N \leq \left\lfloor \frac{2^M}{2\pi}\left(\hat{\theta}_{ZF,N} + \cos^{-1}(k)\right)\right\rfloor, \qquad (5.39)$$

where $\lambda_N = \frac{2^M}{2\pi}\theta_N$ while $\lceil \cdot \rceil$ and $\lfloor \cdot \rfloor$ denote the ceiling and floor functions, respectively.

The previous equation shows that the problem finally reduces to a number of separate enumerations of integers between the lower and upper bounds. The difference with the RSD is that those integers do not reflect the actual modulation symbols values but the order of the symbols points on the M-PSK constellation circle. A schematic of the CSD search at the ith signal dimension is given in Fig. 5.14.

It is apparent that at each step the algorithm enumerates the integers that correspond to the phases of the lattice points (see Eq. (5.32)) that are within the hypersphere. From a geometrical point of view at each dimension i the search interval is not any more a line between the lower and the upper bounds as in RSD, but it is defined as the arc of the M-PSK constellation circle between the intersection points of the latter with a circle whose center is $\hat{S}_{ZF,i}$ and the radius equal to C_i.

The steps described above for the Nth dimension are repeated for the remaining dimensions (signal carriers) in a similar manner with the RSD until a full path across the SD spanning tree is found. It is notable that the proper
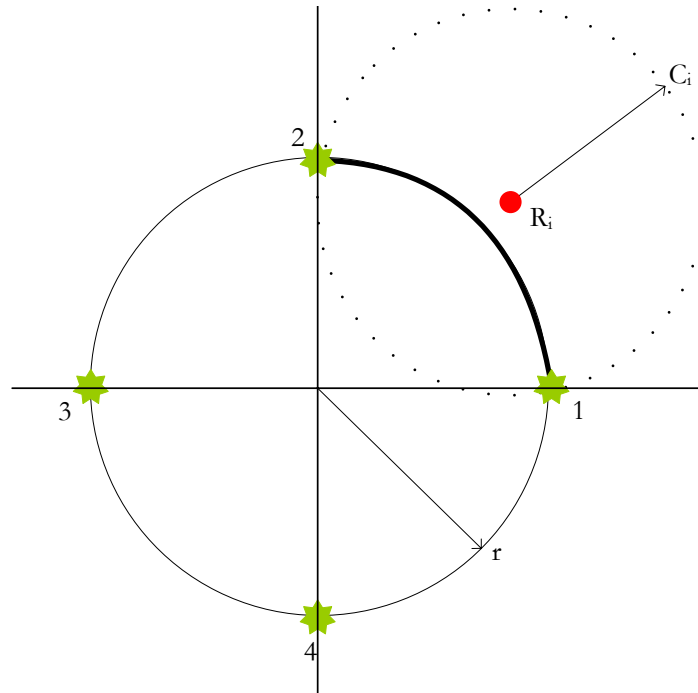
Figure 5.14: A single dimension search for Complex Sphere Decoding (CSD).

implementation of the previous calculations requires that $0 \le \cos k^{-1} \le \pi$ and not $-\pi/2 \le \cos k^{-1} \le \pi/2$. [100].

Before proceeding with simulation results it should be mentioned that CSD can be combined with multi-amplitude modulation schemes considering that M-QAM ($M > 4$) symbols lie on circles of different size. Hence, the problem solution will be given by solving Eq. (5.37) for all the different values of the circle radius r [100].

5.3.2 CSD Results

In order to evaluate the system performance, BER in the presence of AWGN was also measured. In addition, SE reordering was also performed, similarly to the RSD case, to overcome the problem of the radius initial setting. Figs 5.15 and 5.16 show BER versus ΔfT curves in the complex SD detection. It can be seen that CSD achieves optimum performance for both BPSK and
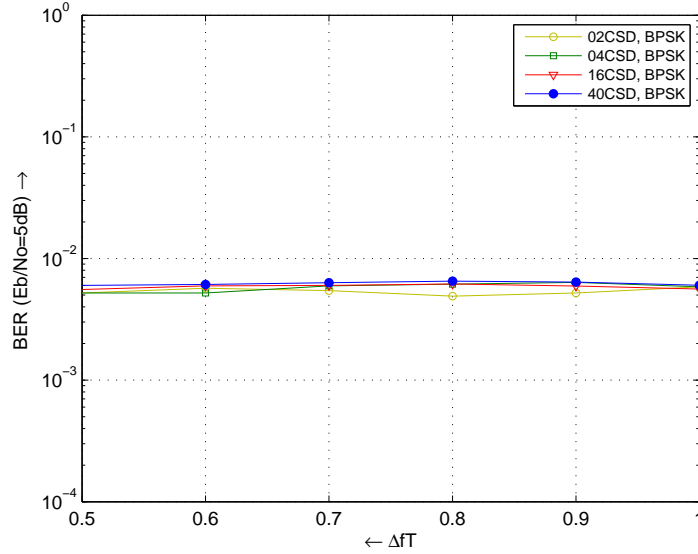
Figure 5.15: Complex SD detection BER for BPSK SEFDM systems.

QPSK modulations. However, due to the large computational cost the size of the detected SEFDM signal is limited in this study to 40 and 24 carriers for BPSK and QPSK, respectively. For the same reason, simulations for 24 QPSK SEFDM carriers were performed for only 1000 SEFDM symbols.

The CSD computational complexity has also been evaluated for different noise values, input data formats (BPSK or QPSK) and the matrix $\mathbf{M}$ properties that change with the number of SEFDM carriers and their frequency separation. The number H of visits to the SD tree nodes was used as a measure of the computational effort required by the algorithm.

Figs 5.17 and 5.18 show that the main factor that affects complexity is the matrix $\mathbf{M}$. As the number of carriers grows and/or their frequency separation decreases, the triangular matrix $\mathbf{M}$ tends to become singular as its diagonal elements (eigenvalues) value approach zero. Consequently, the number of required arithmetic operations increases unacceptably.

Furthermore, the noise variance as well the format of the input data play a significant role. QPSK appears to be computationally more expensive than
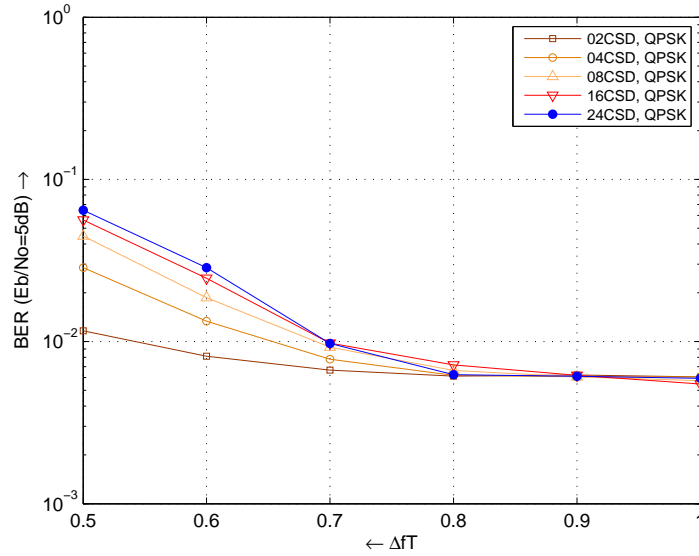
Figure 5.16: Complex SD detection BER for QPSK SEFDM systems.

BPSK since the size of the tree in QPSK is larger. In addition, noise augments complexity since the radius of the sphere is a function of noise and consequently the number of the lattice points included in it, depend on its size.

Finally, Fig. 5.19 shows the significant impact that the use of CSD has on the complexity of the algorithm. In particular, the numbers of the tree nodes visits for a fixed number of carriers $N = 16$ in case of RSD and CSD detection are compared. E_b/N_0 was set either to 5 or 8 dB and ΔfT was equal to 0.75.

The above studies clearly demonstrate that CSD algorithm performs much faster than RSD especially when the matrix **M** properties start degrading. This is attributed to the avoidance of doubling the matrices dimension.

Hence, this work findings about CSD for the SEFDM system proposed in [29], may be summarised in the following:

- First, the complex SEFDM projections matrix **M** is by definition upper triangular, allowing thus omitting the Cholesky decomposition step in the initialisation step of the SD algorithm;
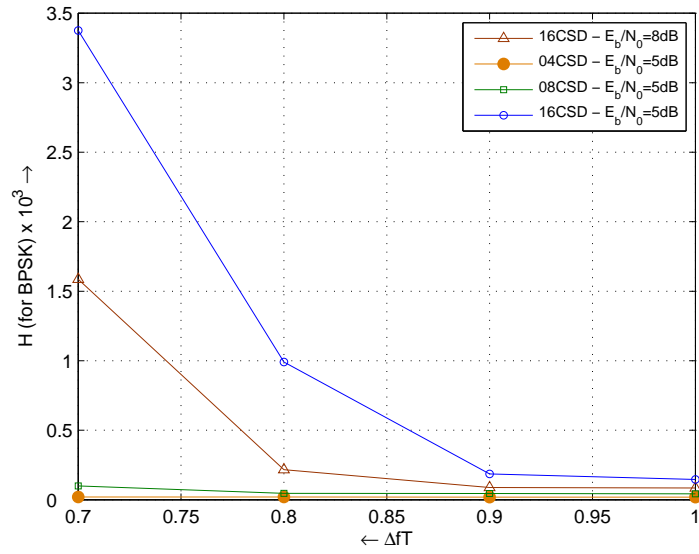
Figure 5.17: CSD detection complexity for BPSK SEFDM systems. The number of SEFDM carriers varies between 4 and 16.
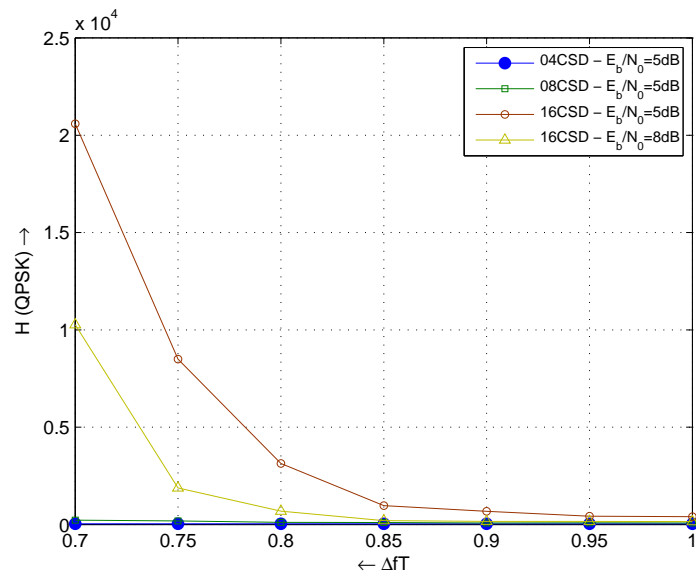
Figure 5.18: CSD detection complexity for QPSK SEFDM systems. The number of FDM carriers varied between 4 and 16.
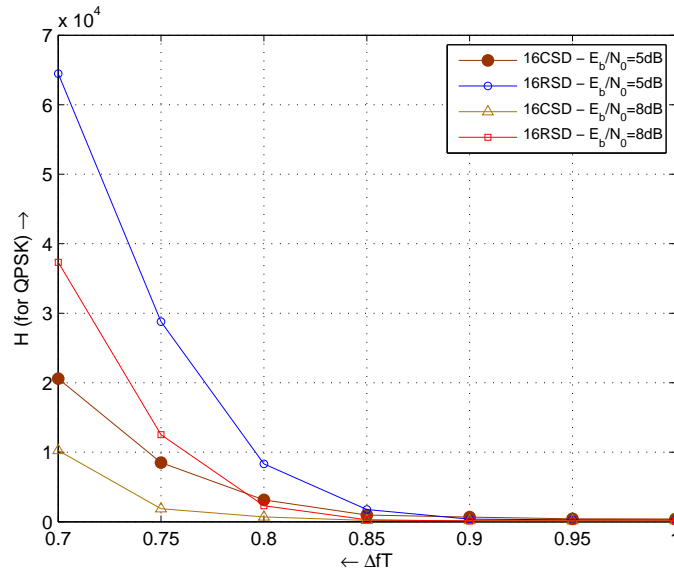
Figure 5.19: CSD vs RSD detection complexity for QPSK SEFDM systems.

- According to this work's numerical results, CSD offers a significant improvement as opposed to the RSD variant due to the avoidance of doubling the dimension of the detection problem;

- Nevertheless, a fast solution is still constrained by the properties of the matrix $\mathbf{M}$. As the latter tends to be singular with the increase of number of carriers and/or the decrease in their frequency separation, the detection problem becomes ill-posed. A possible improvement could be offered by the application of regularisation techniques for ill-posed Least Squares problems like the Tikhonov method [106].

5.4 Regularised Sphere Decoding (RegSD)

5.4.1 SEFDM Grammian Matrix and SD

Efficient detection of SEFDM signals depends on the properties of the covariance matrix $\mathbf{M}$ (i.e. the Gram matrix) that appears in the SEFDM linear

α N	0.7	0.75	0.8	0.85	0.9	0.95	1
8	4.25	2.93	2.12	1.6	1.27	1.07	1
16	33.9	14.71	6.97	3.6	2.03	1.28	1
24	290.11	78.88	24.46	8.59	3.42	1.58	1
32	2554.8	435.3	88.2	21.1	5.9	2	1
40	22860	2440	323	52	10	3	1

Table 5.1: Gram Matrix **M** Condition Number for Varying α and N

statistical model. The Gram matrix is positive semidefinite upper triangular, so its eigenvalues equate to its diagonal elements. In the OFDM case the orthonormal base coincides with the SEFDM carriers and consequently $\mathbf{M} = \mathbf{I_N}$. On the other hand, in the SEFDM case, with decreasing carrier spacing α and/or increasing number of carriers N, the Gram matrix eigenvalues decrease rapidly and $\mathbf{M}$ as well as $\mathbf{M}^H\mathbf{M}$ tend to become singular. Table 5.1 depicts $\mathbf{M}$ condition number (ratio of the largest to the smallest eigenvalue) to illustrate this effect. For large condition number, suboptimum linear detection techniques such as ZF and MMSE, do not result in good BER performance [107], [108] and optimum detection methods like RSD and CSD are not directly applicable. Therefore, other detection techniques have to be explored. The section below examines RegSD detection.

5.4.2 RegSD for SEFDM Detection

The applicability of SD mainly depends on the invertibility of the Gram matrix $\mathbf{M}$. However, as explained in section 5.4.1, one of the main limitations of the introduced non orthogonal FDM system is that $\mathbf{M}$ becomes ill-conditioned as α decreases and/or N increases. In order to ease the severity of this effect, a Regularised SD algorithm [106], [101], [109] is used. In particular, to decrease the matrix $\mathbf{M}$ condition number, regularisation is used by introducing a quadratic

regulator to the cost function of (5.3). Noting that the term $\mathbf{S}^H\mathbf{S}$ is constant for constant modulus schemes (e.g. equal to N), it is possible to transform the original optimisation problem (5.3) into an equivalent problem

$$\text{min.} \quad \left\{ \|\mathbf{R} - \mathbf{MS}\|^2 + \epsilon\mathbf{S}^H\mathbf{S} \right\}, \tag{5.40}$$

$$\text{s.t.} \qquad \mathbf{S} \in Q^N,$$

where ϵ is an arbitrarily selected constant and $(\cdot)^H$ denotes the Hermitian matrix. The above norm could be developed obtaining

$$\text{min.} \quad \{\mathbf{R}^H\mathbf{R} - \mathbf{R}^H\mathbf{MS} - \mathbf{S}^H\mathbf{M}^H\mathbf{R} + \mathbf{S}^H(\mathbf{M}^H\mathbf{M} + \epsilon\mathbf{I_N})\mathbf{S}\},$$

$$\text{s.t.} \qquad \mathbf{S} \in Q^N. \tag{5.41}$$

The full matrix $\mathbf{A} = \mathbf{M}^H\mathbf{M} + \epsilon\mathbf{I_N}$ could also be Cholesky decomposed. The latter is guaranteed to be positive definite, thanks to the added term $\epsilon\mathbf{I_N}$, so that $\mathbf{A} = \mathbf{D}^H\mathbf{D}$, where $\mathbf{D}$ is an upper triangular matrix. Consequently, the optimisation problem reduces to

$$\text{min.} \quad \left\{ \mathbf{R}^H\mathbf{R} - \mathbf{R}^H\mathbf{MS} - \mathbf{S}^H\mathbf{M}^H\mathbf{R} + \mathbf{S}^H\mathbf{D}^H\mathbf{DS} \right\}, \tag{5.42}$$

$$\text{s.t.} \qquad \mathbf{S} \in Q^N.$$

To apply SD to the regularised optimisation problem, the constraint below has to be met

$$\mathbf{R}^H\mathbf{R} - \mathbf{R}^H\mathbf{MS} - \mathbf{S}^H\mathbf{M}^H\mathbf{R} + \mathbf{S}^H\mathbf{D}^H\mathbf{DS} \leq C + \epsilon\mathbf{S}^H\mathbf{S}. \tag{5.43}$$

$\mathbf{P}$ is set to $\mathbf{A}^{-1}\mathbf{M}^H\mathbf{R}$ and the term $\mathbf{P}^H\mathbf{D}^H\mathbf{DP}$ is added to both sides of Eq. (5.43), resulting in the following

$$\mathbf{P}^H\mathbf{D}^H\mathbf{DP} - \mathbf{P}^H\mathbf{AS} - \mathbf{S}^H\mathbf{AP} + \mathbf{S}^H\mathbf{D}^H\mathbf{DS} \leq C'$$

$$\Longleftrightarrow \|\mathbf{D}(\mathbf{P} - \mathbf{S})\|^2 \leq C', \tag{5.44}$$

where:

$$C' = C + \epsilon\mathbf{S}^H\mathbf{S} - \mathbf{R}^H\mathbf{R} + \mathbf{P}^H\mathbf{D}^H\mathbf{DP}. \tag{5.45}$$

α N	0.7	0.75	0.8	0.85	0.9	0.95	1
8	3.15	2.96	2.72	2.26	1.66	1.19	1
16	4.53	4.44	4.31	4.07	3.59	1.93	1
24	5.50	5.40	5.31	5.19	4.85	3.50	1
32	6.33	6.21	6.10	6.01	5.81	4.93	1
40	7.05	6.92	6.80	6.70	6.57	5.80	1

Table 5.2: Matrix $\mathbf{D}$ Condition Number for Varying α and N, for $\epsilon = \frac{1}{N}$

Next, the well known iterative steps of SD, based on the previous formula, are applied. Thanks to Tikhonov regularisation the singular values σ_i' of the Cholesky matrix $\mathbf{D}$ are given by

$$\sigma_i'^2 = \sigma_i^2 + \epsilon, \ i = 1, \ldots, N \tag{5.46}$$

where σ_i are the singular values of the projections matrix $\mathbf{M}$. Since $\epsilon > 0$, then $\mathbf{D}$ is never singular. In addition, numerical results depicted in Table 5.2 demonstrate that its condition is significantly better than that of $\mathbf{M}$ (shown in Table 5.1).

It must also be mentioned that the RegSD based SEFDM detection can be easily expanded to higher level QAM schemes since non-constant modulus [2] M-QAM symbols ($M > 4$) can be expressed as linear combinations of 4-QAM symbols [101], [110]. Finally, in the implementation of the RegSD, the Schnorr-Euchner (SE) enumeration strategy, as applied to MIMO systems in [103], was followed. RegSD pseudocode based on Python symbolics is demonstrated in Fig. 5.20.

---

[2]RegSD detection for SEFDM could also involve higher level M-QAM since non-constant modulus M-QAM can be expressed as linear combinations of 4-QAM symbols [110], [101].

```
def RegSD (M,R, N, lattice_points, SNR)
        ε=1/SNR
        A=M^H M+εI
        D=cholesky{A}
        P=A^-1 M^H R
        C'=∞

        Ŝ_reg=SD (D, P, N, C', lattice_points)
```

Figure 5.20: RegSD pseudocode based on a Python implementation.

5.4.3 RegSD Results

In order to confirm the above theoretical analysis, a number of simulations were performed for different numbers of carriers and frequency distances between them. In the following two sets of results are presented. First, the feasibility of the introduced SEFDM system is investigated by measuring the algorithmic complexity of the RegSD detector. Second, the system concept was validated through BER measurements.

In terms of algorithmic complexity, this work used as a performance measure the logarithmic function $\log(\cdot)$ of the number H of the visits to the RegSD tree nodes, averaged over 1000 SEFDM symbols. Complexity variations were measured versus the number of carriers N and the frequency separation $\alpha = \Delta fT$. In terms of system performance, BER measurements were conducted for up to $N = 32$ carriers with minimum frequency distance equal to $\alpha = 0.7$ of the inverse of the SEFDM symbol, i.e. $\Delta f = \frac{0.7}{T}$. In all simulations, the carriers were modulated by 4-QAM.

Fig. 5.21 demonstrates a first comparison between the typical and regularised versions of SD, both based on real decomposition. It is clear that the regularisation benefits increase as the condition of the matrix $\mathbf{M}$ deteriorates. In particular, for a 4-QAM SEFDM signal of 16 carriers and $\alpha = 0.75$ it can be observed that RegSD runs almost 1000 times faster than RSD.

The following discussion investigates the impact of the Gram matrix condition number and of the noise variance on the computational cost of the proposed
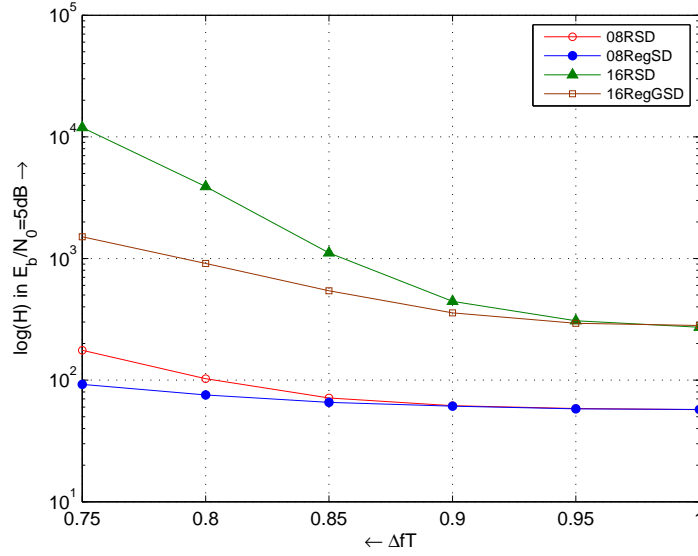
Figure 5.21: Comparison between RegSD and RSD. The number of SEFDM carriers N was either 8 or 16. The modulation scheme was 4-QAM and the E_b/N_0 was set to 5 dB. The RegSD parameter ϵ was set to $\frac{1}{\text{SNR}}$.

RegSD receiver.

In the complexity measurements, the regularisation factor ϵ was set to either σ^2, so that **P** is equal to the MMSE estimate, or $\frac{1}{N}$. Fig. 5.22 shows the SD complexity for different sizes of the SEFDM signal and a fixed value of $E_b/N_0 = 8$ dB. It is clear that for frequency separation $\alpha < 0.9$ and for $N > 16$ carriers the complexity highly increases. Furthermore, it is demonstrated that as N increases, or equivalently as the Gram matrix condition number deteriorates substantially (see Table 5.1), RegSD requires less operations when the regularisation parameter is set to $\epsilon = \sigma^2$ as opposed to $\epsilon = \frac{1}{N}$.

In Fig. 5.23 the measurements were repeated after reducing the amount of noise in the system so that $E_b/N_0 = 15$ dB. The complexity appears to be independent of the carriers frequency separation for $N \leq 40$ carriers and $\Delta f \geq \frac{0.75}{T}$. This confirms theoretical expectations since the number of the RegSD arithmetic operations depends on the number of **MS** points (SEFDM

142
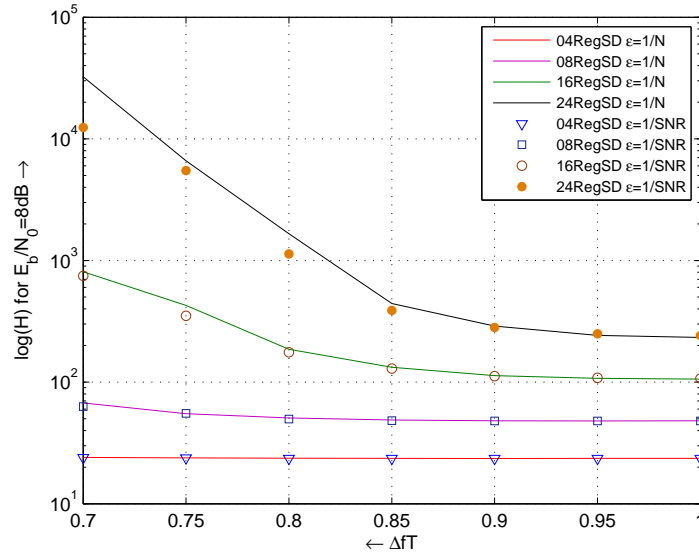
Figure 5.22: Average number of visits of RegSD tree nodes over 1000 SEFDM symbols. The number of SEFDM carriers was $N = 4 \rightarrow 24$ and ϵ was $\frac{1}{N}$ or $\frac{1}{\text{SNR}}$.

symbols transformed by $\mathbf{M}$) that lie within a hypersphere of C radius. As the noise level in the system decreases, the value of the radius decreases and fewer points are enumerated within the sphere.

The complexity for a fixed value of $\Delta fT = 0.75$ for diverse values of E_b/N_0 was also investigated. Fig. 5.24 shows that complexity is independent from the noise only for a small number of carriers ($N = 8$). However, in the high SNR area ($E_b/N_0 > 13$ dB) complexity becomes insensitive to noise for $N \leq 24$.

Summarising the results, it is concluded that RegSD complexity varies with the noise and the matrix $\mathbf{M}$ properties. In particular, the number of arithmetic operations significantly rises as the Gram matrix condition number degrades as well as with increasing noise. Nevertheless, a tolerable cost could be achieved under specific constraints, i.e. $N \leq 40$, $\Delta fT \geq 0.75$, and $E_b/N_0 > 15$ dB.

Error rate simulations were also performed for diverse values of ΔfT as well as for different noise values. Fig. 5.25 shows that with $E_b/N_0 = 8$ dB the system approximates the BER of an OFDM scheme if the frequency separation
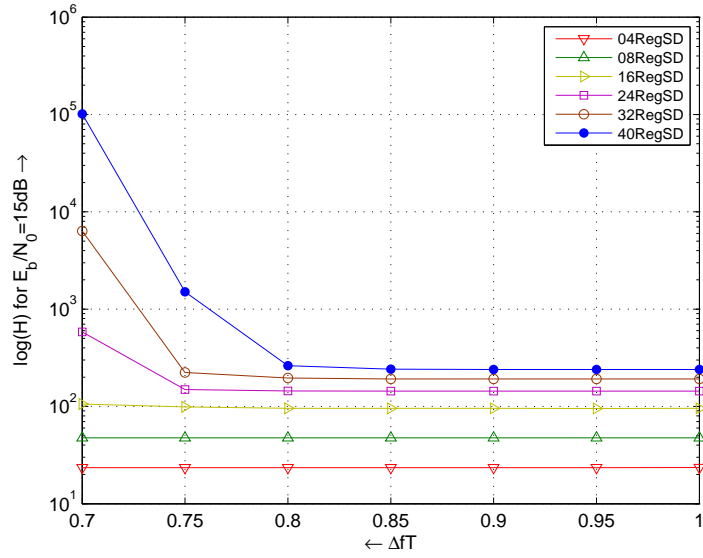
Figure 5.23: Average number of visits of RegSD tree nodes. ϵ was $\frac{1}{\text{SNR}}$.
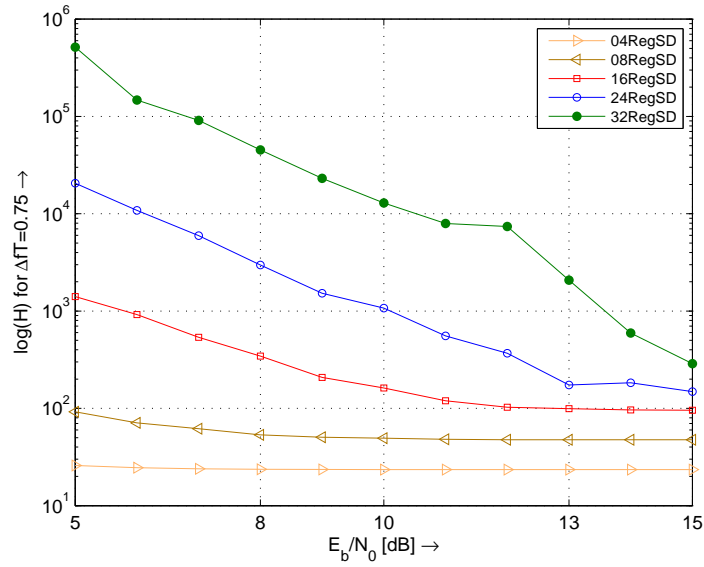
Figure 5.24: Average number of visits of RegSD tree nodes . ϵ was either $\frac{1}{N}$ or $\frac{1}{\text{SNR}}$.

between the SEFDM carriers is reduced to $\frac{0.7}{T}$. Finally, it must be underlined that the regulator ϵ value does not affect the detection error rate thanks to the

144
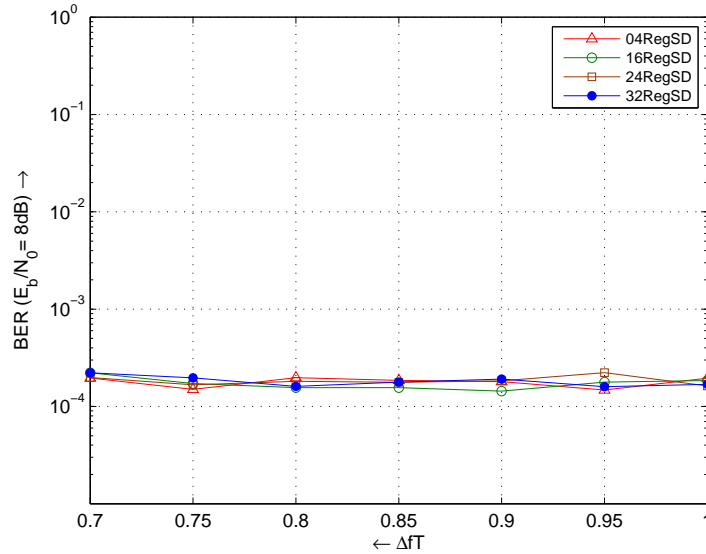
Figure 5.25: BER of 4-QAM SEFDM RegSD detection; ϵ was set to $\frac{1}{\text{SNR}}$

.

equivalence between (5.3) and (5.40). In addition, Fig. 5.26 shows that the SEFDM system with up to 32 carriers and a discount of 25% in the bandwidth of an equivalent OFDM system, approximates the OFDM performance for E_b/N_0 between 5 and 10 dB.

5.5 Summary and Discussion

This chapter addressed the issue of computationally effective optimal detection for non orthogonal SEFDM signals. New algorithms are derived for both the real (RSD) and complex (CSD) versions of the SD detection for SEFDM and the simulation testing of the error performance and complexity of both algorithms. We conclude that CSD is superior to RSD in terms of computational complexity thanks to the avoidance of doubling the depth of the SD tree and the faster initialisation step that takes advantage of the upper triangular nature of the SEFDM system projections matrix. Notwithstanding, it was also found that
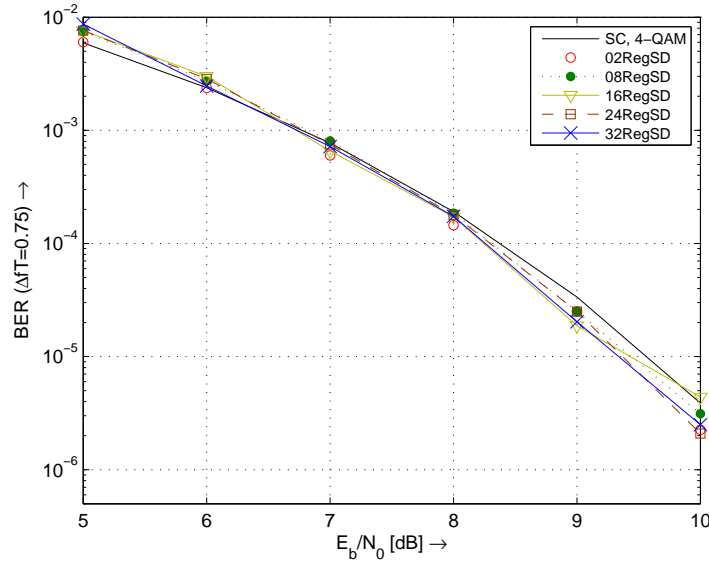
Figure 5.26: BER of 4-QAM SEFDM RegSD detection; ϵ was equal to $\frac{1}{\text{SNR}}$.

the applicability of both SD variances is limited by the severe ill-conditioning of the system Grammian matrix. This is due to the system inherent ICI caused by the deliberate overlapping of the SEFDM sub-bands.

In order to overcome this problem, potential regularisation techniques were explored and the application of the Cui and Tellambura technique, that is based on a modification of the Tikhonov method for the ML unconstrained problem, was explored. In particular, the ill-posed SEFDM ML problem is regularised by adding an extra square term into the LS objective function. It was shown by mathematical derivation and simulation results that the singular values of the new matrix are never zero and that its condition number is significantly improved.

In addition, comparisons between RSD and RegSD were performed and showed that the latter greatly speeds up the SEFDM detection. Consecutively, it was demonstrated that in the region of $E_b/N_0 > 10$ dB the proposed RegSD receiver could afford the computational cost of an optimal detection for a 4-QAM SEFDM signal of $N = 32$ carriers with frequency separation reduced

146

by 25% in relation to an equivalent OFDM system. Moreover, it appears that in higher SNR regimes, i.e. $E_b/N_0 > 15$ dB, the signal dimension could be probably doubled.

Although this work provided some useful insight about the possibility of accomplishing feasible optimal detection for non-orthogonal SEFDM systems, there are still issues that need further clarification. A first important topic is the effect of the regularisation in terms of noise addition in the system. In particular, despite the fact the condition of the regularised inverse matrix is improved, some of the complexity reduction benefit is lost because the radius of the hypersphere is also increased due to the addition of the regularisation penalty term. Thus, the proper choice of the regulator ϵ value should be considered.

Literature is rich of methods (e.g., L-curve, min norm product and U-curve) determining the optimum regulator in the unconstrained regularised LS problem, i.e. where the solution can be any real number [75], [76], [77], [78]. However, there is no such a method for the RegSD application that solves the integer LS (ILS) problem. It must be noticed that in [101], [111] the regulator is set by experimentation, leaving thus a gap for further research of this problem.

Another approach to the same topic could be the investigation of a kind of partial Tikhonov regularisation following the idea introduced in [112]. This would aim to the reduction of the norm of the smoothing term and consequently of the artificial noise introduced in the problem. This could result in a further reduction of SEFDM RegSD complexity.

Finally, we believe that a derivation of a closed formula for the expected complexity of SD over the noise (taking into account the special structure of the SEFDM projections matrix $\mathbf{M}$) may shed some more light on the effect of the noise on the complexity of an SEFDM sphere detector and assist in determining the SNR regimes that allow practical applications of the SEFDM-SD detection.

Chapter 6

Convex optimisation for SEFDM detection

6.1 Introduction

As already seen in the introductory chapters, in the presence of AWGN, the SEFDM detection reduces to a combinatorial optimisation problem. Verdú in [72] showed that a similar ML problem for Multi User Code Division Multiplex Access (MU-CDMA) detection can be classified as an integer linear program and proved that is consequently NP hard to be solved. Moreover, he provided a useful discussion about the possibilities of alternatives based either on investigations for special cases or the application of heuristics that could achieve a faster suboptimal yet accurate enough solution.

Driven by the former observation, research results were later presented demonstrating that a polynomial time solution is tangible when the model coefficients matrix exhibits special properties [123], [124], [125], [126]. Yet, these cases are strictly limited to MU-CDMA scenarios and therefore are out of the scope of this thesis investigations.

In Chapter 5 the problem has been similarly approached by applying dynamic programming techniques like different versions of the SD. It was demon-

strated by modelling and through simulation results that a reliable fast detection could be achievable under special conditions, i.e. for medium size SEFDM systems working in high SNR regimes. However, the proposed technique may prove to be impractical in low SNR even for medium size signals.

In this chapter, work to bridge this gap is attempted following the latter approach suggested by Verdú. To be more specific, the ML detection is reformulated to a semidefinite program that can be solved in polynomial time because to its convex nature [127], [128]. The reformulation method used is well known in the literature and is based on the relaxation of the constraints of the initial NP hard problem. In particular, it was first introduced in communications by Ma et al. [129] as well as Tan et al. [130] for the detection of synchronous MU-CDMA systems. Hence, the fixed complexity of SDP and its sufficient accuracy stimulated further research in different fields like MIMO [131], [132], [133] and more recently spectrally efficient multicarriers systems [46], [48].

Jalden et al. [134], [135] as well as Kisialiou et al. [136], [137] further attempted to derive optimality conditions for the SDP solution. They showed that SDP can achieve the exact ML estimate when the noise level and the coefficients matrix properties comply with specific conditions. Interestingly, initial investigations also showed that a typical SEFDM SDP detector approximates the ML detection but the relaxation gap, i.e. the gap between the optimum and the SDP estimate, broadens as the projections matrix becomes ill conditioned.

In the literature, there are several techniques for the mitigation of the aforementioned gap like the use of Gangster operators [138] or the introduction of cutting planes, i.e. linear inequalities that constrain the feasible set of the SDP program [139], [46].

Following the idea of constraining the feasible set of an optimisation problem, this chapter describes a novel combined SDP-ML algorithm that constrains the feasible set of the original ML problem according to a first SDP estimate. This is conceptually different from existing solutions that apply constraints to

the feasible set of the relaxed problem (not the original ML problem as we use in the new design). Furthermore, in order to reduce the computational effort of the combined SDP-ML detection a novel SD based algorithm, that implements exactly the above concept, is designed and constructed in software. This algorithm appears to be significantly faster than a typical SD in low SNR regimes and for SEFDM signals with $N \leq 48$ carriers, with no more than 1 dB power penalty.

6.2   SDP for the SEFDM detection

Chapter 3 demonstrated that in AWGN the optimum ML detection of the SEFDM signal reduces to the following combinatorial LS problem

$$\text{min.} \quad \|\mathbf{R} - \mathbf{MS}\|^2$$
$$\text{s.t.} \quad \mathbf{S} \in Q^N, \tag{6.1}$$

This section will explore convex optimisation techniques to solve this problem, trading error performance for a fixed computational cost. In particular, it will be adopted a series of reformulation steps of the ML detection problem, which will ultimately lead to an SDP detection problem. In the reformulation, the elements of the vector/matrices in Eq. (6.1) will be represented in their real decoupling versions - rather than their original complex versions - by applying conventional real decomposition methods [130]. Consequently, the problem dimension is effectively doubled from N to $2N$. It will also be assumed that the information symbols take 4-QAM values so that the transformed information symbols take values in the binary $2N$-tuples, $\{\pm 1\}^{2N}$. [1] Hence, it is possible

---

[1] Note that SDP detection for SEFDM could be easily expanded for higher level M-QAM since non-constant modulus M-QAM can be expressed as linear combinations of 4-QAM symbols [110]. Furthermore, relaxations suitable for problems set on higher cardinality alphabets (e.g. M-PSK or 16-QAM) have already been proposed in the literature [139], [132], [133].

to write the problem (6.1) as

$$\text{min.} \quad \tilde{\mathbf{S}}^T \tilde{\mathbf{M}}^T \tilde{\mathbf{M}} \tilde{\mathbf{S}} - \tilde{\mathbf{R}}^T \tilde{\mathbf{M}} \tilde{\mathbf{S}} - \tilde{\mathbf{S}}^T \tilde{\mathbf{M}}^T \tilde{\mathbf{R}}$$

$$\text{s.t.} \qquad \tilde{\mathbf{S}} \in \{\pm 1\}^{2N} , \qquad (6.2)$$

where $(\cdot)^T$ denotes the transpose of a matrix and $\tilde{\mathbf{R}}$, $\tilde{\mathbf{M}}$ and $\tilde{\mathbf{S}}$ are the real versions of the matrices, $\mathbf{R}$, $\mathbf{M}$ and $\mathbf{S}$, respectively.

Adding an extra slack variable $\tilde{S}_{2N+1} = 1$, and thereby increasing the dimension of the problem by one, the cost function of Eq. (6.2) becomes

$$\tilde{\mathbf{S}}^T \tilde{\mathbf{M}}^T \tilde{\mathbf{M}} \tilde{\mathbf{S}} - \tilde{\mathbf{R}}^T \tilde{\mathbf{M}} \tilde{\mathbf{S}} - \tilde{\mathbf{S}}^T \tilde{\mathbf{M}}^T \tilde{\mathbf{R}} = \mathbf{x}^T \mathbf{L} \mathbf{x}, \qquad (6.3)$$

where $\mathbf{L}$ and $\mathbf{x}$ are block matrices given by

$$\mathbf{L} = \begin{bmatrix} \tilde{\mathbf{M}}^T \tilde{\mathbf{M}} & -\tilde{\mathbf{M}}^T \tilde{\mathbf{R}} \\ -\tilde{\mathbf{R}}^T \tilde{\mathbf{M}} & 0 \end{bmatrix} , \quad \mathbf{x} = \begin{bmatrix} \tilde{\mathbf{S}} \\ \tilde{S}_{2N+1} \end{bmatrix} . \qquad (6.4)$$

According to the definition of matrices inner product [53] the Right Hand Side (RHS) of Eq. (6.3) is equal to

$$\mathbf{x}^T \mathbf{L} \mathbf{x} = \left(\mathbf{L}^T \mathbf{x} \right)^T \mathbf{x} = \left\langle \left(\mathbf{L}^T \mathbf{x} \right), \mathbf{x} \right\rangle = \text{Tr}\{ \left(\mathbf{L}^T \mathbf{x} \right), \mathbf{x}^T \} = \text{Tr}\{ \mathbf{L}^T \mathbf{x} \mathbf{x}^T \} \quad (6.5)$$

where $\langle \cdot \rangle$ denotes the matrices inner product and the operator $\text{Tr}\{\cdot\}$ denotes the 'trace' function. The Hermitian nature (by its construction) of the block matrix $\mathbf{L}$ makes the RHS of Eq. (6.5) is equal $\text{Tr}\{\mathbf{L}\mathbf{X}\}$, where $\mathbf{X} = \mathbf{x}\mathbf{x}^T$.

The square matrix $\mathbf{X} = \begin{bmatrix} \tilde{\mathbf{S}} \tilde{\mathbf{S}}^T & \tilde{\mathbf{S}} \\ \tilde{\mathbf{S}}^T & 1 \end{bmatrix}$ has the following properties: its diagonal elements should be equal to unity, its eigenvalues cannot be negative and finally it is of rank 1. Consequently, Eq. (6.2) is equivalent to

$$\text{min.} \qquad \text{Tr}\{\mathbf{L}\mathbf{X}\}$$

$$\text{s.t.} \quad \text{diag}\{\mathbf{X}\} = \mathbf{e}$$

$$\mathbf{X} \succeq 0$$

$$\text{rank}\{\mathbf{X}\} = 1, \qquad (6.6)$$

where the curly inequality $\succeq$ indicates that $\mathbf{X} = \mathbf{x}\mathbf{x}^\mathbf{T}$ is a positive semidefinite matrix (see Appendix C). In addition, $\mathbf{e}$ is a $(2N+1) \times 1$ vector of ones and the diag$\{\cdot\}$ operator generates a $(2N + 1) \times 1$ vector that includes all the diagonal elements of the argument matrix. Finally, the rank$\{\cdot\}$ operator provides the rank of the square matrix $\mathbf{X}$.

The ML problem in (6.1) is non convex because of the non convex domain Q^N of the objective function. Hence, the equivalent problem of (6.6) is also non convex (see Appendix C). Consequently, it is still NP hard. However, convexity can be accomplished by relaxing the constraints of Eq. (6.6) after discarding the non affine rank$\{\mathbf{X}\} = 1$. Thus, Eq. (6.6) is transformed to

$$
\begin{aligned}
&\text{min.} && \text{Tr}\{\mathbf{L}\mathbf{X}\} \\
&\text{s.t.} && \text{diag}\{\mathbf{X}\} = \mathbf{e} \\
& && -\mathbf{X} \preceq 0.
\end{aligned} \tag{6.7}
$$

Further, this problem is an SDP owing to the positive semidefinite constraint $\mathbf{X} \succeq 0$, so that it can be very efficiently solved using well known Interior Point Methods (IPM) [140] applied for the solution of such programs with linear objectives and constraints.

It would be useful to mention that this is not the only way to reformulate the ILS problem of the ML detection to an SDP program. Another approach is to solve the so called bi-dual problem [132], i.e. the dual (see Appendix C) of the dual, of the primal ML detection as this is described in Eqs (6.1) and (6.6). This is always convex yet not equivalent to the initial non-convex primal problem described in Eq. (6.1).

Finally, it is necessary to underline that SDP is a sub-optimum technique since its solution does not always coincide with the solution of the initial ML problem. In order to decrease the so called relaxation gap between these two solutions, a new technique, combining SDP with brute force ML, has been designed and will be introduced below.

6.2.1 Recovery of the SEFDM symbol

The outcome of the SDP is not the desired vector $\tilde{\mathbf{S}}$ but the square matrix $\mathbf{X}$. Yet, a method for the recovery of the estimate $\hat{\mathbf{S}}$ of the SEFDM symbol is needed. In the literature, a number of different methods are proposed. In this paragraph, the most common ones are described, that can be categorised in the following: i) the rank-1, ii) the dominant eigenvector and iii) the randomisation techniques.

i) Starting by the simplest, the rank-1 method [131] is based on the assumption that SDP returns the exact solution of the ML problem. This implies that $\text{rank}\{\mathbf{X}\} = 1$ and consequently $\mathbf{X}$ last column should correspond to the vector $\mathbf{x}^T = \begin{bmatrix} \tilde{\mathbf{S}} \\ 1 \end{bmatrix}$. Hence, the last column of the optimal $\mathbf{X}$ is chosen and a slicing function $\text{sign}\{\cdot\}$ is applied over the first $2N$ elements of the column. The final SDP estimate of the SEFDM symbol $\hat{\mathbf{S}}$ is given by

$$\hat{\mathbf{S}} = \text{sign}\{\mathbf{X}_{i,2N+1}\}, \ i = 1, \ldots, 2N, \tag{6.8}$$

with

$$\text{sign}\{\mathbf{X}_{i,2N+1}\} = \begin{cases} +1 & , & \mathbf{X}_{i,2N+1} > 0 \\ -1 & , & \mathbf{X}_{i,2N+1} \leq 0 \end{cases}.$$

Another approximation is the so called Dominant EigenVector (DEV) method [139] that comprises of the following steps:

1. The solution of (6.7) matrix $\mathbf{X}$ is eigenvalue decomposed so that $\mathbf{X} = \mathbf{U}\text{diag}(\lambda_i)\mathbf{U}^T$, where λ_i are its eigenvalues and $\mathbf{U}$ the matrix of its eigenvectors $\mathbf{u_i}$, $i = 1, \ldots, 2N + 1$, respectively;

2. Pick up the vector $\mathbf{v_m} = \sqrt{\lambda_m}\mathbf{u_m}$ that is associated to the maximum eigenvalue λ_m;

3. Set $\mathbf{x} = \begin{cases} \mathbf{v_m} & \textit{if } \mathbf{v_m}[2N + 1] \geq 0 \\ -\mathbf{v_m} & \textit{if } \mathbf{v}_m[2N + 1] < 0 \end{cases}$;

4. Then, $\hat{\mathbf{S}} = \text{sign}\{\mathbf{x}\}$.

Finally, the randomisation process [129], [136] and [128] is described in the following:

1. Generate a vector $\mathbf{v_m}$ applying the first two steps of the DEV method;

2. For each of the $2N + 1$ entries of the estimate $\hat{\mathbf{x}}$ of the $\mathbf{x}$ vector, set up a Bernoulli distribution with the following probabilities

   $P\{\hat{x}_i = 1\} = \frac{1+v_{m,i}}{2}$,

   $P\{\hat{x}_i = -1\} = \frac{1-v_{m,i}}{2}$;

3. Set $\hat{x}_i = -\hat{x}_i$ if $\hat{x}_{2N+1} = -1$, $\forall i$.

4. Create a number of K random outputs $[\hat{x}_1, \hat{x}_2, \ldots, \hat{x}_{2N+1}]^T$ and choose the one that minimizes the cost of RHS of Eq. (6.3).

5. Set the SDP FDM solution $\hat{\mathbf{S}}_{SDP}$ equal to the first $2N$ entries of the selected random output $\hat{\mathbf{x}}$.

Since, in the literature there is no close formula for the performance of the above heuristics, some preliminary simulations were run in order to evaluate their suitability for the SEFDM detection. In particular, BER was measured for all three different techniques for a fixed size $N = 8$ or $N = 16$ SEFDM signal, different values of $\alpha = \Delta f T$ and for a fixed E_b/N_0 of 5 dB.

Fig. 6.1 demonstrates findings that show that until the $\alpha = 0.8$ point the DEV and the randomisation techniques are quasi-optimal while the rank-1 starts deviating from the optimal solution (as represented by the Regularised SD curve). It is further observed that as the matrix condition deteriorates with increased N and reduced α, due to α reduction, this gap broadens and the randomisation appears to work better. Hence, in the modelling it is this method that is applied since cases where the projections matrix is severely ill-conditioned, due to the overly ICI among the SEFDM sub-bands are the cases of interest in this research.
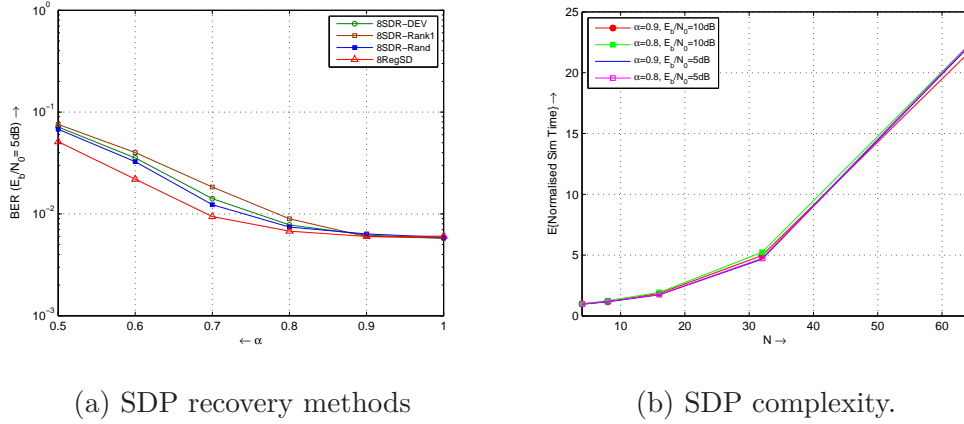
(a) SDP recovery methods

(b) SDP complexity.

Figure 6.1: (a) Comparisons of recovery methods of the transmitted SEFDM symbol from the SDP estimate. 'DEV' and 'Rand' correspond to the Dominant Eigenvector and the Randomisation techniques, respectively. (b) Complexity of SDP versus the size of the SEFDM signal.

6.2.2 SDP Complexity

In the SDP implementations, the CVX optimisation tool [141], [142] was used. CVX provides the user with an easy way of formulating convex optimisation problems in Matlab language. Then, CVX calls the Self Dual Minimization (SeDuMi) solver for the solution of the introduced convex programs.

The SeDuMi solver applies well known primal-dual Interior Point Methods (IPM) [143] that have a polynomial order of complexity [140]. The solution of SDP based on IPM is $O(N^{3.5})$. This is because IPM approximate the solution through an iterative process. The complexity of each iteration is $O(N^3)$ while for a good accuracy the number of iterations required is at most $O(N^{0.5})$ [139].

It is noted that the real decoupling has an effect on the process complexity since it results in the doubling of the dimension of the SEFDM detection problem. Consequently, the computational effort for each iteration is $O((2N)^3)$ and the overall IPM $O((2N)^3 N^{0.5})$.

Nevertheless, the advantage of the SDP relaxation is that it has a fixed

complexity, insensitive to the noise in the system in contrast to the Sphere Decoders studied in Chapter 5. Fig. 6.1 shows indicative simulation results for the normalised average SDP detection time of one SEFDM symbol for N ranging from 4 to 64 sub-carriers, $\alpha \in \{0.8, 0.9\}$ and $E_b/N_0 \in \{5, 10\}$ dBs. It is apparent that the SDP complexity depends only on the signal dimension and is immune to the noise and $\mathbf{M}$ ill conditioning.

6.3 A new SDP based Boxed ML detection

In SDP-ML technique, a two step procedure is used. Initially, the SDP estimate $\tilde{\mathbf{S}}$ of the originally transmitted symbols $\mathbf{S}$ is generated. Subsequently, it is used the ML principle in a neighborhood, $\mathcal{D}$, of $\tilde{\mathbf{S}}$. The neighborhood consists of the set of transmitted symbols whose binary representation is within a certain Hamming distance parameter, ρ, from the binary representation of $\tilde{\mathbf{S}}$. This procedure is commonly known as boxed ML [144].

The neighborhood $\mathcal{D}$ consists of the set of transmitted vectors $\mathbf{S}$ obeying the relationship: $d_H \left\{ \mathbf{S}', \tilde{\mathbf{S}}' \right\} \leq \rho$ where $d_H \left\{ \cdot, \cdot \right\}$ represents the Hamming distance operator , $\mathbf{S}'$ represents the binary version of $\mathbf{S}$, and $\tilde{\mathbf{S}}'$ represents the binary version of $\tilde{\mathbf{S}}$, i.e.

$$\mathbf{S} \in \mathcal{D} \text{ iff } d_H \left\{ \mathbf{S}', \tilde{\mathbf{S}}' \right\} \leq \rho \tag{6.9}$$

A block diagram of the proposed receiver is given in Fig. 6.2.

To demonstrate the way the proposed algorithm works, a numerical example is given for a 4-QAM SEFDM signal of only $N = 2$ sub-carriers with $\alpha = 0.8$. The 2×2 complex projections matrix $\mathbf{M}$ of the SEFDM system is

$$\mathbf{M} = \begin{bmatrix} 1 & -0.1892 + 0.1375i \\ 0 & 0.9723 \end{bmatrix}. \tag{6.10}$$

The actually transmitted SEFDM symbol $\mathbf{S}$ and a random generation of
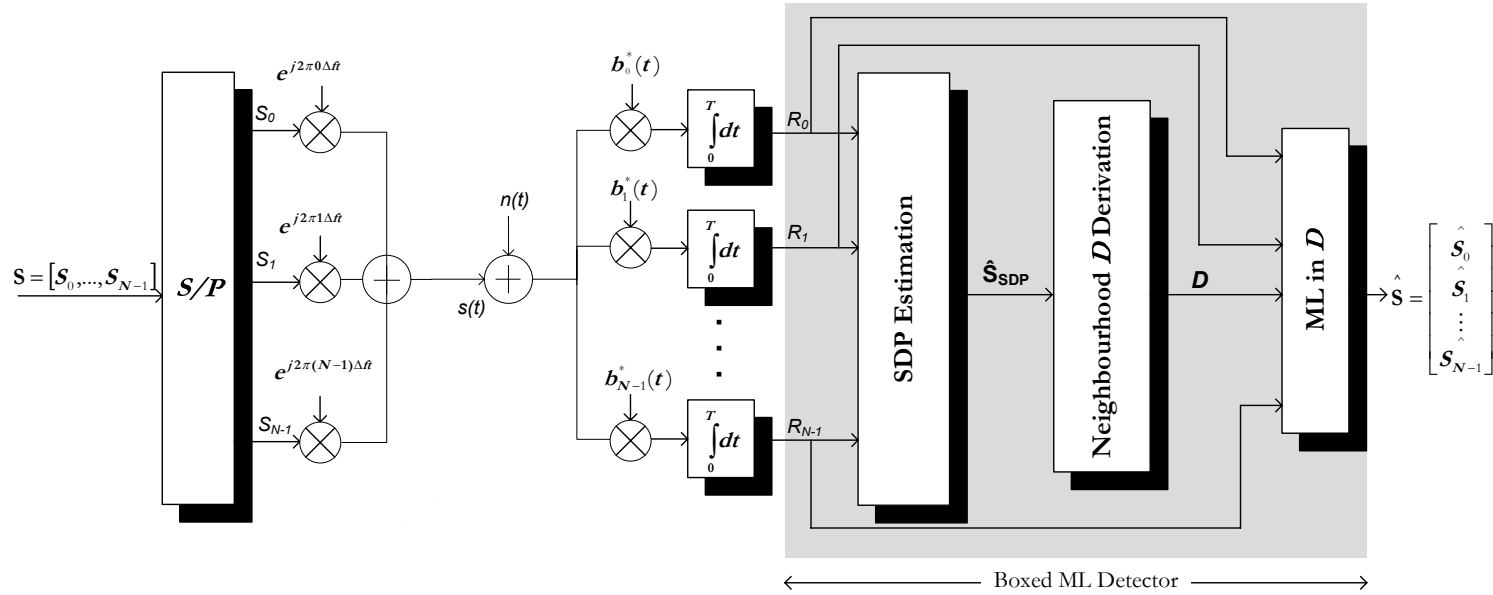
Figure 6.2: A coarse block diagram of the boxed SDP-ML detector.

the statistics vector $\mathbf{R}$ are, respectively

$$\mathbf{S} = \begin{bmatrix} 1.0 + 1.0i \\ 1.0 - 1.0i \end{bmatrix}, \ \mathbf{R} = \begin{bmatrix} -0.2401 + 0.9511i \\ 1.5583 - 1.2897i \end{bmatrix}. \tag{6.11}$$

After the real decoupling process, the SDP calculates an estimate of the SEFDM symbol whose real decoupled version $\tilde{\mathbf{S}}$ is

$$\tilde{\mathbf{S}} = \begin{bmatrix} -1.0 \\ +1.0 \\ +1.0 \\ -1.0 \end{bmatrix}, \tag{6.12}$$

that obviously diverges from the optimal solution $\mathbf{S}$. If $\rho = 1$, the following neighborhood D is created by flipping the binary version of $\tilde{\mathbf{S}}$ $(2 \times \log_2 4) = 4$ times by 1 bit at a time

$$D = \left\{ \begin{bmatrix} -1 \\ +1 \\ +1 \\ -1 \end{bmatrix}, \begin{bmatrix} +1 \\ +1 \\ +1 \\ -1 \end{bmatrix}, \begin{bmatrix} -1 \\ -1 \\ +1 \\ -1 \end{bmatrix}, \begin{bmatrix} -1 \\ +1 \\ -1 \\ -1 \end{bmatrix}, \begin{bmatrix} -1 \\ +1 \\ +1 \\ +1 \end{bmatrix} \right\}, \tag{6.13}$$

Finally, the metric of the problem of Eq. (6.1) is calculated over the columns of D that is a subset of the initial feasible set $(|D| = 5$ while $\left| Q^N \right| = 16$, where $|\cdot|$ denotes the set cardinality).

The combined SDP-ML estimate $\hat{\mathbf{S}}$ is

$$\hat{\mathbf{S}} = \begin{bmatrix} 1.0 + 1.0i \\ 1.0 - 1.0i \end{bmatrix}, \tag{6.14}$$

that is apparently equal to the transmitted symbol.

6.3.1 SDP-ML Complexity

The complexity of the proposed method depends on the number of calculations of both the SDP and ML components of the algorithm. The former has

polynomial complexity of order $O((2N)^3 N^{0.5})$ over the number of sub-carriers N [140]. The computational cost of ML depends on the size of the SDP neighborhood $\mathcal{D}$, since this determines the number of the executed ML comparisons. The length of the expanded SEFDM symbols is equal to $N \times \log_2 M$. Consequently, the size of the neighborhood $\mathcal{D}$ will be equal to the sum of all possible combinations of $N \times \log_2 M$ bits with k flipped bits taken at a time, where k runs from 1 to ρ, i.e.

$$
\begin{aligned}
size(D) &= \sum_{k=1}^{\rho} \binom{N \log_2 M}{k} + 1, \\
&= \sum_{k=1}^{\rho} \frac{(N \log_2 M)!}{(N \log_2 M - k)! k!} + 1.
\end{aligned} \tag{6.15}
$$

The unity term is due to the inclusion of the $\hat{\mathbf{S}}$ in the brute force part.

It is apparent that for ρ equal to unity, the number of necessary boxed ML comparisons is $N \log_2 M$, as opposed to the M^N comparisons required for the ML implementation over the entire group of SEFDM symbols. Table 6.1 provides the ratio γ of the number of ML over SDP-ML comparisons for various 4-QAM SEFDM signal dimensions and ρ equal to 1 or 2.

ρ	$\gamma, N = 8$	$\gamma, N = 16$	$\gamma, N = 32$
1	4096	$> 10^8$	$> 10^{17}$
2	480	$> 10^6$	$> 10^{15}$

Table 6.1: Ratio γ of ML over the SDP-ML Comparisons

6.3.2 Numerical Results

Simulations were performed to investigate the efficiency of the SDP-ML detection. A pseudocode for the SDP in this work modelling is given in Fig. 6.3.

Results were taken for different numbers N of 4-QAM modulated SEFDM sub-carriers with normalised frequency separation $\alpha \in [0.5, 1]$. E_b/N_0 range was

```
def SDP (M,R)
        M̃=decouple{M},
        R̃=decouple{R}
        L = [ M̃^T M̃    − M̃^T R̃ ]
            [ − R̃^T M      0    ]
            cvx_begin sdp
                        variable x(2N+1, 2N+1)
                        minimize(Tr{Lx])
                        diag(x)==ones(2N+1,1)
                        x==semidefinite(2N+1)
            cvx_end

        Ŝ_SDP=randomise{x}
```

Figure 6.3: Pseudocode for the SDP implementation using the CVX tool. The shadowed part corresponds to the CVX SDP formulation.

set from 0 to 8 dB. In all simulations, the number of iterations of the randomisation process [136] was set to be equal to 10. In addition, the performance curves corresponding to MMSE and SD receivers were used for comparison purposes.

Fig. 6.4 demonstrates the complexity of the single SDP and the proposed SDP-ML techniques versus α. In particular, the normalised simulation time was used as an indicative measure of comparison. Results were taken for different numbers of SEFDM sub-carriers and a fixed value of E_b/N_0 equal to 5 dB. The Hamming distance parameter ρ was set to be either 1 or 2. From the simulations outcome two conclusions are made: First, the computational effort required by both schemes, SDP and SDP-ML, is fixed with respect to α. Second, the SDP-ML detection with $\rho = 1$ approximates the single SDP in terms of complexity. However, for $\rho = 2$ the simulation time of the former appears to be approximately 100 times larger than the latter. Therefore, it is heuristically concluded that $\rho = 1$ would be a suitable choice for a practical implementation of the introduced scheme.

In Fig. 6.5 the BER performance of the SDP and SDP-ML based detection techniques is evaluated. Measurements were taken for 8 to 32 SEFDM
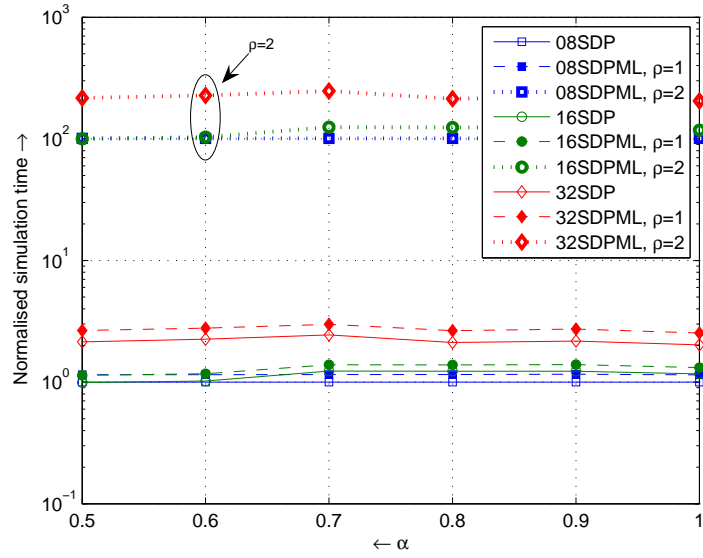
Figure 6.4: Complexity comparison of SDP and SDP-ML detection (Hamming distance $\rho = 1$ and 2) versus α; N ranged from 8 to 32 and E_b/N_0 set to 5 dB.
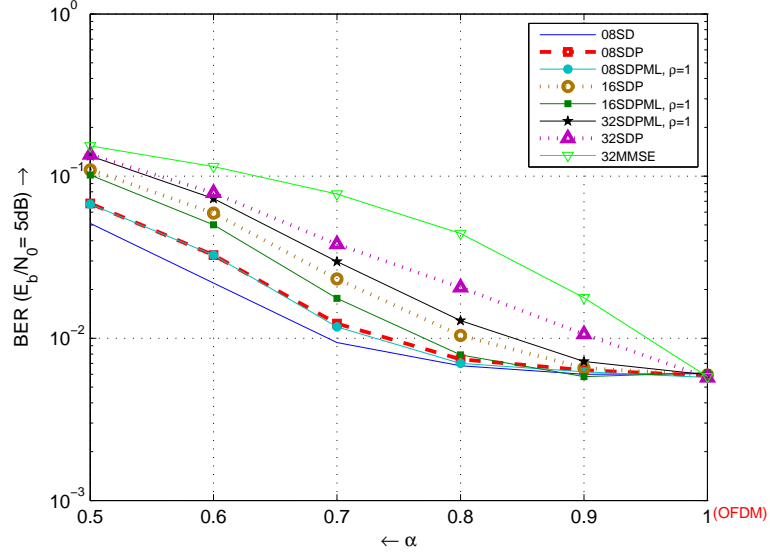
Figure 6.5: Error Performance of the SDP and SDP-ML detection techniques versus α; E_b/N_0 set to 5 dB.

sub-carriers, with frequency separation ranging from the OFDM ($\alpha = 1$) to the half OFDM ($\alpha = 0.5$) ones. In addition, E_b/N_0 was set to a fixed value of 5 dB. Results show that for small signal dimensions ($N = 8, 16$) and for $\alpha \geq 0.8$ SDP performs close to optimum. However, as α further decreases and/or the dimension of the SEFDM signal N increases the relaxation gap opens as a consequence of the deterioration of the projections matrix $\mathbf{M}$ condition, resulting in a significant detection degradation. Notwithstanding, for $N > 8$ it is apparent that the relaxation gap with the SDP-ML detection is much smaller than in the case of the SDP.

Fig. 6.6 illustrates the BER versus E_b/N_0 curves for the SDP and SDP-ML, respectively. The normalised frequency separation α of the SEFDM sub-carriers was fixed and equal to 0.8 since it appears from Fig. 6.5 that for this value the relaxation gap is relatively small. Results show that for $N = 8$ and 16 SEFDM performance is very close to ideal/Single Carrier (SC). However, as N increases it can be seen that the relaxation gap results in diverging from the ideal OFDM case. Nevertheless, in all simulations SDP performed better than the linear MMSE detector that is actually a looser than SDP relaxation of the ML problem [129], [145]. Furthermore, it is notable that for $\alpha = 0.8$ and $N = 32$ the proposed SDP-ML method offers a modest 1 dB E_b/N_0 gain with respect to the single SDP detection.

Fig. 6.7 also shows the error performance of the SDP-ML detection versus E_b/N_0 for different dimensions of the SEFDM signal and with varying α. In the figure, the BER value of 6×10^{-3}, correspondent to a single carrier E_b/N_0 of 5db, is plotted as a reference line for the sake of comparison. It appears that as the size of the signal increases and/or α decreases extra power is required so that the SDP-ML with $\rho = 1$ detection achieves this BER target.

Finally, Fig. 6.8 demonstrates the Spectral Efficiency (SpE) of the SDP-ML 4-QAM SEFDM scheme with $\rho = 1$, versus the E_b/N_0 required to achieve a BER of 6×10^{-3}. The SpE of such SEFDM systems with 16 and 32 sub-carriers
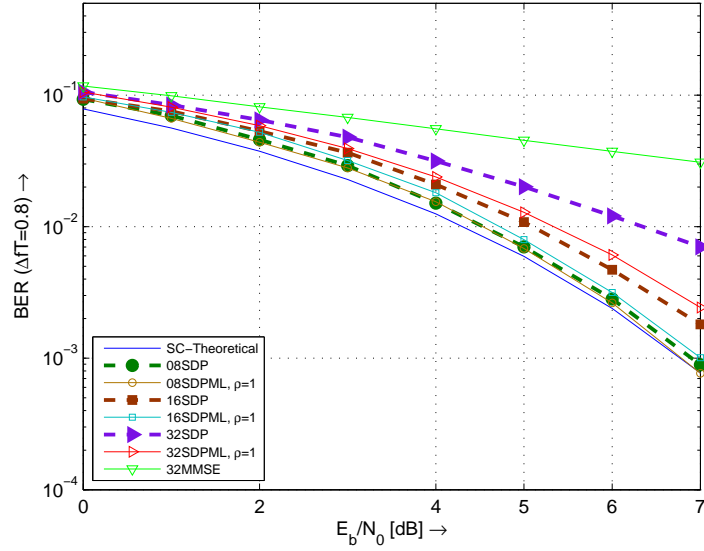
Figure 6.6: Error Performance of the SDP and SDP-ML detection techniques for different values of E_b/N_0 and SEFDM sub-carriers number N; α set to 0.8.
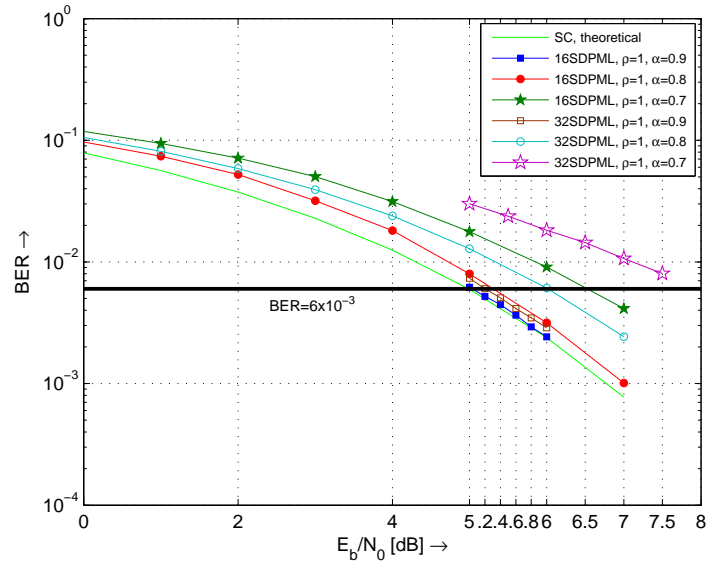
Figure 6.7: Error Performance of the SDP-ML detection ($\rho = 1$) for different values of E_b/N_0; N equal to 16 or 32 and $\alpha = \Delta fT$ set from 0.9 to 0.7.
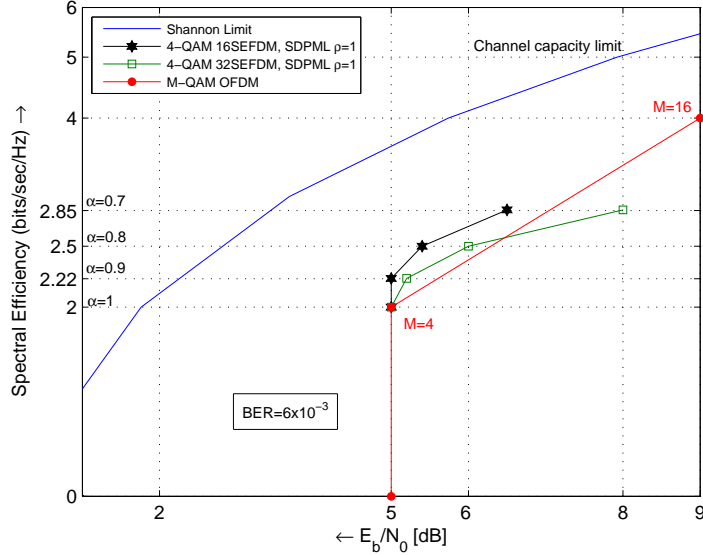
Figure 6.8: Spectral efficiency of an SDP-ML non-orthogonal FDM system versus the E_b/N_0, for a BER target of 6×10^{-3}; the SDP-ML ρ set to 1.

is compared to the SpE of a symbol rate/equivalent OFDM. The Shannon limit for the normalised capacity of a band-limited AWGN channel [52] serves as an upper bound. It is clear that SEFDM is superior as opposed to OFDM for $\alpha \geq 0.8$ (that achieves a SpE of 2.5). Notwithstanding, the larger SEFDM with $N = 32$ sub-carriers does not offer absolute SpE benefit for $\alpha = 0.7$ though the SEFDM signal occupies a smaller bandwidth than OFDM. This is due to the power penalty that should be paid because of the degradation of the error performance of the SDP-ML detection as the size of the SEFDM signal increases and/or the SEFDM sub-carriers frequency separation decreases.

6.4 Pruned Sphere Decoder (PSD)

Motivated by the SDP-ML finding, this work proposes a modified SD version that could implement faster the SDP-ML method thanks to the reduction in the computation of the brute force ML part. The apparent benefit of such

an arrangement could be a further increase in the dimension of the detectable signal thanks to the smaller computational effort and/or the use of a larger than 1 Hamming distance parameter.

1. In particular, the proposed algorithm involves two consecutive steps: Initially, the SDP estimate $\tilde{\mathbf{S}}$ of the transmitted SEFDM symbol is calculated. Furthermore, the new radius C' of the RegSD hypersphere is derived according to Eq. (5.45) as

$$C' = \left\| \mathbf{R} - \mathbf{M}\tilde{\mathbf{S}} \right\|^2 + \epsilon \tilde{\mathbf{S}}^T \tilde{\mathbf{S}} - \mathbf{R}^T \mathbf{R} + \mathbf{P}^T \mathbf{D}^T \mathbf{D} \mathbf{P}. \tag{6.16}$$

Consequently, $\tilde{\mathbf{S}}$ lies on the surface of the RegSD sphere.

2. An extra condition is added in the RegSD implementation of Section 5.4 so that the algorithm never traces the RegSD tree paths that correspond to the SEFDM symbols that have larger Hamming distance from the calculated $\tilde{\mathbf{S}}$ than a selected ρ value. This pruning results in reducing the RegSD in the

$$
\begin{aligned}
\text{min.} \quad & \left\| \mathbf{D} \left(\mathbf{P} - \mathbf{S} \right) \right\|^2, \\
\text{s.t.} \quad & \left\| \mathbf{D} \left(\mathbf{P} - \mathbf{S} \right) \right\|^2 \leq C', \\
& \mathbf{S} \in \{\pm 1\}^{2N}, \\
& d_H = \text{HD} \left\{ \mathbf{S}, \tilde{\mathbf{S}} \right\} \leq \rho, \tag{6.17}
\end{aligned}
$$

where the HD $\{\cdot, \cdot\}$ operator calculates the Hamming distance between the argument vectors and ρ is the heuristically predefined value of d_H that could range from 0 to $N\log_2 M$ (i.e., the length of the binary representation of $\tilde{\mathbf{S}}$).

Fig. 6.9 provides a flow chart of the pruned SD algorithm. The red dotted lined boxes correspond to the add-in modifications of the algorithm. It is obvious that the main alteration is the addition of an if loop that checks the Hamming distance between the path and the respective part of the SDP estimate at each visited tree node. Should $d_H \geq \rho$ at a node, the algorithm cuts the attached subtree and continues the search going backwards.
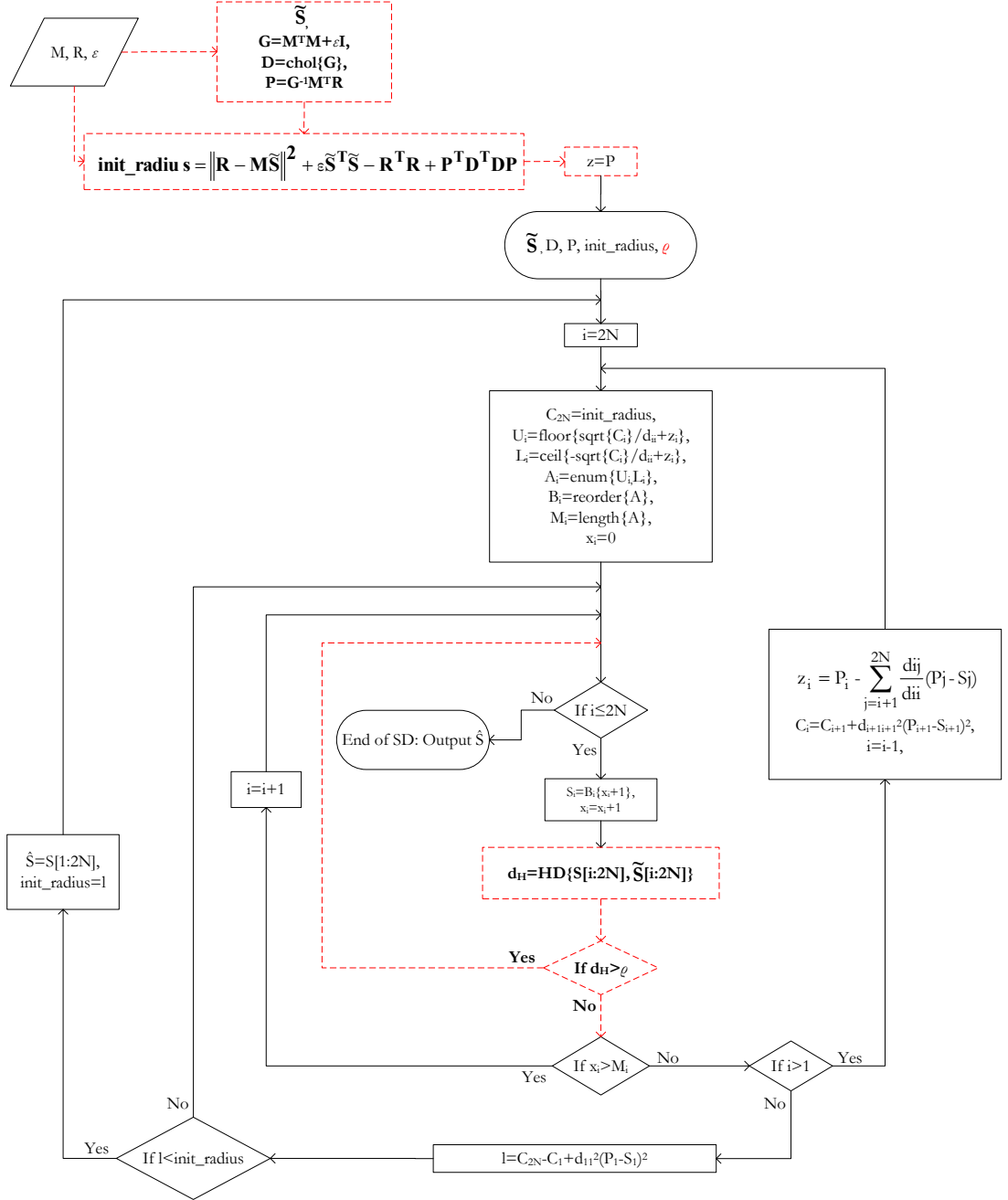
Figure 6.9: A flow chart of the Pruned Sphere Decoding (PSD) algorithm.

In order to simplify the understanding of the pruning of the PSD tree, the following example is provided: a BPSK SEFDM signal of $N = 3$ carriers is assumed. The full RegSD tree has $2^3 = 8$ different paths that correspond to the full feasible set of the ML optimisation problem. If the derived $\tilde{\mathbf{S}}$ is $[-1, +1, +1]^T$ and the Hamming distance is $\rho = 1$ then the pruned SD tree includes only 4 (out of 8) paths as shown in Fig. 6.10. As a consequence, it will be expected that the number of the visits to the SD nodes will be significantly reduced as opposed to the full SD at the expense of a penalty in the optimality of the achieved BER.

Moreover, as opposed to the SDP-ML, the pruned SD is expected to achieve the same error performance for the same given d_H without necessarily tracing all the 4 paths of the pruned SD tree as in the boxed ML case.

6.4.1 PSD modelling and Simulation Results

An algorithmic implementation of the PSD was done through MATLAB coding in order to evaluate performance. A set of simulations was run for varying number of SEFDM carriers N and frequency separation ranging from $\alpha = 1$ (OFDM) to $\alpha = 0.5$ (half OFDM). The proposed scheme was also tested for
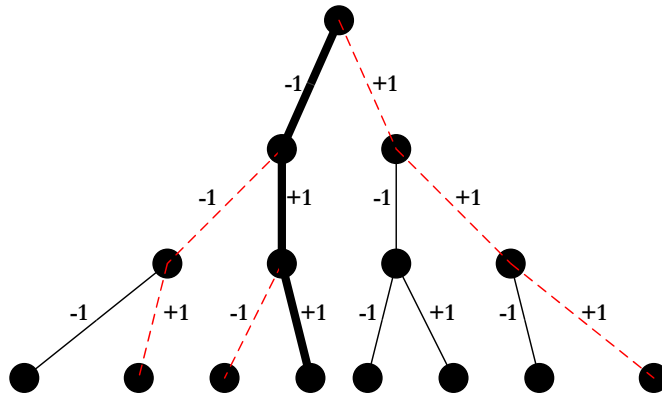
Figure 6.10: Full (all lines) and Pruned (dotted lines) SD tree. The SDP estimate is represented by the bold solid line.

various values of the parameter ρ of the added constraint of Eq. (6.17).

In all cases, the error performance and complexity of the proposed PSD algorithm were compared through simulation to those of the SDP-ML approach, as well as to the optimal RegSD. As far as the error performance is concerned, the BER, versus the normalised frequency separation α or the Energy of the bit over the Noise power density E_b/N_0, was used as a measure of comparison. Moreover, the complexity was evaluated in terms of simulation time and visits to the RegSD tree nodes for the comparison with SDP-ML and simple RegSD, respectively. A simplified pseudocode for this work implementation is given in Fig. 6.11.

6.4.2 PSD Error Performance

Fig. 6.12 depicts the error performance of the PSD scheme versus the normalised frequency separation α of the SEFDM carriers. The PSD results are compared to the SDP-ML detection error rates for different number of carriers N and values of the Hamming distance parameter ρ. In addition, the BER curves of the simple RegSD detection for $N = 8$ and $N = 16$ represent the optimal detection for these SEFDM signal dimensions. It is apparent that in all cases the performance of the PSD method is equivalent to the performance of the SDP-ML scheme with the same ρ. Furthermore, the proposed scheme offers a suboptimal solution since it diverges from the RegSD curves especially after the $\alpha = 0.8$ point. However, as the condition for the Hamming distance relaxes (i.e. ρ becomes larger) the performance difference between RegSD and PSD results decreases. In particular, it is notable that for $N \leq 32$ and $\rho \leq 2$ PSD approximates the optimal detection.

The simulations were repeated for $\alpha = 0.8$ and E_b/N_0 that ranged from 0 to 7 dB. In Fig. 6.13, it can be seen that PSD achieves exactly the SDP-ML performance for $\rho = 1$. In addition, it is observed that for $N = 32$, a larger $\rho = 2$ improves further the PSD performance offering an almost 2 dB

```
def   PSD (M, R, N, SNR, lattice_points, ρ)
          S'   = SDP(M,R)
          A   = M^H M+(1/SNR)I_N
          D   = cholesky(A)
          P   = A^-1 M^H R
          C   = (R-MS')^H(R-MS')+(1/SNR)–R^H R+P^H D^H DP
          D'=decouple{D}, P'=decouple{P}
          ρ = P', L=D'
          i=2N,  C_i= C,  ξ_i=ρ_i
          LB_i = ceil{-√(C_i/l_i,i²)+ξ_i}
          UB_i = floor{√(C_i/l_i,i²)+ξ_i}
          A_i   = enum{lattice_points, LB_i, UB_i}
          B_i   = sortSE{A_i, ξ_i}
          M_i   = length{B_i}, x_i=0
          while i<=2N:
                    S_i= B_i,x
                    x_i+=1
                    d_H=HD{S(i:2N),S'(i:2N)}
                    if d_H>ρ & x_i<= M_i:
                              continue
                    else:
                              if x_i> M_i:
                                        i+=1
                                        continue
                              elif i>1:
                                        i-=1
                                        C_i     = C_i+1 - l_i+1,i+1²(ξ_i+1 - S_i+1)²
                                        ξ_i=ρ_i + l_i,i+1:2N/l_i,i (ρ_i+1:2N - S_i+1:2N)
                                        LB_i   = ceil{-√(C_i/l_i,i²)+ξ_i}
                                        UB_i   = floor{√(C_i/l_i,i²)+ξ_i}
                                        A_i     = enum{lattice_points, LB_i, UB_i }
                                        B_i     = sortSE{A_i, ξ_i}
                                        M_i     = length{B_i}, x_i = 0
                              elif C_N-1 – C_1+l_1,1²(ξ_1-S_1)² < C:
                                        C       = C_N-1 – C_1+l_1,1²(ξ_1 - S_1)²
                                        C_N-1   = C_N-1 – C_1+l_1,1²(ξ_1 - S_1)²
                                        Ŝ  = S, i = 2N
                                        LB_i   = ceil{-√(C_i/l_i,i²)+ξ_i}
                                        UB_i   = floor{√(C_i/l_i,i²)+ξ_i}
                                        A_i     = enum{lattice_points, LB_i, UB_i }
                                        B_i     = sortSE{A_i, ξ_i}
                                        M_i     = length{B_i}, x_i = 0
          Solution = recomp{Ŝ}
return [Solution]
```

Figure 6.11: Pseudocode for PSD. The shadowed areas depict the modifications in the proposed algorithm as opposed to a typical Sphere Detector.
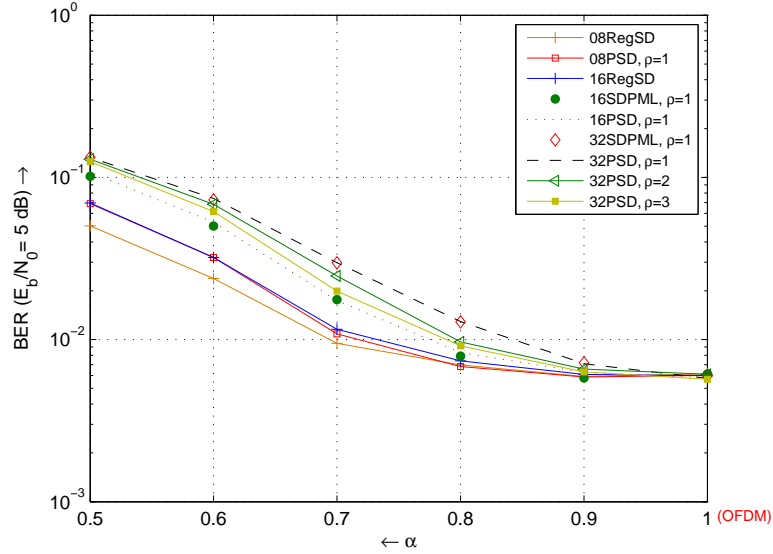
Figure 6.12: Error Performance of the proposed PSD scheme versus α.

gain as opposed to the simple Semidefinite Programming (SDP) detection. Results depicted in 6.14 show that PSD achieves a quasi optimal BER for $N \leq 48$ upon the selection of the proper value for the Hamming distance parameter. Heuristically, this is found to be $\rho = 1, 2$ and 3 for $N = 16, 32$ and 48, respectively. It is notable that for $N = 48$ a small tightening of the d_H constraint so that $\rho = 2$, introduces no more than an extra 0.5 dB of error penalty.

6.4.3 PSD Complexity

The computational complexity of the proposed method was evaluated and compared to the SDP-ML and the full tree RegSD methods. Fig. 6.15 shows the simulation time required by the SD or the ML parts of the pruned SD and SDP-ML, respectively. All the results were normalised over the values of the 32SDP-ML with $\rho = 1$. It is clear that PSD performs faster than an equivalent, i.e. using the same ρ, SDP-ML scheme. For example, it can be seen that for the detection of an SEFDM signal with $N = 32$ and $\alpha = 0.8$, PSD performs almost
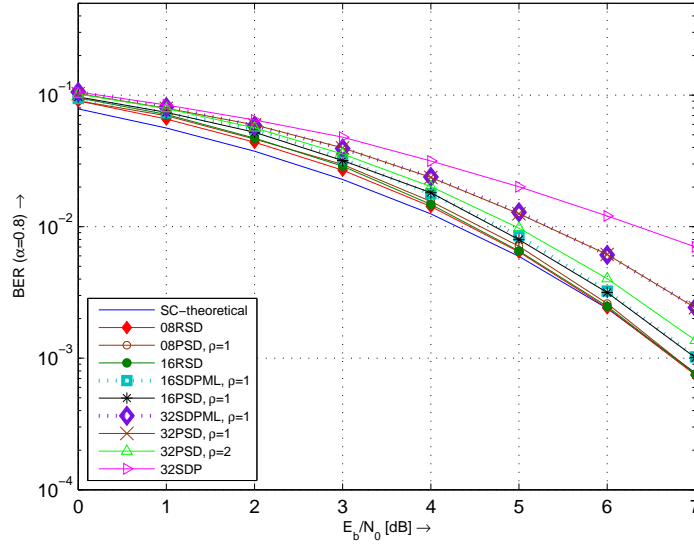
Figure 6.13: Error Performance of the proposed PSD scheme versus the E_b/N_0.
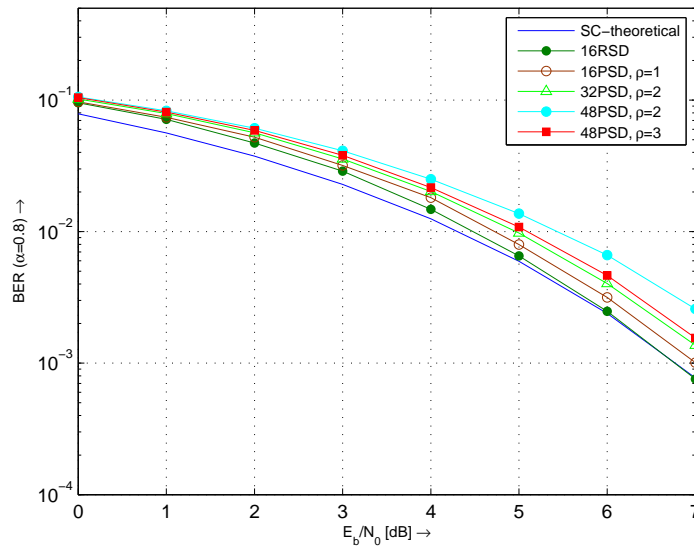
Figure 6.14: Quasi-optimal error Performance of the proposed PSD scheme versus the E_b/N_0 for $N \in \{16, 32, 48\}$ and $\rho \in \{1, 2, 3\}$, respectively.

15 times faster than the SDP-ML with $\rho = 2$. This improvement is due to the SD that investigates only the fraction of the SEFDM lattice points [73] with a
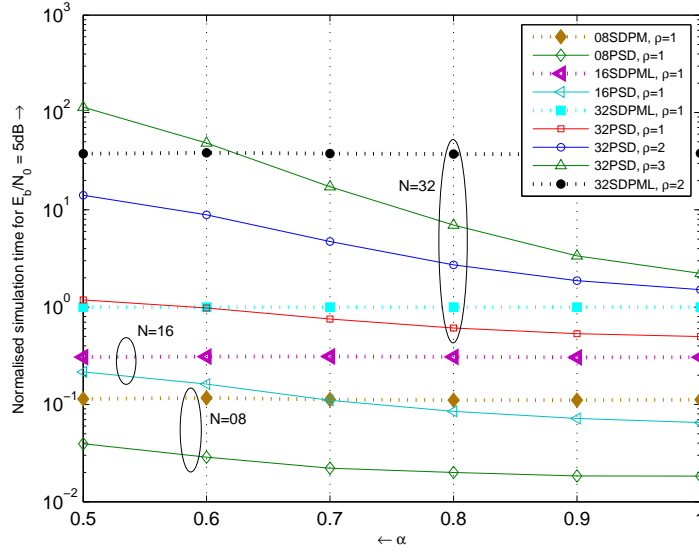
Figure 6.15: Complexity comparison between PSD and SDP-ML detection.

specific Hamming distance d_H from $\tilde{\mathbf{S}}$ that are within the SD hypersphere.

In addition, in Fig. 6.16 the complexity of the pruned SD is compared to the complexity of a simple RegSD that traces a full tree. We see that in the PSD case the number of the visits to the tree nodes is significantly lower than that of the RegSD, even though a Schnorr Euchner [103] reordering strategy is used. In particular, for all combinations of N and α, results show that the number of the node visits is reduced by at least 30% with respect to the single RegSD algorithm. In addition, for $N = 32$ and $\alpha = 0.8$ PSD with $\rho = 1$ and 2, appears to use 70 and 15 times, respectively, fewer visits to the tree nodes than RegSD. Furthermore, PSD for $N = 48$ and $\rho = 2$ appears to be computationally cheaper than RegSD for a smaller dimension $N = 32$ SEFDM signal. This is clearly due to the addition of the Hamming distance d_H constraint as described in Eq. (6.17). Consequently, the relaxation of this constraint (i.e. the increase of the parameter ρ) results in a degradation of the PSD computational complexity.

Furthermore, Fig. 6.17 depicts the simulation time of the Sphere decoder part as a percentage of the entire PSD detection simulation time. Four different
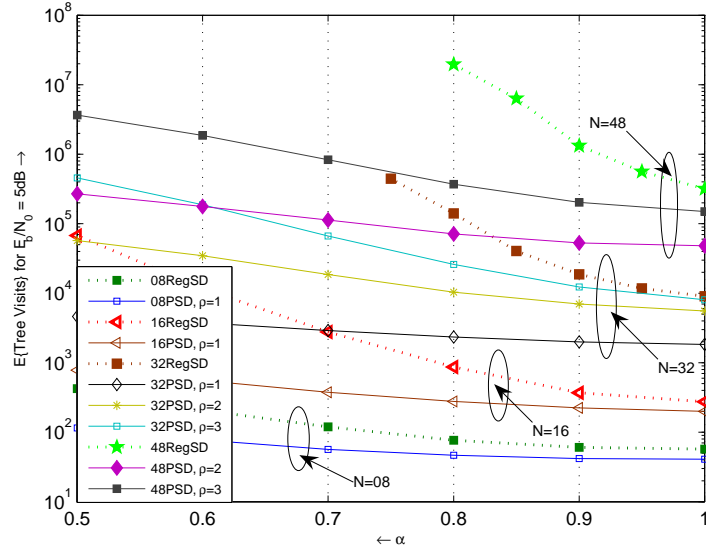
Figure 6.16: Complexity comparison between PSD and a full tree SD.

scenarios are examined; for $N = 32$ with $\rho = 1$ or 2 and for $N = 48$ with $\rho = 2$ or 3, respectively. It is observed that for $\rho < 3$, the PSD algorithm computational cost is dominated by the initial SDP calculation step. This could be further reduced by using more appropriate SDP implementations for SEFDM as discussed in the conclusions chapter of the thesis.

Finally, PSD and typical SD are compared in terms of distribution of node visits at each level of the SD tree. In particular, possible benefits are explored as offered by PSD in low SNR regimes, represented by an E_b/N_0 value of 5 dB, and for large dimension 4-QAM SEFDM signals, i.e. N is 32 or 48. It is notable that this means that the actual dimension of the PSD and SD problems are 64 and 96, respectively, due to the decoupling process. Figs 6.18 and 6.19 show that the distribution of tree visits for PSD is much lower than for a typical SD. In addition, the tighter d_H, the better the distribution of the points as expected because of the larger pruning of the SD tree. This is quite important for practical implementations where the size of the tree matters as stated in [146].
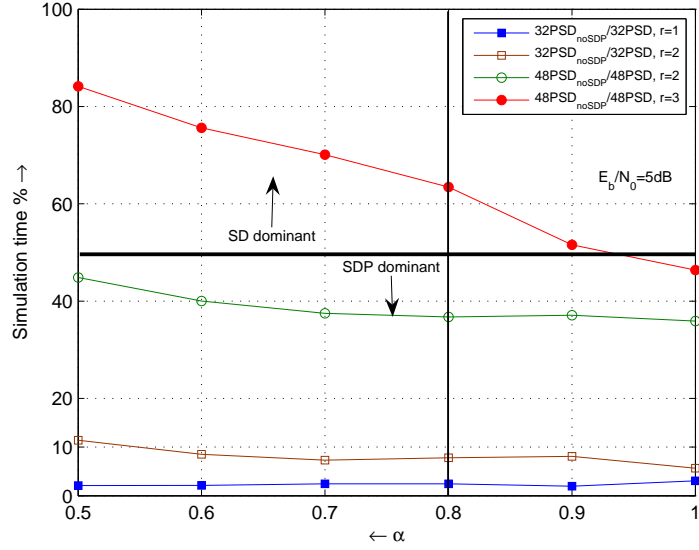
Figure 6.17: Percentage of the SD part over the entire PSD simulation time.
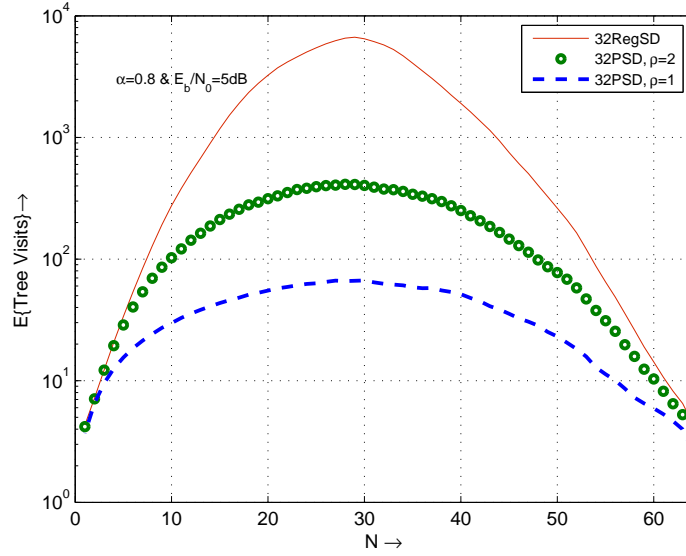
Figure 6.18: Distribution of the visits to the tree for PSD and typical SD detectors for SEFDM. $N = 32$, $\mathbf{S} \in \{\pm 1 \pm j\}^N$, $\alpha = 0.8$ and E_b/N_0 set to 5 db.

6.5 Summary and Discussion

Motivated by recent results in the area of MIMO and MU-CDMA detection, this chapter considers the examination of the possibility of a fast and adequately
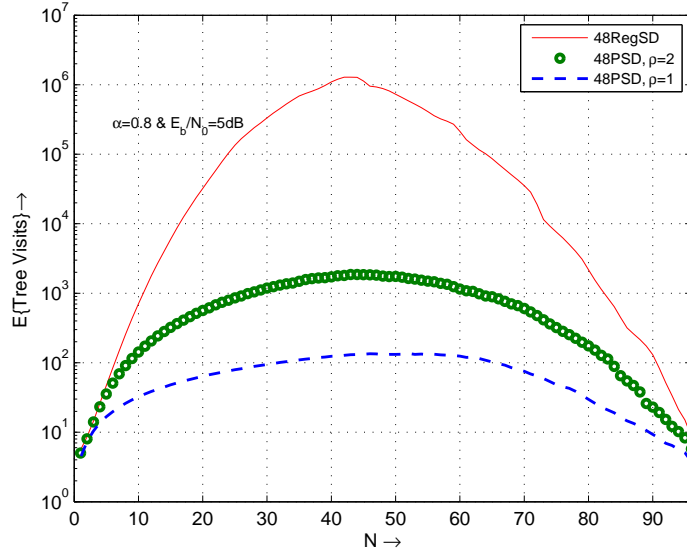
Figure 6.19: Distribution of the visits to the tree for PSD and typical SD detectors for SEFDM. $N = 48$, $\mathbf{S} \in \{\pm 1 \pm j\}^N$, $\alpha = 0.8$ and E_b/N_0 set to 5 db.

reliable suboptimal detection for the SEFDM system described in Chapter 2. The so called Semidefinite relaxation method is well known in the literature and is based on the reformulation of the Maximum Likelihood problem into a convex Semidefinite Program. Initial simulation results show that the error penalty incurred by the relaxation using SDP detection depends on the properties of the matrix $\mathbf{M}$ of the SEFDM system model. As the number of the SEFDM sub-carriers increases and/or their frequency separation decreases the matrix becomes ill conditioned and the SEFDM detection deteriorates. In order to mitigate the opening of the relaxation gap, i.e. the difference between the optimal and the SDP solution, a combined SDP-ML scheme is introduced. Simulation results show that for 4-QAM SEFDM systems of moderate size ($N \leq 32$), a bandwidth reduction of 20% could be achieved with respect to an equivalent OFDM system at the expense of a small error rate degradation. Furthermore, the SDP-ML complexity is insensitive to the noise level. Consequently, SDP-ML could represent a feasible solution in low SNR environments

in contrast to optimal typical Sphere Detectors whose practicality is limited due to the overly increase of complexity with the problem dimension and the noise level in the system.

Notwithstanding, larger SEFDM signals require the application of an exhaustive search over a larger subset of possible solutions, incurring thus a significant increase of the SDP-ML computational complexity. On such basis this chapter proposed a new modified Sphere Decoder algorithm, termed Pruned Sphere Decoder (PSD), that implements faster the combined Semidefinite Programming and brute force ML. The number of branches of the PSD tree is restricted due to the addition of an extra constraint so that the feasibility set includes only the SEFDM vectors that have a predefined Hamming distance d_H from an initial SDP estimate. It was shown by simulation that for $d_H \leq 2$ the new scheme achieves a quasi-optimal error performance for SEFDM systems with $N \leq 48$ and $\Delta fT = 0.8$ in low SNR regimes. In addition, PSD offers the same solution in terms of BER with an equivalent combined SDP-ML scheme but in a fraction of the computational effort. Finally, simulation results showed that PSD significantly reduces the required effort for the tree search of an optimal SD at the expense of a small penalty in the BER and the initialisation cost of the SDP calculation.

As far as the SDP calculations is concerned, it is notable that almost all simulations times were dominated by the time required for the SDP. In order to reduce this, other implementations than the one based on the Boyd's CVX tool [141], [142], as used in the modelling of this chapter, could be explored. To mention but a few, SDP solutions for complex systems that avoid doubling the dimension of the SDP program, efficient SDP formulations for large dimension optimisation problems like the one proposed in [147], or finally solutions tailored for the SEFDM case.

Finally, over the past few years, there has been a wealth of research in the area of designing new detection algorithms, specifically in the area of MIMO

communication systems. The application of such algorithms to the SEFDM detection problem is outside the scope of this work. However, it may well be of interest to researchers to compare the performance of similar algorithms, in terms of system performance and computational complexity, to the new algorithms reported in this chapter. Of the newly published material, we outline two relevant and recent developments. First, the SD outlined by Barbero et al. [115], [113] propose a quasi-optimal SD that is not necessarily faster than a typical SD but more suitable for hardware implementation because of its fixed complexity. This is contrasted to the algorithm proposed in this chapter where the complexity is random, although polynomially bound but the operation is expected to be faster than SD. Second, new work by Stojnic et al. [148], [118], [117] proposes a combined SDP-SD algorithm with aims similar to those of the author of this thesis; i.e. to find a faster than SD solution to large dimension problems in low SNR. The authors also propose an intelligent "pruning" of the typical SD by using a similar to this work SDP initialisation step and then calculating tight bounds at each level enumeration. This results in a better error performance than the technique reported in this chapter as it achieves an optimal solution. However, further investigations and comparisons should be included in future work in order to examine if the novel PSD is faster, and consequently more suitable for SEFDM detection, thanks to the use of the Hamming distance constraint instead of the their bounds calculations.

Chapter 7

Conclusions

This thesis has dealt with the problem of designing reliable and computationally tangible receivers for spectrally efficient FDM systems. Such systems are designed to occupy less than the OFDM bandwidth by squeezing the frequency separation between the adjacent FDM sub-bands. The problem was split into two parts: first, the generation of a receiver base that optimises the SEFDM detection in presence of additive white Gaussian noise. Second, the derivation of optimal detector was done with detector's limitations in terms of error rate and computational complexity were investigated. In addition, different approaches to design computationally tangible detection algorithms were proposed following either sub-optimal techniques or techniques suitable under special signal and noise conditions.

In Chapter 2, the principles of multicarrier signals representation were given, with discussion of the advantage of using orthogonal bases in terms of ease of signal detection and noise minimisation. Yet, this is not the case in frequency dispersive channels where the use of orthonormal bases suffers poor localisation due to the wide spread of signal in the frequency domain. Notwithstanding, the work of this thesis was limited to the simpler scenarios

where the signal is corrupted by noise only [1]. In addition, the Mazo limit for faster than Nyquist transmission and recent work on the dual Mazo limit were shortly discussed. The latter reveals that the Euclidean distance between the transmitted signal waveforms does not shrink when the frequency separation of the rectangularly shaped signal carriers is larger than 80% of an equivalent OFDM system. This result motivated the rest of this work that mainly comprises investigations of detection techniques for such systems.

Chapter 3 included a detailed description of the first SEFDM system introduced by Rodrigues and Darwazeh in [29]. Initially, for the sake of system completeness recent proposals for the signal generation upon digital transformations were described with emphasis on recent work at UCL [73], [60]. Regarding the receiver demodulator, it was found and shown by simulation that the Gram Schmidt method used in the introductory work [29] suffers severe numerical errors. As a result, it is inefficient for the generation of a large dimension orthonormal projections base. Hence, the use of the modified and the iterative modified GS variances was proposed. It was shown by simulation that IMGS is able to generate an orthogonal base for large dimensional SEFDM signals. Further to this, the Lowdin method - typically used in the field of quantum chemistry - was also used leading to the generation of orthonormal functions that are closer in the least square sense to the initial FDM carriers. Following the derivation of an orthonormal base, the noise variables at the output of the receiver correlators were proven to be independent with zero mean and variances equal to the noise channel power spectral density. As a result, the noise is not colored and therefore joint probability of correct detection as expressed by the maximum a posteriori criterion reduces to a well known combinatorial least squares problem. A first solver based on an exhaustive enumeration of the possible transmitted SEFDM waveforms was designed and implemented in

---

[1]Recent work based on the regularised SD detection of Chapter 5 using a more complete channel model and accounting for the effects of time dispersive channels such as ISI and frequency selective fading, has shown promising results and is reported in [149].

software. The simulation results confirmed dual Mazo limit discussed in chapter 2. In particular, it was found that the SEFDM systems conveying BPSK and 4-QAM data symbols achieve the same error rates as equivalent OFDM systems as long as the normalised carriers frequency separation α is ≥ 0.8. Nevertheless, the initial results were limited to 8 carrier SEFDM systems due to the exponential increase of the detection complexity over the constellation cardinality M and the signal dimension N. Motivated by Verdu's recommendations in [72], where he also proved that such combinatorial problems are non polynomial hard, two different approaches were followed in this thesis in order to find a fast and reliable detection; either apply fixed and polynomial complexity algorithms that are sub-optimal (Chapters 4 and 6) or investigate the possibility of an optimal solution under special circumstances, e.g. very low noise in the system (Chapter 5).

Chapter 4 provided the results of this work's first investigations in linear detection techniques. Initially, zero forcing was applied as a relaxation of the initial optimal maximum likelihood problem. It was shown that this technique eliminates the system inherent interference. Yet, it suffers severe error penalties due to the ill conditioning of the receiver projections matrix. In order to cope with the latter effect regularisation techniques of the ML problem were investigated. In particular, it was shown that the noise enhancement at the output of the demodulator can be decreased if the correlators outputs are filtered using a regularised projections matrix. Consecutively, a minimum mean squared error (MMSE) detector was derived and shown to constitute a special case of Tikhonov regularisation where the regulator is defined according to the receiver SNR. MMSE performance was also evaluated and it was proven that MMSE offers great improvement relative to ZF. Nevertheless, MMSE was considerably sub-optimal when the signal dimension increases and/ or the carriers frequency separation decreases. In order to narrow the error rate gap between ML and MMSE a new combined method was designed and implemented. In

particular, the ML exhaustive search was limited to a subset of transmitted waveforms whose binary versions deviate from the binary version of an initial MMSE estimate up to a predefined Hamming distance. It must be mentioned that the creation of this subset would not require a priori knowledge of the entire feasible set of SEFDM transmitted symbols, for it was created by flipping the bits of the binary version of the MMSE estimate. It was also shown that the number of floating operations required by the ML part of this technique depended on the value of the Hamming distance parameter ρ. The tighter the latter, the smaller the feasible subset and the computational complexity. It was demonstrated by simulation that MMSE-ML with $\rho = 1$ approximates optimal detection for BPSK SEFDM signals with $N \leq 48$. However, similar 4-QAM SEFDM detection suffers from local minima. Consequently, such detection requires a relaxation of the Hamming distance constraint that renders MMSE-ML detection unfeasible.

Chapter 5 approached SEFDM detection from a different perspective. In particular, the potential of the popular lattice detector called Sphere decoder was examined. The SEFDM system was modelled as a lattice whose generator matrix is the SEFDM system projections matrix. Then, the solution search space was reduced to the volume of a hypersphere that extends around the observations vector. SD achieved the optimal solution by applying dynamic programming, i.e. splitting the detection into a recursive process comprising N consecutive steps. The SD search process is equivalent to an in-depth search of a spanning tree. Initially, the standard real and complex variants of SD were examined. It was found by simulation that both schemes achieve the optimal solution but complex SD performs faster since it searches a smaller in depth tree. It was also confirmed that SD complexity is greatly affected by the noise and the internal interference of the system. Furthermore, the SD implementation is not possible as soon as the projections matrix becomes numerically singular. To overcome this particular limitation, the application

of a regularised variance of SD (RegSD), introduced by Cui and Tellambura in [101], was proposed. Through detailed modelling it was shown that RegSD reduces considerably SD complexity and that a tangible detection of medium sized SEFDM signals could be accomplished in high SNR regimes, i.e. when $E_b/N_0 \geq 10$dB.

However, the detection in low SNRs still posed open research questions. Therefore, Chapter 6 examined fixed complexity convex optimisation techniques. In particular, the ML problem was reformulated to an equivalent optimisation problem. By relaxing the non convex constraints of the latter, the SEFDM detection is reduced to a semidefinite program (SDP). This is a linear optimisation program that is solved using - well known from linear programming - interior point methods. Simulation were run for different signal settings and confirmed that SDP is a better relaxation, in terms of error rate, than both ZF and MMSE. Notwithstanding, the SDP solution is sub-optimal due to the growth of the feasible set. In addition, it was seen that the relaxation gap, i.e. the gap between the SDP and the optimal solution, widens with the worsening of the projections matrix condition. In order to reduce the gap, a similar to MMSE-ML combined method of chapter 4, an SDP-ML combined method was designed. It was found that this constrained ML performs satisfactorily for 4-QAM SEFDM when the system dimension is relatively small $N \leq 16$. Yet, larger dimensions require a larger Hamming distance parameter. Finally, to speed up the SDP-ML method, a modified sphere decoder was introduced. The new method limits the enumeration of the brute force ML at the feasible transmitted symbols that have a specific Hamming distance from the SDP estimate and they further lie within the SD hypersphere. It was shown by simulation that this novel pruned SD (PSD) reduces significantly the simulation time required by SDP-ML. Consequently, the use of larger than unity Hamming distance parameters is possible and reliable detection for larger dimensions $N \leq 48$ could be accomplished. Moreover, it was demonstrated that

PSD requires much fewer visits to the spanning tree nodes than the regularised SD, especially when the ill condition of the projections matrix and/or the noise in the system increase.

Overall, this thesis provided investigations of possible detection techniques for spectrally efficient FDM systems that suffer severe intercarrier interference due to the deliberate overlapping of the individual sub-bands. Through various studies, it was shown that the optimal detection of such a system in AWGN can be reduced to a combinatorial LS problem that can be solved without error penalties for SEFDM signals with $\alpha \geq 0.8$. Furthermore, it was demonstrated that tangible solutions could be accomplished by a regularised sphere decoder for small dimension SEFDM signals of $N \leq 48$ under high SNR conditions. In addition, a sub-optimal novel SD modification was also proposed as a complementary solution for the detection of such signals in low SNR regimes.

7.1 Proposals for future work

Despite this work contributions, research for computationally efficient detection techniques for SEFDM is still an open area. In addition, this work investigations revealed collateral gaps that need to be filled in. In particular, in the author's view it is worthy to investigate further the following issues:

- **The properties of the projection matrix**. It was shown by simulation that for 'sufficiently' large number of carriers or small frequency separation, the receiver base functions tend to be linear dependent and the matrix tends to singularity. Nevertheless, there is no mathematical definition for the above mentioned 'sufficiently'. Therefore, it would be useful to attempt a mathematical derivation of a closed formula for the decay rate of the matrix singular values and identify a numerical bound after which the matrix becomes practically singular. Hence, the limits for a feasible implementation of an SEFDM system in terms of signal

dimension and carriers frequency separation would be identified. A proposed area of research could be in the field of the finite dimensional linear independent Gabor frames [37], [150];

- **The expected complexity of the sphere decoder**. It would be desirable to derive mathematically the expected SD complexity over the noise taking into account the special properties of the SEFDM detection, i.e. that the coefficients matrix is an ill conditioned upper triangular matrix. Consequently, the SNR regions where SD could be applied with a reasonable complexity could be defined. Examples of such research efforts can be found in [74], [96] and [97];

- **The optimum regulator for the Cui and Tellambura regularised SD [101]**. As proven by simulation, the regulator value plays an important role since it determines the regularisation efficiency. Yet, the regularisation process adds some artificial noise in the system that affects negatively SD performance in terms of complexity. Consequently, the derivation of the optimal, from the complexity perspective, regulator constitutes a crucial matter. In Chapter 5, it was mentioned that there are such derivations for the unconstrained LS problem. To the author's knowledge there is no similar method for the regularisation of the integer LS problem representing the regularised sphere detection. Consequently, this leaves a research gap to be filled;

- **The effect of the projections matrix ill conditioning on the semidefinite programming**. It was seen by simulation that the opening of the SDP relaxation gap increases as the inherent interference of the SEFDM system deteriorates with the number of the carriers and/or the decrease in their frequency separation. Causes of this degradation could be revealed through detailed algorithmic analysis, so that suitable regularisation techniques could be applied;

- **The implementation speed of SDP**. This is another essential issue. Although it is well established in the literature that the complexities of SDP and MMSE are comparable, the actual simulation time of the former was considerably larger in our simulations. A possible cause of this could be the use of the CVX tool [141], [142] that probably slows the SDP process. In any case, techniques that speed up the SDP solution of problems with size similar to the SEFDM signal dimension should be investigated;

- **Further investigations on the introduced pruned SD**. This novel SD appears to be very efficient especially when the condition of the projections matrix is bad. Consequently, its applicability in different systems like ill conditioned MIMO [151] or ill conditioned CDMA systems [152] should be examined. Within the same scope, it would be useful to compare PSD with other fast SD variants like the fixed complexity SD [115] or the SDP-SD proposed in [117]. Finally, it would be useful to study further PSD complexity. A recommended start point could be to demonstrate that the PSD worst case complexity is bounded by the complexity of the equivalent SDP-ML scheme described in chapter 6. As already shown, the order of the latter increases according to the heuristic Hamming parameter;

- **Studies of other SEFDM detection tecniques**. New approaches could be based on the Likelihood Ascent Sequence (LAS) method that was recently proposed for the detection of MIMO systems [153], [154]. LAS appears to be a very promising technique since it converges to the optimal error rate in problems of large dimension. In addition, proposals for practical LAS detectors implementations based on Field Programmable Gate Array (FPGA) have already come to light [155]. Alternative detections could be based on Truncated Singular Value Decomposition (TSVD)

or partial Tikhonov regularisations [75], where the level of truncation or regularisation are determined according to the properties of the SEFDM projections matrix (as in Chapter 3). Finally, the author would recommend further research for recent findings in the integer programming domain.

To conclude, this work should extend to subjects other than the detection in AWGN so that the SEFDM system description becomes realistic. For example, the detection techniques should be tested in the presence of fading channels. Notwithstanding, note that some initial results of SEFDM system studies in AWGN and fading are to be presented in [149]. In addition, other important issues are the sensitivity to frequency and phase offsets and to amplifier non linearity as well as the Adjacent Channel Interference (ACI). Regarding the latter, it is interesting to mention that a significant merit of OFDM is its sharp edged 50 dB bandwidth that results into a low ACI level. Consequently, a similar SEFDM behavior should be confirmed. Finally, SEFDM research should lead to real systems implementations. Such work is already underway at UCL and FPGA based prototypes are expected in 2011.

Overall, the different detection techniques designed in this thesis confirm the practicability of SEFDM signals and systems. Much work is yet to be done to optimise further the detection techniques and to study their different effects on SEFDM systems under realistic performance scenarios.

Appendix A: Regularised matrix SVD

In the following, a simple proof for Eq. (5.46) is provided. A Singular Value Decomposition (SVD) of matrix $\mathbf{M}$ is:

$$\mathbf{M} = \mathbf{U}\boldsymbol{\Sigma}\mathbf{V}^H, \tag{1}$$

where $\mathbf{U}$ and $\mathbf{V}$ are two square $N \times N$ orthonormal matrices and $\boldsymbol{\Sigma}$ is a $N \times N$ diagonal matrix with diagonal elements the singular values $\sigma_i, \ i = 1, \ldots, N$ of $\mathbf{M}$. Thus, the Grammian $\mathbf{M}^H\mathbf{M}$ is:

$$\begin{aligned}
\mathbf{M}^H\mathbf{M} &= \left(\mathbf{U}\boldsymbol{\Sigma}\mathbf{V}^H\right)^H \mathbf{U}\boldsymbol{\Sigma}\mathbf{V}^H = \mathbf{V}\boldsymbol{\Sigma}^H\mathbf{U}^H\mathbf{U}\boldsymbol{\Sigma}\mathbf{V}^H \Longleftrightarrow \\
\mathbf{M}^H\mathbf{M} &= \mathbf{V}\boldsymbol{\Sigma}^H\boldsymbol{\Sigma}\mathbf{V}^H = \mathbf{V}\boldsymbol{\Sigma}^2\mathbf{V}^H.
\end{aligned} \tag{2}$$

Consecutively, the regularised matrix $\mathbf{A}$ is:

$$\begin{aligned}
\mathbf{A} &= \mathbf{M}^H\mathbf{M} + \epsilon\mathbf{I} = \mathbf{V}\boldsymbol{\Sigma}^2\mathbf{V}^H + \epsilon\mathbf{I} \Longleftrightarrow \\
\mathbf{A} &= \mathbf{V}\boldsymbol{\Psi}\mathbf{V}^H,
\end{aligned} \tag{3}$$

where $\boldsymbol{\Psi}$ is the following diagonal matrix:

$$\boldsymbol{\Psi} = \begin{bmatrix} \sigma_1^2 + \epsilon & 0 & \cdots & 0 \\ 0 & \sigma_2^2 + \epsilon & \cdots & 0 \\ \vdots & 0 & \ddots & 0 \\ 0 & \cdots & 0 & \sigma_N^2 + \epsilon \end{bmatrix}. \tag{4}$$

From Eqs. (3) and (4) it is obvious that the eigenvalues ψ_i, $i = 1, \ldots, N$ of $\mathbf{A}$ are:

$$\psi = \sigma_i^2 + \epsilon, \ , i = 1, \ldots, N. \tag{5}$$

Since $\epsilon > 0$ the regularised $\mathbf{A}$ has non zero eigenvalues and it is always positive definite. Hence, it can be Cholesky decomposed and written as the Grammian of an upper triangular matrix $\mathbf{D}$. The squares of the singular values σ_i' of the latter are by definition equal to ψ_i. From Eq. (5) is concluded that:

$$\sigma_i'^2 = \sigma_i^2 + \epsilon. \tag{6}$$

Appendix B: Preliminaries on lattice theory

Lattice theory is a mathematical frame work that describes the operation over partially ordered sets known as lattices. Such sets are central to the operation of Sphere Decoders. In this section, the basic concepts and defintions of Lattice theory, taken from [156] are outlined as they will aide understanding of the SD concept.

Definition 1: Let $\mathbf{u}_1, \mathbf{u}_2, \ldots, \mathbf{u}_N$ be N linear independent vectors on p-dimensional Euclidean space R^p ($N \leq p$). A lattice Λ is the set of vectors:

$$b_1 \times \mathbf{u}_1 + b_2 \times \mathbf{u}_2 + \ldots + b_N \times \mathbf{u}_N \mid b_1, b_2, \ldots, b_N \in \mathbb{Z}, \tag{7}$$

where $\mathbb{Z}$ is the set of all integers. In other words, the lattice Λ is composed of the linear combinations of the vectors $\mathbf{u}_i$ subject to the constraint that their coefficients are integer numbers.

The matrix whose columns are constituted by the lattice vectors $\mathbf{u}_i$, with $i = 1, \ldots, N$, is called the lattice generator matrix $\mathbf{M}$, i.e.:

$$\mathbf{M} = \left[\begin{array}{cccc} \mathbf{u}_1 & \mathbf{u}_2 & \ldots & \mathbf{u}_N \end{array} \right]. \tag{8}$$

In matrix representation, $\mathbf{M}$ generates the lattice Λ in the following way:

$$\Lambda = \{\mathbf{MB}\}, \tag{9}$$

where $\mathbf{B}$ is the vector column of the integer coefficients $[b_1, b_2, \ldots, b_N]^T$.

Definition 2: A deep hole of a lattice Λ is the furthest point of the Euclidean

space R^p from Λ.

Definition 3: The lattice covering radius is the minimum distance of the lattice from a deep hole.
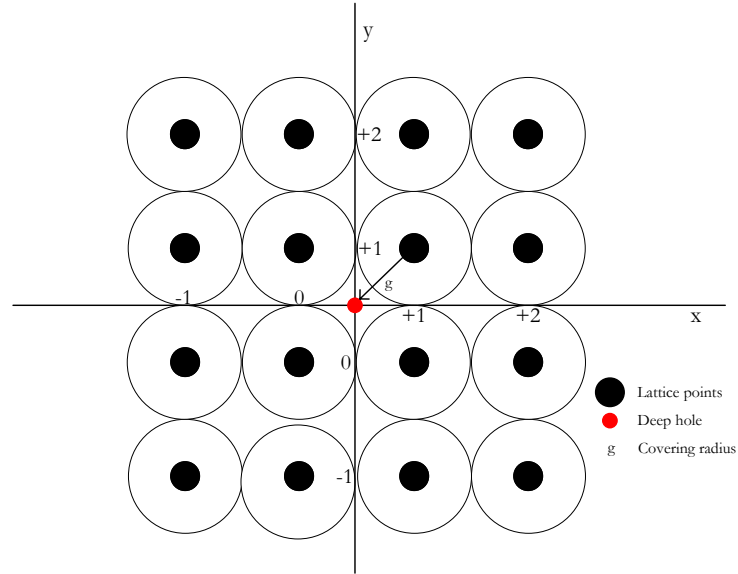
Figure 1: Illustration of a 2-dimensional integer lattice. The $(1/2, 1/2)$ point is a lattice deep.

Fig. 1 illustrates the integer 2-dimensional lattice and the respective sphere packing. In addition, the deep holes and the covering radius of the lattice are demonstrated.

Definition 4: The volume $d(\Lambda)$ of a lattice Λ is equal to the determinant of the generator matrix $\det(\mathbf{M})$, with $\det(\cdot)$ denoting the determinant of a matrix.

Definition 5: The volume of a N-dimensional hypersphere of radius ρ is:

$$V_N \rho^N, \tag{10}$$

where V_N is the volume of the N-dimensional hypersphere with radius $\rho = 1$:

$$V_N = \frac{\pi/2^{n/2}}{n/2!}. \tag{11}$$

In lattice sphere packings, ρ is also called the packing radius.

Definition 6: The density Δ of a lattice sphere packing is given by the pro-

190

portion of the space occupied by the sphere layers, i.e.:

$$\Delta = \frac{sV_N\rho^N}{d(\Lambda)},$$ (12)

where s is the number of the spheres in the lattice packing.

A very typical example of lattices is the cubic or integer lattice $\mathbb{Z}^N$ that consists of all the integer N-tuples, i.e.:

$$\mathbb{Z}^N = \Lambda \,|\mathbf{u}_i = \mathbf{e}_i, \ i = 1, \ldots, N \ ,$$ (13)

where $\mathbf{e}_i, \ldots, \mathbf{e}_N$ is the N-dimensional standard basis. A generator matrix of $\mathbb{Z}^N$ is simply the N-dimensional identity matrix $\mathbf{I}_N$. Its packing radius is $\rho = 1/2$, its covering radius is $\sqrt{N}/2$ and its density is equal to $V_N 2^{-N}$.

Appendix C: Preliminaries on convex optimisation

The following paragraphs cite basic convex optimisation definitions, utilised in Chapter 6 that would be useful for this thesis reader.

Definition 1. *Convex Sets* - A set $S \subset R^N$ is a convex set if:

$$\forall x, y \in S, \ \theta x + (1 - \theta) y \in S, \ \text{with } \theta \in [0, 1] \tag{14}$$

In other words a set is convex when it contains the cord that joins any two points in the set. Examples of a convex and non convex set are given in Fig. 2 (a) and (b), respectively.

Definition 2. *Convex cone* - It is the set of all points x in a convex set S so that:

$$x = \theta_1 x_1 + \theta_2 x_2 \ \forall x_1, x_2 \in S, \ \text{with } \theta_1 \geq 0, \theta_2 \geq 0 \tag{15}$$

In other words it is the set that contains all the conic combinations of the points in the set S. It must be mentioned that a conic set is always convex. An example of a cone set is the positive semidefinite cone $\mathbf{S}_+^N$, i.e. the set of all the symmetric positive semidefinite matrices X of N dimension.

Definition 3. *Matrix inequality* - It is the generalised inequality set over the positive semidefinite cone, i.e.:

$$\mathbf{X} \preceq_{\mathbf{S}_+^N} \mathbf{Y} \iff Y - X \succeq_{\mathbf{S}_+^N} 0 \iff Y - X \in \mathbf{S}_+^N \tag{16}$$

Definition 4. *Convex function* - A function $f(x)$ is convex when its domain $S = \text{dom}\{f\}$ is convex and $\forall x, y \in S$:

$$f(\theta x + (1 - \theta) y) \leq \theta f(x) + (1 - \theta) f(y) \qquad (17)$$

Examples of convex functions are all the linear functions and all the norms.
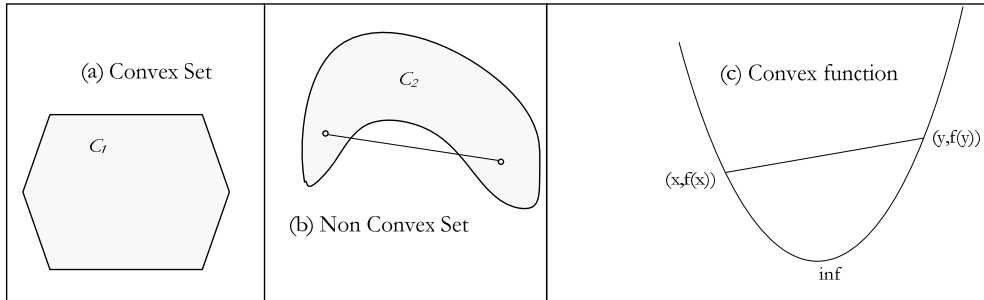
Figure 2: Convex and non-convex sets and functionsrepresentations.

Definition 5. *Convex optimisation problem* - An optimisation problem of the following general form:

$$
\begin{aligned}
\text{min.} \quad & f_0(x) \\
\text{s.t.} \quad & f_i(x) \leq 0, \; i = 1, \ldots, m \\
& h_j(x) = 0, \; j = 1, \ldots, n
\end{aligned}
\qquad (18)
$$

is convex when the objective $f_0(x)$, its domain and the inequality constraints $f_i(x)$ are convex, and the equality constraints are affine. The parameters m and n can be any integer numbers. It must be noticed that the feasible set, i.e. the set of the objective domain points that meet the problem constraints, of a convex optimisation problem is also convex [144].

Proposition 1: Any locally optimal point of a convex problem is (globally) optimal. The proof is given in [144].

Proposition 2: *Equivalent convex problems*: Two convex optimisation problems are equivalent if the solution of one is obtained from the solution of the other and vice-versa [144]

Definition 6. *Semidefinite program* - A convex optimisation problem is classified as a Semidefinite program when it can be formulated as follows:

$$\begin{aligned}
\min. \quad & \mathbf{c}^T \mathbf{x} \\
\text{s.t.} \quad & \mathbf{x_1 F_1} + \mathbf{x_2 F_2} + \ldots + \mathbf{x_n F_n} + \mathbf{G} \succeq 0 \\
& \mathbf{A x} = \mathbf{b}, \; i = 1, \ldots, n
\end{aligned} \tag{19}$$

where $\mathbf{c}, \mathbf{x}, \mathbf{F_i}, \mathbf{G}, \mathbf{A}, \mathbf{b}$ are vectors/matrices and $\mathbf{F_i}, \mathbf{G} \in \mathbf{S}_K$, i.e. they are symmetric matrices of k dimension. The inequality constraint is commonly called the Linear Matrix Inequality (LMI).

Definition 7. *Lagrangian and Lagrange dual functions* - The Lagrangian function L of an optimisation problem as described in equation (18) is given by:

$$L(x, \lambda, \nu) = f_0(x) + \sum_{i=1}^{n} \lambda_i f_i(x) + \sum_{j=1}^{m} \nu_i h_i(x) \tag{20}$$

where the Lagrangian multipliers λ_i and ν_i are called dual variables. It is apparent that the Lagrangian is the linear combination of the objective with its constraints.

The Lagrange dual g is the minimum of the Lagrangian over x, i.e.

$$g(\lambda, \nu) = \underbrace{\inf}_{x \in D} L(x, \lambda, \nu) \tag{21}$$

where D is the domain of the objective function and inf denotes the infimum. The Lagrange dual is important thanks to its lower bound property, i.e. for $\lambda \geq 0$, $g(\lambda, \nu) \leq p^*$. Hence, it is a useful tool for a derivation of a lower bound for the solution p^* of any primal optimisation problem.

Definition 8. *The dual problem* - The (Lagrange) dual problem is the following optimisation problem:

$$\begin{aligned}
\max. \quad & g(\lambda, \nu) \\
\text{s.t.} \quad & \lambda \preceq 0
\end{aligned} \tag{22}$$

It must be noticed that the solution of the dual problem g^* is by definition the best lower bound for the solution of the primal problem.

Definition 9. *Weak and strong duality*: When the solution p^* of the primal optimisation problem and its dual g^* are the same, then the duality is called strong. Otherwise, when the duality gap, i.e. $p^* - g^*$, is non zero the duality is called weak.

Definition 10. *KKT conditions*: The Karush-Kuhn-Tucker (KKT) conditions for the problem of Eq. (18) are the following:

1. $f_i(x) \leq 0$ and $h_j = 0$ for $i = 1, \ldots, n$ and $j = 1, \ldots, m$, respectively;

2. $\lambda_i \geq 0$ for $i = 1, \ldots, n$;

3. $\lambda_i f_i = 0$ for $i = 1, \ldots, n$;

4. $\nabla_x L = 0$

Proposition 4: For a convex optimisation problem, the strong duality holds if and only if the KKT conditions are met. Note that if the problem is not convex KKT conditions fulfillment is necessary but not sufficient for the strong duality.

The interest reader could find in [144], [127], [157], [128] detailed analysis and descriptions of convex optimisation and semidefinite programming for a variety of different applications.

List of References

[1] R. R. Mosier and R. G. Clabaugh. Kineplex, a bandwidth efficient binary transmission system. *AIEE Transactions (Part I: Communications and Electronics)*, 76:723–728, January 1958.

[2] R. W. Chang. Synthesis of band-limited orthogonal signals for multi-channel data transmission. *Bell System Tech. J.*, 45:1775âĂŞ1796, Dec. 1966.

[3] US3488445A. US Patent - Orthogonal Frequency Division Multiplex Data Transmission System, January 1970. Filed in November 1966 by R. W. Chang.

[4] B. Saltzberg. Performance of an Efficient Parallel Data Transmission System. *IEEE Transactions on Communication Technology*, 15(6):805 –811, december 1967.

[5] S. Weinstein and P. Ebert. Data Transmission by Frequency-Division Multiplexing Using the Discrete Fourier Transform. *IEEE Transactions on Communications*, 19(5):628–634, Oct 1971.

[6] J. M. Cioffi. A Multicarrier Primer. *ANSI T1E1.4/91-157*, Nov 1991.

[7] European Telecommunication Standard Institute. Digital Audio Broadcasting (DAB); DAB to Mobile, Portable and Fixed Receivers, ETS 300 401 ed.1, Feb 1995.

[8] European Telecommunication Standard Institute. Digital Video Broadcasting (DVB); Framing Structure, Channel Coding and Modulation for Digital Terrestrial Television (DVB-T), ETSI ETS 300 744 ed.1, Mar 1997.

[9] U.H. Reimers. DVB-The Family of International Standards for Digital Video Broadcasting. *Proceedings of the IEEE*, 94(1):173 –182, jan. 2006.

[10] Institute of Electrical and Electronics Engineers. IEEE 802.11, IEEE Standard for Information technology-Telecommunications and information exchange between systems-Local and metropolitan area networks-Specific requirements - Part 11: Wireless LAN Medium Access Control (MAC) and Physical Layer (PHY) Specifications, 2007.

[11] E. Perahia. IEEE 802.11n Development: History, Process, and Technology. *IEEE Communications Magazine*, 46(7):48 –55, july 2008.

[12] Institute of Electrical and Electronics Engineers. IEEE 802.16, IEEE Standard for Local and metropolitan area networks Part16: Air Interface for Broadband Wireless Access Systems, 2009.

[13] Fan Wang, A. Ghosh, C. Sankaran, P. Fleming, F. Hsieh, and S. Benes. Mobile WiMAX systems: performance and evolution. *IEEE Communications Magazine*, 46(10):41 –49, october 2008.

[14] E. Dahlman, H. Ekstrom, A. Furuskar, Y. Jading, J. Karlsson, M. Lundevall, and S. Parkvall. The 3G Long-Term Evolution - Radio Interface Concepts and Performance Evaluation. 1:137 –141, may 2006.

[15] D. Astely, E. Dahlman, A. Furuskar, Y. Jading, M. Lindstrom, and S. Parkvall. LTE: the evolution of mobile broadband. *IEEE Communications Magazine*, 47(4):44 –51, april 2009.

197

[16] Arogyaswami J. Paulraj, Dhananjay A. Gore, Rohit U. Nabar, and Helmut Bölcskei. An overview of MIMO communications - A key to gigabit wireless. *IEEE Proceedings*, 92(2):198–218, February 2004.

[17] Ming Jiang and L. Hanzo. Multiuser MIMO-OFDM for Next-Generation Wireless Systems. *Proceedings of the IEEE*, 95(7):1430–1469, July 2007.

[18] S. Ramseler, M. Arzberger, and A. Hauser. MV and LV powerline communications: new proposed IEC standards. In *IEEE Transmission and Distribution Conference, 1999*, volume 1, pages 235 –239 vol.1, apr 1999.

[19] HomePlug. AV White Paper. www.homeplug.org, 2005.

[20] A. Skrzypczak, P. Siohan, and J.-P. Javaudin. Application of the OFDM/OQAM Modulation to Power Line Communications. *IEEE International Symposium on Power Line Communications and Its Applications, 2007. ISPLC '07.*, pages 71 –76, march 2007.

[21] J. Armstrong. OFDM for Optical Communications. *Lightwave Technology, Journal of*, 27(3):189 –204, feb.1, 2009.

[22] W. Shieh and C. Athaudage. Coherent optical orthogonal frequency division multiplexing. *Electronics Letters*, 42(10):587 – 589, may 2006.

[23] Ralf Haas and Jean-Claude Belfiore. A Time-Frequency Well-localized Pulse for Multiple Carrier Transmission. *Wirel. Pers. Commun.*, 5(1):1–18, 1997.

[24] W. Kozek and A.F. Molisch. Nonorthogonal pulseshapes for multicarrier communications in doubly dispersive channels. *IEEE Journal on Selected Areas in Communications*, 16(8):1579–1589, Oct 1998.

[25] T. Strohmer and S. Beaver. Optimal OFDM design for time-frequency dispersive channels. *IEEE Transactions on Communications*, 51(7):1111–1122, July 2003.

[26] B. Hirosaki. An Orthogonally Multiplexed QAM System Using the Discrete Fourier Transform. *IEEE Transactions on Communications*, 29(7):982 – 989, jul 1981.

[27] M.R.D. Rodrigues and I. Darwazeh. Fast OFDM: A proposal for doubling the data rate of OFDM schemes. In *Proceedings of the International Conference on Telecommunications*, pages 484–487, Beijing, China, June 2002.

[28] Fuqin Xiong. M-ary amplitude shift keying OFDM system. *IEEE Transactions on Communications*, 51(10):1638–1642, Oct. 2003.

[29] M.R.D. Rodrigues and I. Darwazeh. A spectrally efficient frequency division multiplexing based communication system. In *8th International OFDM-Workshop*, pages 70–74, Hamburg, Germany, September 2003.

[30] M. Hamamura and S. Tachikawa. Bandwidth efficiency improvement for multi-carrier systems. *15th IEEE International Symposium on Personal, Indoor and Mobile Radio Communications, 2004. PIMRC 2004*, 1:48–52 Vol.1, Sept. 2004.

[31] Wang Jian, Yang Xun, Zhang Xi-lin, and Daoben Li. The Prefix Design and Performance Analysis of DFT-based Overlapped Frequency Division Multiplexing (OvFDM-DFT) System. In *3rd International Workshop on Signal Design and Its Applications in Communications, 2007. IWSDA 2007*, pages 361–364, 23-27 Sept. 2007.

[32] F. Rusek and J.B. Anderson. The two dimensional Mazo limit. *International Symposium on Information Theory, 2005. ISIT 2005. Proceedings.*, pages 970–974, Sept. 2005.

[33] F. Rusek and J.B. Anderson. Multistream Faster than Nyquist Signaling. *IEEE Transactions on Communications*, 57(5):1329–1340, May 2009.

199

[34] J. E. Mazo. Faster-than-Nyquist signaling. *Bell Syst. Tech. J*, 54:1451–1462, Oct 1975.

[35] Louis L. Scharf. *Statistical Signal Processing*. Addison-Wesley, 1991.

[36] Martin Vetterli and Jelena Kovacevic. *Wavelets and Subband Coding*. Prentice Hall, 1995.

[37] Soo-Chang Pei and Min-Hung Yeh. An introduction to discrete finite frames. *IEEE Signal Processing Magazine*, 14(6):84–96, Nov 1997.

[38] D. Gabor. Theory of communication. *J. IEE*, 93:429–457, 1946.

[39] B. Le Floch, M. Alard, and C. Berrou. Coded orthogonal frequency division multiplex [TV broadcasting]. *Proceedings of the IEEE*, 83(6):982–996, Jun 1995.

[40] Theodore S. Rappaport. *Wireless Communications*. Prentice Hall, 1996.

[41] Scott Beaver. *Banach Algebras of Integral Operators, Off-Diagonal Decay, and Applications in Wireless Communications*. PhD thesis, University of California Davis, 2004.

[42] A. Vahlin and N. Holte. Optimal finite duration pulses for OFDM. *IEEE Transactions on Communications*, 44(1):10–14, Jan 1996.

[43] J.-P. Javaudin and P.-J. Bouvet. Use of Signals in Quadrature Over OFDM/OQAM. *IEEE 65th Vehicular Technology Conference, 2007. VTC2007-Spring.*, pages 1891 –1895, april 2007.

[44] Hui Jiang and Daoben Li. A New Time Division Multiplexing Technique. In *International Conference on Wireless Communications, Networking and Mobile Computing, 2007. WiCom 2007*, pages 771–774, 21-25 Sept. 2007.

[45] Hui Jiang, Daoben Li, and Weidong Li. Performance Analysis of Over-lapped Multiplexing Techniques. In *3rd International Workshop on Signal Design and Its Applications in Communications, 2007. IWSDA 2007*, pages 233–237, 23-27 Sept. 2007.

[46] Xing Yang, Wenbao Ai, Tianping Shuai, and Daoben Li. A Fast Decoding Algorithm for Non-orthogonal Frequency Division Multiplexing Signals. *Second International Conference on Communications and Networking in China, 2007. CHINACOM '07.*, pages 595–598, Aug. 2007.

[47] Peng Sun, Xing Yang, and Daoben Li. Lattice reduction aided MMSE-SIC detection for non-orthogonal frequency division multiplexing signals. *Third International Conference on Communications and Networking in China, 2008. ChinaCom 2008*, pages 527–532, Aug. 2008.

[48] Yong MO, Xing YANG, and Dao ben LI. Semidefinite programming detection for OvHDM signal. *The Journal of China Universities of Posts and Telecommunications*, 15(3):8 – 12, 18, 2008.

[49] Fredrik Rusek and John B. Anderson. Successive interference cancellation in multistream faster-than-Nyquist Signaling. In *IWCMC '06: Proceedings of the 2006 international conference on Wireless communications and mobile computing*, pages 1021–1026, New York, NY, USA, 2006. ACM.

[50] Yafei Hou and M. Hamamura. Bandwidth efficiency of PC-OFDM systems with high compaction multi-carrier modulation. *2005 International Conference on Wireless Communications, Networking and Mobile Computing, 2005. Proceedings*, 1:197–200, Sept. 2005.

[51] D. Dasalukunte, F. Rusek, J.B. Anderson, and V. Owall. Transmitter architecture for faster-than-Nyquist signaling systems. *IEEE Interna-*

tional Symposium on Circuits and Systems, 2009. ISCAS 2009, pages 1028 –1031, may 2009.

[52] John G. Proakis. *Digital Communications 4th Edition*. McGraw Hill, 4th edition, 2001.

[53] Gene H. Golub and Charles F. Van Loan. *Matrix Computations*. The John Hopkins University Press, 3rd edition, 1996.

[54] Julien Langou Luc Giraud and Miroslav Rozloznik. On the loss of orthogonality in the Gram Schmidt orthogonalisation process. Technical report, CERFACS, 2003.

[55] A. Bjorck and C. C. Paige. Loss and Recapture of Orthogonality in the Modified Gram–Schmidt Algorithm. *SIAM Journal on Matrix Analysis and Applications*, 13(1):176–190, 1992.

[56] Janet C. Rutledge A.Bruce Carlson, Paul. B. Crilly. *Communication Systems: An introductyion to signal and noise in communication systems*. McGraw-Hill, 4th edition, 2002.

[57] D.H. Bailey and P.N. Swarztrauber. The Fractional Fourier Transform and Applications. *SIAM Review*, 33(3):389–404, September 1991.

[58] L. Bluestein. A linear filtering approach to the computation of discrete Fourier transform. *IEEE Transactions on Audio and Electroacoustics*, 18(4):451 – 455, dec 1970.

[59] Safa I A Ahmed and Izzat Darwazeh. DFT Based Transmitter for Spectrally Efficient FDM Systems. In *London Communications Symposium, LCS 2009*, 2009.

[60] Safa I A Ahmed and Izzat Darwazeh. Simple DSP - IDFT techniques for generating Spectrally Efficient FDM Signals. In *IEEE, IET Inter-*

national Symposium on Communication Systems, Networks and Digital Signal Processing, 2010.

[61] James W. Daniel Ben Noble. *Applied Linear Algebra*. Prentice Hall, 2nd edition, 1977.

[62] Walter Hoffmann. Iterative algorithms for Gram-Schmidt orthogonalization. *Computing*, 41(4):335–348, December 1989.

[63] Miro Rozloznik Luc Giraud, Julien Langou and Jasper van den Eshof. Rounding Error Analysis of the Classical Gram Schmidt process. Technical report, CERFACS, 2004.

[64] Vipin Srivastava. A unified view of the orthogonalization methods. *Journal of Physics A: Mathematical and General*, 33(35):6219–6222, 2000.

[65] H. C. Schweinler and E. P. Wigner. Orthogonalization Methods. *Journal of Mathematical Physics*, 11:1693–1694, May 1970.

[66] John A. Erdos John G. Aiken and Jerome A. Goldstein. On Lowdin orthogonalization. *International Journal of Quantum Chemistry*, XVIII:1101–1108, 1980.

[67] I. Mayer. On Lowdin's method of symmetric orthogonalization. *International Journal of Quantum Chemistry*, 90:63–65, 2002.

[68] S Chaturvedi, A K Kapoor, and V Srinivasan. A new orthogonalization procedure with an extremal property. *Journal of Physics A: Mathematical and General*, 31(19):L367–L370, 1998.

[69] D. F. Scofield. A note on Lowdin orthogonalization and the square root of a positive self-adjoint matrix. *International Journal of Quantum Chemistry*, 7:561–568, 1972.

[70] Bakopoulos A. and Chrysovergis I. *Introduction in the Numerical Analysis*. Symeon Publishing Co., 1993.

[71] Athanasios Papoulis and S. Unnikrishna Pillai. *Probability, Random Variables and Stohastic Processes.* McGraw-Hill, 4th edition, 2002.

[72] Sergio Verdu. Computational complexity of optimum multiuser detection. *Algorithmica*, 4:303–312, 1989.

[73] I. Kanaras, A. Chorti, M.R.D. Rodrigues, and I. Darwazeh. Spectrally Efficient FDM Signals: Bandwidth Gain at the Expense of Receiver Complexity. In *IEEE International Conference on Communications, 2009. ICC '09.*, pages 1–6, June 2009.

[74] B. Hassibi and H. Vikalo. On the sphere-decoding algorithm I. Expected complexity. *IEEE Transactions on Signal Processing*, 53(8):2806–2818, Aug. 2005.

[75] Christian Hansen. *Rank Deficient and Discrete Ill Posed Problems.* SIAM, 1998.

[76] T. Reginska. A regularization parameter in discrete ill–posed problems. *SIAM J. Sci. Comput.*, 17(3):740–749, 1996.

[77] Marek Rudnicki Dorota Krawczyk-Stando. Regularisation Parameters Selection in Discrete Ill-Posed Problems - The Use of the U-Curve. *International Journal in Applied Mathematics and Computer Science*, 17:157–164, 2007.

[78] E.M. Ventouras, C.C. Papageorgiou, N.K. Uzunoglu, and G.N. Christodoulou. Tikhonov regularization using a minimum-product criterion: Application to brain electrical tomography. *Proceedings of the 23rd Annual International Conference of the IEEE Engineering in Medicine and Biology Society, 2001*, 1:608–611 vol.1, 2001.

[79] John G. Proakis Tiejun (Ronald) Wang and James R. Zeidler. Techniques for suppression of intercarrier interference in OFDM systems. In *IEEE Communications Society / WCNC 2005*, 2005.

[80] V. Kuhn R. Bohnke, D. Wubben and K.D. Kammeyer. Reduced complexity MMSE Detection for BLAST architectures. In *IEEE Global Telecommunications Conference, 2003 - GLOBECOM '03*, pages 2258–2262, San Fransisco, USA, December 2003.

[81] V. Pammer, Y. Delignon, W. Sawaya, and D. Boulinguez. A low complexity suboptimal MIMO receiver: The combined ZF-MLD algorithm. *14th IEEE Proceedings on Personal, Indoor and Mobile Radio Communications, 2003. PIMRC 2003*, 3:2271–2275 vol.3, 7-10 Sept. 2003.

[82] Fan Wang, Yong Xiong, and Xiumei Yang. Approximate ML detection based on MMSE for MIMO systems. *PIERS Online*, 3(4):475–480, 2007.

[83] Hui Zhao, Hang Long, and Wenbo Wang. Tabu Search Detection for MIMO Systems. *Personal, Indoor and Mobile Radio Communications, 2007. PIMRC 2007. IEEE 18th International Symposium on*, pages 1 –5, sept. 2007.

[84] N. Srinidhi, Saif K. Mohammed, A. Chockalingam, and B. Sundar Rajan. Near-ML Signal Detection in Large-Dimension Linear Vector Channels Using Reactive Tabu Search. 2009.

[85] A. Wiesel, Y.C. Eldar, and S. Shamai. Zero-Forcing Precoding and Generalized Inverses. *IEEE Transactions on Signal Processing*, 56(9):4409 –4418, sept. 2008.

[86] B. Hassibi and H. Vikalo. On the expected complexity of integer least-squares problems. *IEEE International Conference on Acoustics, Speech, and Signal Processing, 2002. Proceedings. (ICASSP '02)*, 2:1497–1500, 2002.

[87] U. Fincke and M. Pohst. Improved methods for calculating vectors of short length in a lattice, including a complexity analysis. *Mathematics on Computation*, 44(170):463–471, April 1985.

[88] E. Viterbo and E. Biglieri. A Universal Decoding Algorithm for Lattice Codes. In *14th Colloq. GRETSI Juan-les-Pins, France*, pages 611–614, Sept 1993.

[89] E. Viterbo and J. Boutros. A universal lattice code decoder for fading channels. *IEEE Transactions on Information Theory*, 45(5):1639–1642, Jul 1999.

[90] D. Pham, K.R. Pattipati, P.K. Willett, and Jie Luo. An improved complex sphere decoder for V-BLAST systems. *IEEE Signal Processing Letters*, 11(9):748–751, Sept. 2004.

[91] A.M. Chan and Inkyu Lee. A new reduced-complexity sphere decoder for multiple antenna systems. *IEEE International Conference on Communications, 2002. ICC 2002*, 1:460–464, 2002.

[92] O. Damen, A. Chkeif, and J.-C. Belfiore. Lattice code decoder for space-time codes. *IEEE Communications Letters*, 4(5):161–163, May 2000.

[93] R. Santiago Mozos and M.J. Fernandez-Getino Garcia. Efficient complex sphere decoding for MC-CDMA systems. *IEEE Transactions on Wireless Communications*, 5(11):2992–2996, Nov. 2006.

[94] Dung Ngoc Dao and Chintha Tellambura. A general combinatorial sphere decoder and its application. *IEEE Communications Letters*, 10(12):810–812, December 2006.

[95] K.K. Soo Y.M. Siu L. Yang, R.S. Chen. An efficient sphere decoding approach for PTS assisted PAPR reduction of OFDM signals. *AEU -*

International Journal of Electronics and Communications, 61(10):684–688, November 2007.

[96] H. Vikalo and B. Hassibi. On the sphere-decoding algorithm II. Generalizations, second-order statistics, and applications to communications. *IEEE Transactions on Signal Processing*, 53(8):2819–2834, Aug. 2005.

[97] J. Jalden and B. Ottersten. On the complexity of sphere decoding in digital communications. *IEEE Transactions on Signal Processing*, 53(4):1474–1484, April 2005.

[98] J. Jalde and B. Ottersten. On the limits of sphere decoding. *International Symposium on Information Theory, 2005. ISIT 2005. Proceedings*, pages 1691–1695, 4-9 Sept. 2005.

[99] Hamid Jafarkhani. *Space - Time Coding, Theory and Practice*. Cambridge University Press, 2005.

[100] B.M. Hochwald and S. ten Brink. Achieving near-capacity on a multiple-antenna channel. *IEEE Transactions on Communications*, 51(3):389–399, March 2003.

[101] T. Cui and C. Tellambura. An efficient generalized sphere decoder for rank-deficient MIMO systems. *IEEE Communications Letters*, 9(5):423–425, May 2005.

[102] E. Agrell, T. Eriksson, A. Vardy, and K. Zeger. Closest point search in lattices. *IEEE Transactions on Information Theory*, 48(8):2201–2214, Aug 2002.

[103] M.O. Damen, H. El Gamal, and G. Caire. On maximum-likelihood detection and the search for the closest lattice point. *IEEE Transactions on Information Theory*, 49(10):2389–2402, Oct. 2003.

[104] Chris Meyers Allen Downey, Jeffrey Elkner. *How to Think Like a Computer Scientist Learning with Python.* Green Tea Press, 2002.

[105] Lei Zhang, Haipeng Lei, Xin Zhang, and Dacheng Yang. Efficient Complex Sphere Decoding Framework for Linear Dispersion Space-Time Block Codes. In *IEEE 18th International Symposium on Personal, Indoor and Mobile Radio Communications, 2007. PIMRC 2007*, pages 1–4, Sept. 2007.

[106] Ake Bjorck. *Numerical Methods for Least Squares Problems.* Society for Industrial and Applied Mathematics, 1996.

[107] I. Kanaras, A. Chorti, M.R.D. Rodrigues, and I. Darwazeh. An Optimum Detection for a Spectrally Efficient non Orthogonal FDM System. In *13th International OFDM-Workshop 2008, InOWo'08, Hamburg, Germany.* OFDM International Workshop 2008, August 2008.

[108] I. Kanaras, A. Chorti, M.R.D. Rodrigues, and I. Darwazeh. A combined MMSE-ML detection for a spectrally efficient non orthogonal FDM signal. *5th International Conference on Broadband Communications, Networks and Systems, 2008. BROADNETS 2008.*, pages 421–425, Sept. 2008.

[109] A. Alavi, C. Tellambura, and I. Fair. PAPR reduction of OFDM signals using partial transmit sequence: an optimal approach using sphere decoding. *IEEE Communications Letters*, 9(11):982–984, Nov. 2005.

[110] B. Tarokh and H.R. Sadjadpour. Construction of OFDM M-QAM sequences with low peak-to-average power ratio. *IEEE Transactions on Communications*, 51(1):25–28, Jan 2003.

[111] X.-W. Chang, X. Yang, T. Le-Ngoc, and P. Wang. Partial regularisation approach for detection problems in underdetermined linear systems. *Communications, IET*, 3(1):17–24, January 2009.

[112] Xiao-Wen Chang and Xiaohua Yang. An efficient regularization approach for underdetermined MIMO system decoding. In *IWCMC '07: Proceedings of the 2007 international conference on Wireless communications and mobile computing*, pages 349–353, New York, NY, USA, 2007. ACM.

[113] L.G. Barbero and J.S. Thompson. A fixed-complexity MIMO detector based on the complex sphere decoder. *IEEE 7th Workshop on Signal Processing Advances in Wireless Communications, 2006. SPAWC '06*, pages 1–5, 2-5 July 2006.

[114] L.G. Barbero and J.S. Thompson. Rapid prototyping of the sphere decoder for MIMO systems. In *The 2nd IEE/EURASIP Conference on DSPenabledRadio, 2005*, pages 9 pp.–, Sept. 2005.

[115] L.G. Barbero and J.S. Thompson. Fixing the Complexity of the Sphere Decoder for MIMO Detection. *IEEE Transactions on Wireless Communications*, 7(6):2131–2142, June 2008.

[116] J. Jalden, L.G. Barbero, B. Ottersten, and J.S. Thompson. The Error Probability of the Fixed-Complexity Sphere Decoder. *IEEE Transactions on Signal Processing*, 57(7):2711–2720, July 2009.

[117] M. Stojnic, H. Vikalo, and B. Hassibi. Speeding up the Sphere Decoder With HâĹđ and SDP Inspired Lower Bounds. *IEEE Transactions on Signal Processing*, 56(2):712–726, Feb. 2008.

[118] M. Stojnic, H. Vikalo, and B. Hassibi. Further Results on Speeding up the Sphere Decoder. *IEEE International Conference on Acoustics, Speech and Signal Processing, 2006. ICASSP 2006 Proceedings*, 4:IV–IV, May 2006.

[119] C. Windpassinger, L. Lampe, R.F.H. Fischer, and T. Hehn. A performance study of MIMO detectors. *IEEE Transactions on Wireless Communications*, 5(8):2004–2008, Aug. 2006.

[120] C. Windpassinger and R.F.H. Fischer. Low-complexity near-maximum-likelihood detection and precoding for MIMO systems using lattice reduction. In *2003 IEEE Information Theory Workshop, 2003. Proceedings*, pages 345–348, 31 March-4 April 2003.

[121] M. Taherzadeh, A. Mobasher, and A.K. Khandani. Communication Over MIMO Broadcast Channels Using Lattice-Basis Reduction. *IEEE Transactions on Information Theory*, 53(12):4567–4582, Dec. 2007.

[122] J. Adeane, M.R.D. Rodrigues, and I.J. Wassell. Lattice-reduction-aided detection for MIMO-OFDM-CDM communication systems. *IET Communications*, 1(3):526–531, June 2007.

[123] S. Ulukus and R.D. Yates. Optimum multiuser detection is tractable for synchronous CDMA systems using m-sequences. *IEEE Communications Letters*, 2(4):89 –91, apr 1998.

[124] C. Sankaran and A. Ephremides. Solving a class of optimum multiuser detection problems with polynomial complexity. *IEEE Transactions on Information Theory*, 44(5):1958 –1961, sep 1998.

[125] M. Motani. Polynomial complexity optimal multiuser detection for a wider class of problems. *Wireless Communications and Networking, 2003. WCNC 2003. 2003 IEEE*, 1:375 –378 vol.1, march 2003.

[126] M. Motani. Polynomial complexity optimal multiuser detection for wider class of problems. *Electronics Letters*, 39(16):1214 – 1215, aug. 2003.

[127] Lieven Vandenberghe and Stephen Boyd. Semidefinite Programming. *SIAM Review*, 38(1):49–95, 1996.

[128] Z.-Q. Luo and W. Yu. An Introduction to Convex Optimization for Communications and Signal Processing. *IEEE Journal on Selected Areas in Communications*, 24(8):1426–1438, Aug. 2006.

[129] Wing-Kin Ma, T.N. Davidson, Kon Max Wong, Zhi-Quan Luo, and Pak-Chung Ching. Quasi-maximum-likelihood multiuser detection using semi-definite relaxation with application to synchronous CDMA. *IEEE Transactions on Signal Processing*, 50(4):912–922, Apr 2002.

[130] Peng Hui Tan and L.K. Rasmussen. The application of semidefinite programming for detection in CDMA. *IEEE Journal on Selected Areas in Communications*, 19(8):1442–1449, Aug 2001.

[131] J. Jalden and B. Ottersten. The Diversity Order of the Semidefinite Relaxation Detector. *IEEE Transactions on Information Theory*, 54(4):1406–1422, April 2008.

[132] A. Wiesel, Y.C. Eldar, and S.S. Shitz. Semidefinite Relaxation for Detection of 16-QAM Signaling in MIMO Channels. *IEEE Signal Processing Letters*, 12(9):653–656, Sept. 2005.

[133] N.D. Sidiropoulos and Z.-Q. Luo. A Semidefinite Relaxation Approach to MIMO Detection for High-Order QAM Constellations. *IEEE Signal Processing Letters*, 13(9):525–528, Sept. 2006.

[134] J. Jalden, C. Martin, and B. Ottersten. Semidefinite programming for detection in linear systems - optimality conditions and space-time decoding. *2003 IEEE International Conference on Acoustics, Speech, and Signal Processing, 2003. Proceedings. (ICASSP '03)*, 4:IV–9–12 vol.4, April 2003.

[135] J. Jalden, B. Ottersten, and Wing-Kin Ma. Reducing the average complexity of ML detection using semidefinite relaxation. *IEEE International Conference on Acoustics, Speech, and Signal Processing, 2005. Proceedings. (ICASSP '05)*, 3:iii/1021–iii/1024 Vol. 3, 18-23 March 2005.

[136] M. Kisialiou and Zhi-Quan Luo. Performance analysis of quasi-maximum-likelihood detector based on semi-definite programming. In *IEEE Inter-*

national Conference on Acoustics, Speech, and Signal Processing, 2005. Proceedings. (ICASSP '05), volume 3, pages 433–436, March 2005.

[137] M. Kisialiou and Zhi-Quan Luo. Efficient Implementation of a Quasi-Maximum-Likelihood Detector Based on Semi-Definite Relaxation. In IEEE International Conference on Acoustics, Speech and Signal Processing, 2007. ICASSP 2007, volume 4, pages IV–1329–IV–1332, 15-20 April 2007.

[138] A. Mobasher, M. Taherzadeh, R. Sotirov, and A.K. Khandani. A Near-Maximum-Likelihood Decoding Algorithm for MIMO Systems Based on Semi-Definite Programming. IEEE Transactions on Information Theory, 53(11):3869–3886, Nov. 2007.

[139] Wing-Kin Ma, Pak-Chung Ching, and Zhi Ding. Semidefinite relaxation based multiuser detection for M-ary PSK multiuser systems. IEEE Transactions on Signal Processing, 52(10):2862–2872, Oct. 2004.

[140] Christoph Helmberg, Franz Rendl, Robert J. Vanderbei, and Henry Wolkowicz. An interior-point method for semidefinite programming. SIAM Journal on Optimization, 6:342–361, 1996.

[141] M. Grant and S. Boyd. Graph implementations for nonsmooth convex programs, Recent Advances in Learning and Control (a tribute to M. Vidyasagar), V. Blondel, S. Boyd, and H. Kimura, editors, pages 95-110, Lecture Notes in Control and Information Sciences, Springer, 2008.

[142] M. Grant and S. Boyd. CVX: Matlab software for disciplined convex programming (web page and software). http://stanford.edu/ boyd/cvx. Stanford University, September 2008.

[143] H.D. Mittelmann. An independent benchmarking of SDP and SOCP solvers. Mathematical Programming, 95(2):407–430, February 2003.

[144] Stephen Boyd and Lieven Vandenberghe. *Convex Optimization.* Cambridge University Press, 2004.

[145] Joakim Jalden and Bjorn Ottersten. High Diversity Detection Using Semidefinite Relaxation. *Fortieth Asilomar Conference on Signals, Systems and Computers, 2006. ACSSC '06*, pages 2082–2086, Oct.-Nov. 2006.

[146] A. Burg, M. Borgmann, M. Wenk, M. Zellweger, W. Fichtner, and H. Bolcskei. VLSI implementation of MIMO detection using the sphere decoding algorithm. *IEEE Journal of Solid-State Circuits*, 40(7):1566–1577, July 2005.

[147] M. Abdi, H. El Nahas, A. Jard, and E. Moulines. Semidefinite positive relaxation of the maximum-likelihood criterion applied to multiuser detection in a CDMA context. *IEEE Signal Processing Letters*, 9(6):165–167, Jun 2002.

[148] M. Stojnic, H. Vikalo, and B. Hassibi. A branch and bound approach to speed up the sphere decoder. *IEEE International Conference on Acoustics, Speech, and Signal Processing, 2005. Proceedings. (ICASSP '05)*, 3:iii/429 – iii/432 Vol. 3, march 2005.

[149] A. Chorti, I. Kanaras, M.R.D. Rodrigues, and I. Darwazeh. Joint Channel Equalization and Detection of Spectrally Efficient FDM Signals. In *submitted to IEEE PIMRC'10*, 2010.

[150] Jim Lawrence, GÃűtz E. Pfander, and David Walnut. Linear independence of Gabor systems in finite dimensional vector spaces. *J. FOURIER ANAL. APPL*, 11:2005, 2005.

[151] D. Gesbert. Minimum-error linear receivers for ill-conditioned MIMO channels. In *Signal Processing Advances in Wireless Communications, 2003. SPAWC 2003. 4th IEEE Workshop on*, pages 462 – 466, june 2003.

[152] L. Rugini, P. Banelli, and S. Cacopardi. A full-rank regularization technique for MMSE detection in multiuser CDMA systems. *Communications Letters, IEEE*, 9(1):34 – 36, jan. 2005.

[153] Yi Sun. A family of linear complexity likelihood ascent search detectors for CDMA multiuser detection. *2000 IEEE Sixth International Symposium on Spread Spectrum Techniques and Applications*, 2:713 –717 vol.2, 2000.

[154] K. Vishnu Vardhan, S.K. Mohammed, A. Chockalingam, and B. Sundar Rajan. A Low-Complexity Detector for Large MIMO Systems and Multicarrier CDMA Systems. *IEEE Journal on Selected Areas in Communications*, 26(3):473 –485, april 2008.

[155] B. Cerato and E. Viterbo. Hardware implementation of a low-complexity detector for large MIMO. *Circuits and Systems, 2009. ISCAS 2009. IEEE International Symposium on*, pages 593 –596, may 2009.

[156] J.H. Conway and N.J.A. Sloane. *Sphere Packings, Lattices and Groups*. Springer, 3rd edition, 1999.

[157] H. Hindi. A tutorial on convex optimization. *American Control Conference, 2004. Proceedings of the 2004*, 4:3252–3265 vol.4, June-2 July 2004.